Zein-based nanoparticles for drug delivery applications

Jitkasem Meewan

University of Strathclyde

Strathclyde Institute of Pharmacy and Biomedical Sciences

A thesis presented in fulfilment of the requirements for the degree of Doctor of Philosophy

2021

Declaration of Authenticity

‘This thesis is the result of the author’s original research. It has been composed by the author and has not been previously submitted for examination which has led to the award of a degree.’

Signed:

Date:

Acknowledgements

I would like to express my sincere appreciation to my supervisor Dr. Christine Dufès for giving me the opportunity to work on this project and also for her invaluable support and mentorship throughout the entire study.

I would like to thank Margaret Mullin from the University of Glasgow for her help with TEM, Craig Irving for his help with NMR, Dr. Valerie A. Ferro and Abdullah R. Alzahrani for providing training on SDS-PAGE, Graeme MacKenzie for his help with confocal imaging, and Dr. Richard Burchmore and his team from Glasgow Polyomics, University of Glasgow, for their help with proteomic analysis. I would also like to thank Professor Craig Roberts and Dr. Stuart Woods for providing me with macrophages and dendritic cells. I am grateful to Professor Yvonne Perrie for allowing me to use her centrifuge and NanoAssemblr™ equipment. This thesis could not have been accomplished without the great support from the aforementioned individuals.

I wish to extend my gratitude to Dr. Sukrut Somani and Dr. Partha Laskar for their kind advice and help on my research. Big thanks also to the people who worked alongside me at Lab 224 during my research years, especially Intouch and Jamal, for their kindness, friendship, and most of all - thanks for all the time we shared together.

Special thanks are directed to my best buddy, P' Ik, who always supports, encourages, and stands by me in every moment.

Whole-hearted thanks to my family for their support throughout my life. Without their encouragement and understanding, none of this would have been possible.

Contents

Table of Contents……..…..... II

List of Figures……...… VII

List of Tables…… XII

Abbreviations……...… XIII

Abstract ……...… XVI

Table of Contents

Chapter 1: Introduction……..….. 1

1.1 Nanoparticles for drug delivery in cancer …… 2

1.2 Protein-based nanoparticles.…… 6

1.3 Zein……...……... 7

1.3.1 Characteristics of zein…….… 7

1.3.1.1 Fractions…….…… 7

1.3.1.2 Structure……. 8

1.3.1.3 Solubility…… 9

1.3.1.4 Biocompatibility……. 10

1.3.1.5 Degradation…… 10

1.3.2 Zein-based carrier systems……. 11

1.3.2.1 Micro/nanospheres……. 11

1.3.2.2 Micelles…….. 16

1.3.3 Combination of zein with other materials…….. 18

1.3.4 Zein for drug delivery applications……..…….. 19

1.4 Protein corona…….. 21

1.4.1 Formation of protein corona……... 23

1.4.2 Impact of the protein corona on the systemic circulation time of nanoparticles…….. 24

1.5 PEGylation and its significance…….…….. 26

1.6 Mechanisms of cellular uptake of nanoparticles……... 29

1.7 Aim and objectives…….…….. 33

Chapter 2: PEGylated zein micelles for cancer therapy……. 34

2.1 Introduction……. 35

2.2 Aim and Objectives…….. 35

2.3 Materials…….. 36

2.4 Methods……... 38

2.4.1 PEGylation of zein…….. 38

2.4.2 Attenuated Total Reflection - Fourier Transform Infrared spectroscopy (ATR-FTIR) analysis…….. 39

2.4.3 Proton Nuclear Magnetic Resonance (^{1}H NMR) analysis..... 40
2.4.4 Determination of Critical Micelle Concentration (CMC)..... 40
2.4.5 Preparation of Nile red-loaded mPEG-zein micelles 41
2.4.6 Transmission electron microscopy (TEM)..... 41
2.4.7 Size and zeta potential measurement 41
2.4.8 Determination of Nile red encapsulation efficiency..... 42
2.4.9 *In vitro* evaluation..... 42
2.4.9.1 Cell culture..... 42
2.4.9.2 *In vitro* cytotoxicity..... 43
2.4.9.3 Cellular uptake..... 43
2.4.9.3.1 Qualitative analysis..... 43
2.4.9.3.2 Quantitative analysis..... 44
2.4.9.3.3 Mechanisms of cellular uptake..... 44
2.4.10 Statistical analysis..... 45
2.5 Results..... 46
2.5.1 ATR-FTIR analysis..... 46
2.5.2 ^{1}H NMR analysis 48
2.5.3 Determination of the CMC..... 52
2.5.4 Characterisation of mPEG-zein micelles..... 54
2.5.5 Determination of Nile red encapsulation efficiency..... 56
2.5.6 *In vitro* cytotoxicity..... 59
2.5.7 Cellular uptake..... 61
2.5.7.1 Qualitative analysis..... 61
2.5.7.2 Quantitative analysis..... 62
2.5.7.3 Mechanisms of cellular uptake 64
2.6 Discussion..... 66
Chapter 3: Impact of protein corona on PEGylated zein micelles..... 73
3.1 Introduction..... 74
3.2 Aim and Objectives..... 75
3.3 Materials..... 76
3.4 Methods..... 78
3.4.1 Stability of mPEG-zein micelles in the presence of proteins.... 78

3.4.1.1 Proteins from FBS……..…… 78
3.4.1.2 Proteins from human plasma (HP)……..….. 78
3.4.2 Cell culture……...….. 78
3.4.3 Effect of the protein corona on the cellular uptake of mPEG-zein micelles……... 79
3.4.3.1 Proteins from FBS……..…… 79
3.4.3.2 Proteins from HP..……..…… 80
3.4.4 Evaluation of cell viability……..……... 80
3.4.5 Preparation of hard corona samples……...…… 81
3.4.5.1 Hard corona from FBS…….……..…… 81
3.4.5.2 Hard corona from HP……..…..……..…… 81
3.4.6 Analysis of protein corona……..……... 81
3.4.6.1 Sodium dodecyl sulphate polyacrylamide gel electrophoresis (SDS-PAGE)……. 81
3.4.6.2 Liquid chromatography-mass spectrometry (LC-MS) analysis……...……. 82
3.4.6.3 Protein identification…….. 83
3.4.7 Statistical analysis……..…… 83
3.5 Results……. 85
3.5.1 Stability of mPEG-zein micelles in the presence of proteins…. 85
3.5.2 Effect of protein corona on the cellular uptake of mPEG-zein micelles……..... 87
3.5.2.1 Proteins from FBS……..…… 87
3.5.2.2 Proteins from HP……..……..…… 92
3.5.3 Evaluation of cell viability……. 95
3.5.4 Analysis of the protein corona……...…… 97
3.5.4.1 SDS-PAGE……...……..…… 97
3.5.4.2 LC-MS analysis……...…….……..…… 98
3.6 Discussion…… 102
Chapter 4: Microfluidic versus manual manufacturing of zein-based nanoparticles……..… **110**
4.1 Introduction…….…… 111

4.2 Aim and Objectives……. 112
4.3 Materials…….. 113
4.4 Methods……... 115
4.4.1 Optimisation of production parameters…….. 115
4.4.1.1 Microfluidic system…… 115
4.4.1.2 Nanoprecipitation method……...…… 116
4.4.2 Preparation of zein nanoparticles…… 117
4.4.2.1 Microfluidics……...…… 117
4.4.2.2 Nanoprecipitation…….……...…… 118
4.4.3 Preparation of mPEG-zein nanoparticles entrapping CR6…….. 118
4.4.4 Nanoparticle characterisation …… 118
4.4.4.1 Nanoparticle morphology……...…….…… 118
4.4.4.2 Determination of particle diameter, size distribution, and zeta potential.……...……...…..…… 119
4.4.4.3 CR6 encapsulation efficiency…….…….…… 119
4.4.4.4 Nanoparticle yield……...……...…….…… 119
4.4.5 Stability study…….…… 120
4.4.6 *In vitro* analysis……..……..…….. 121
4.4.6.1 Cellular uptake……...…….…… 121
4.4.6.1.1 Qualitative analysis……..… 121
4.4.6.1.2 Quantitative analysis…… 121
4.4.6.1.3 Mechanisms of cellular uptake…….… 122
4.4.7 Statistical analysis……..…… 122
4.5 Results……...…….. 123
4.5.1 Optimisation of production parameters.…….…… 123
4.5.1.1 Microfluidic system…… 123
4.5.1.2 Nanoprecipitation method…….....…… 125
4.5.2 Impact of manufacturing method on zein nanoparticle characteristics……. 127
4.5.3 Characterisation of PEGylated zein nanoparticles entrapping CR6…….…... 131
4.5.4 Stability of zein and mPEG-zein nanoparticles.……..…… 133

4.5.5 Cellular uptake……... 135
4.5.6 Mechanisms of cellular uptake……... 138
4.6 Discussion……..... 140
Chapter 5: Conclusions and future works……..…… **146**
5.1 Conclusions…….…… 147
5.2 Future works…… 150
References……..…… **153**
Appendices…… **170**
Appendix I: Table A-1. List of hard corona proteins on mPEG5K-zein (0.5:1) and mPEG10K-zein micelles after exposure to human plasma at 37°C for 1 h (n.d.: not detected)…… 171
Appendix II: Conference proceedings and Publications..…… 176

List of Figures

Figure 1-1 Illustration of the enhanced permeation and retention (EPR) effect of macromolecular structures as drug delivery systems and small molecules through healthy (top) and cancer (bottom) tissues (Adapted from Stockhofe *et al*., 2014)…… 4

Figure 1-2 Tertiary structure model of α-zein proposed by Matsushima *et al*. (Adapted from Wang *et al.*, 2008)…… 9

Figure 1-3 Phase separation process to fabricate zein-based micro/nanospheres (Adapted from Zhang *et al.*, 2016)……. 13

Figure 1-4 Emulsification/solvent evaporation process (Adapted from Zhang *et al.*, 2016)…… 15

Figure 1-5 Relationship between the synthetic identity, biological identity, and physiological response. The synthetic identity corresponds to the size, shape, and surface chemistry of a nanomaterial post-synthesis. The biological identity is the size and aggregation state of the nanomaterial in a physiological environment, along with the structure and composition of the protein corona. The physiological response is the subsequent interaction of nanomaterials with biomolecules, biological barriers, and cells in the body (Adapted from Walkey and Chan, 2012)…….. 22

Figure 1-6 Formation of the biomolecular corona. From left to right: The biomolecules (typically highly abundant proteins) (in green) that arrive first to the surface of nanoparticles form an initial corona. Some of the initially adsorbed molecules with low affinity (in green) are subsequently displaced by molecules with a higher affinity that arrive later (in blue). Then, molecules that have a low affinity for the bare surface of nanoparticles (in yellow) can adsorb on the surface, owing to favourable interactions with the adsorbed (green and blue)

biomolecules. Other biomolecules (in red) do not adsorb at all. (Adapted from Monopoli *et al*., 2012)…….. 23

Figure 1-7 Passive targeting of nanoparticles to tumour cells with stealth characteristics. PEGylated nanoparticles are capable of evading the reticuloendothelial system (RES), thus delaying their elimination by the liver and spleen. In contrast, non-PEGylated nanoparticles are easily recognised by the immune cells, resulting in rapid clearance from blood circulation. (Adapted from Ranganathan *et al*., 2012)……. 28

Figure 1-8 Summary of cellular uptake pathways of nanoparticles (Adapted from Panariti *et al*., 2012)…….. 30

Figure 2-1 Schematic reaction of the PEGylation of zein…….. 46

Figure 2-2 FTIR spectra of A) zein, B) mPEG5K, C) mPEG10K, D) mPEG5K-zein conjugate (0.5:1), E) mPEG5K-zein conjugate (1:1), F) mPEG10K-zein conjugate, G) physical mixture of mPEG5K with zein, and H) physical mixture of mPEG10K with zein…… 48

Figure 2-3 ^{1}H NMR spectra of A) zein in DMSO-d_6, B) mPEG5K in D_2O, C) mPEG10K in D_2O, D) mPEG5K-zein (0.5:1) in DMSO-d_6, E) mPEG5K-zein (0.5:1) in D_2O, F) mPEG5K-zein (1:1) in DMSO-d_6, G) mPEG5K-zein (1:1) in D_2O, H) mPEG10K-zein in DMSO-d_6, and I) mPEG10K-zein in D_2O……..... 51

Figure 2-4 Relative fluorescence intensity (I/I_0) of Nile Red in the function of the concentration of mPEG5K-zein (0.5:1) (A), mPEG5K-zein (1:1) (B), and mPEG10K-zein (C). Results represent the mean ± standard deviation (SD) of 3 mPEG-zein batches……. 53

Figure 2-5 TEM images of mPEG-zein micelles (scale bar: 200 nm)……. 54

Figure 2-6 Standard calibration curve of Nile red in methanol for quantification determination of one assay (n = 5). Error bars are smaller than the symbols when not visible…….. 57

Figure 2-7 Cell viability of B16-F10-luc-G5 (A) and T98G (B) cells treated with empty mPEG5K-zein (0.5:1) (dark grey), mPEG5K-zein (1:1) (grey), or mPEG10K-zein (light grey) micelles for 72 hours (*: P < 0.05, compared with control of each group). Results represent mean ± SEM of 3 independent experiments…….. 60

Figure 2-8 Confocal images of B16-F10-luc-G5 cells after incubation with Nile red loaded in mPEG-zein micelles or as a solution (DIC: Differential Interference Contrast) (scale bar: 50 μm)… 62

Figure 2-9 Flow cytometry analysis of the cellular uptake of Nile red loaded in mPEG-zein micelles or as a solution, in B16-F10-luc-G5 cells (a.u.: arbitrary units) (*: P < 0.05). Results represent mean ± SEM of 3 independent experiments.……..… 63

Figure 2-10 Effects of endocytosis inhibitors on the uptake of Nile red loaded in mPEG-zein micelles by B16-F10-luc-G5 cells (*: P < 0.05, compared with control). Results represent mean ± SEM of 3 independent experiments.……. 65

Figure 2-11 Schematic mPEG-zein micelle formation (Adapted from Podaralla *et al.*, 2011)…….. 67

Figure 3-1 Stability of mPEG5K-zein (0.5:1) and mPEG10K-zein micelles in the presence or absence of 10% v/v FBS (A) or HP (B) (cDMEM: complete DMEM medium, sfDMEM: serum-free DMEM medium, sfRPMI: serum-free RPMI medium, sfRPMI + HP: serum-free RPMI medium + 10% v/v HP) (*: P < 0.05, compared with its serum-free counterpart at the same incubation time). Results represents mean ± SD of one sample, triplicate readings.……. 86

Figure 3-2 Time-dependent uptake of pre-formed corona mPEG5K-zein (0.5:1) and mPEG10K-zein micelles in complete and serum-free media by B16-F10-luc-G5 cells (A) and T98G (B) (cRPMI: complete RPMI medium, sfRPMI: serum-free RPMI medium, cDMEM: complete DMEM medium, sfDMEM:

serum-free DMEM medium) (*: P < 0.05, compared between serum-free condition and its serum-containing counterpart at the same treatment time). Results represent mean ± SEM of 3 independent experiments……. 89

Figure 3-3 Uptake of the pre-formed corona micelles in cRPMI (dark grey) or sfRPMI (light grey) by macrophages (A) and dendritic cells (B) (*: P < 0.05, compared with sfRPMI). Results represent mean ± SEM of 3 independent experiments. 91

Figure 3-4 Cellular uptake of Nile red-loaded in mPEG5K-zein (0.5:1) and mPEG10K-zein micelles pre-coated with HP (dark grey) or glucose 5% w/v solution as control (light grey), by B16-F10-luc-G5 cancer cells (A), macrophages (B), and dendritic cells (C) (*: P < 0.05, compared with controls without protein corona). Results represent mean ± SEM of 3 independent experiments.……...….... 94

Figure 3-5 Viability of B16-F10-luc-G5 (A) and T98G (B) cancer cells, macrophages (C), and dendritic cells (D) treated with Nile red-loaded mPEG-zein micelles for 4 h (cancer cells) or 2 h (macrophages, dendritic cells). Results represent mean ± SEM of 3 independent experiments. There was no statistical difference between the treatments……. 97

Figure 3-6 SDS-PAGE gels of protein corona surrounding mPEG-zein micelles following incubation in cDMEM, sfDMEM (A) and HP (B) at 37°C for 1 h. The analysis was performed in duplicate - for clarity only one replicate is shown……. 98

Figure 3-7 Proteomic analysis of the protein corona surrounding mPEG5K-zein (0.5:1) and mPEG10K-zein micelles. Proteins were classified by function (A) and weight (kDa) (B). The 20 most abundant proteins in the corona of mPEG-zein micelles were used to create the heat map (C)……. 101

Figure 4-1 Zein nanoparticles manufacture using a microfluidic cartridge coupled with a NanoAssemblr™ device…….. 116

Figure 4-2 Nanoprecipitation methods used to prepare zein nanoparticles. Nanoparticles were formed either by addition of the organic phase to the aqueous phase (Method 1) or by addition of the aqueous phase to the organic phase (Method 2). This figure was created with Biorender.com..…….....… 117
Figure 4-3 Morphology of CR6-loaded zein nanoparticles using TEM (scale bar: 200 nm)…… 128
Figure 4-4 Size and polydispersity index (PDI) (A), zeta potential (B), encapsulation efficiency (EE) (C), and yield (D) of CR6-loaded zein nanoparticles (*: P < 0.05). Results represent mean ± SEM of 3 samples.…… 131
Figure 4-5 Unstained TEM images of zein, mPEG5K-zein (0.5:1), mPEG5K-zein (1:1), and mPEG10K-zein nanoparticles. All nanoparticles were prepared using nanoprecipitation Method 2 (scale bar: 200 nm)…… 132
Figure 4-6 Stability of zein (A) and mPEG-zein (B) nanoparticles loading CR6 after storage at 4°C for 4 weeks. Results represent mean ± SEM of 3 samples. Nanoparticles were prepared by nanoprecipitation Method 2. Error bars are smaller than the symbols when not visible……..... 134
Figure 4-7 Confocal images of the cellular uptake of CR6 loaded in zein and mPEG-zein nanoparticles, or as a solution, in B16-F10-luc-G5 cells (scale bar: 25 μm)…….. 136
Figure 4-8 Flow cytometry analysis of the cellular uptake of CR6 loaded in zein and mPEG-zein nanoparticles, or as a solution (a.u.: arbitrary units) (*: P < 0.05). Results represent mean ± SEM of 3 independent experiments.…….. 137
Figure 4-9 Effects of endocytosis inhibitors on the cellular uptake of CR6-loaded zein/mPEG-zein nanoparticles (*: P < 0.05, compared with control of each system). Results represent mean ± SEM of 3 independent experiments.……. 139

List of Tables

Table 1-1	The role of the physicochemical and environmental parameters of the nanoparticles on the protein corona.……	25
Table 2-1	Composition of the three mPEG-zein synthesised in the study.	38
Table 2-2	Particle size and zeta potential of empty and Nile red-loaded mPEG-zein micelles. Results represent mean ± SEM of 4 samples.……	55
Table 2-3	Encapsulation efficiency of Nile red in mPEG-zein formulations. Results represent mean ± SEM of 4 samples.….	58
Table 2-4	Amount of Nile red per mg of mPEG-zein in three micelle formulations. Results represent mean ± SEM of 4 samples.….	58
Table 4-1	Characteristics of zein nanoparticles synthesised in the microfluidic Y-junction and the effect of various experimental parameters used in this work. Results represent mean ± SD of triplicate readings……..	124
Table 4-2	Characteristics of zein nanoparticles prepared by nanoprecipitation method optimised by variation of the following parameters: preparation method and volume ratio of aqueous to organic phase. Results represent mean ± SD of triplicate readings…….....	127
Table 4-3	Characteristics of zein and mPEG-zein nanoparticles prepared by nanoprecipitation Method 2. Results represent mean ± SEM of 3 samples. ……...	133

Abbreviations

ATR-FTIR	Attenuated total reflection - Fourier transform infrared
a.u.	Arbitrary units
BCRP	Breast cancer resistance protein
BMD	Bone marrow-derived
BSA	Bovine serum albumin
cDMEM	Complete Dulbecco’s modified Eagle medium
CMC	Critical micelle concentration
cRPMI	Complete Roswell Park Memorial Institute medium
CR6	Coumarin-6
DAPI	4’,6-diamidino-2-phenylindole
DI	Deionised
DIC	Differential interference contrast
DLS	Dynamic light scattering
DMEM	Dulbecco's modified Eagle medium
DMSO	Dimethyl sulfoxide
DMSO-d_6	Deuterated dimethyl sulfoxide
DOX	Doxorubicin
D_2O	Deuterium oxide
EE	Encapsulation efficiency
emPAI	Exponentially modified protein abundance index
EPR	Enhanced permeability and retention
FRR	Flow rate ratio

FBS	Foetal bovine serum
FDA	Food and Drug Administration
FTIR	Fourier transform infrared
GI	Gastrointestinal
GLOBOCAN	Global Cancer Incidence, Mortality and Prevalence
GRAS	Generally recognised as safe
HP	Human plasma
IC_{50}	Half-maximal inhibitory concentration
LC-MS	Liquid chromatography-mass spectrometry
MFI	Mean fluorescence intensity
MOWSE	Molecular weight search
mPEG	Methoxy polyethylene glycol
mPEG-SCM	Methoxy polyethylene glycol succinimidyl carboxymethyl
MPS	Mononuclear phagocyte system
MRP1	Multidrug resistance-associated protein 1
MSCs	Mesenchymal stem cells
MTT	3-(4,5-dimethylthiazol-2-yl)-2,5-diphenyltetrazolium bromide
MW	Molecular weight
NHS	N-hydroxysuccinimide
nLC-ESI-MS/MS	Nanoscale liquid chromatography coupled to electrospray ionisation tandem mass spectrometry
PBS	Phosphate buffered saline
PDI	Polydispersity index
pDNA	plasmid DNA

PEG	Polyethylene glycol
P-gp	P-glycoprotein
PLA	Poly(lactic acid)
PLGA	Poly(lactic-co-glycolic acid)
RES	Reticuloendothelial system
RPMI 1640	Roswell Park Memorial Institute medium
SD	Standard deviation
SDS-PAGE	Sodium dodecyl sulphate polyacrylamide gel electrophoresis
SEM	Standard error of the mean
sfDMEM	Serum-free Dulbecco's modified Eagle medium
sfRPMI	Serum-free Roswell Park Memorial Institute medium
SOD	Superoxide dismutase
TEM	Transmission electron microscopy
TFR	Total flow rate
TOC	α-tocopherol
TPGS 1000	D-α-tocopheryl polyethylene glycol 1000 succinate
^{1}H NMR	Proton nuclear magnetic resonance
5-FU	5-fluorouracil

Abstract

Zein's protein origin and hydrophobicity has raised concerns about its potential use as a delivery system in humans. To overcome this issue, it has been hypothesised that conjugating zein with polyethylene glycol (PEG) could provide steric shielding to the delivery system, thus preventing its opsonisation and increasing its half-life in the blood. The overall goal of this thesis was therefore to synthesise zein micelles conjugated with PEG and assess the possibility of using them for cancer drug delivery. First, we demonstrated that zein could be successfully conjugated with PEG and self-assembled into micelles with sizes ranging from 100 to 300 nm, depending on the molecular weight of PEG and PEG to zein ratio. *In vitro* studies revealed that PEGylated zein micelles could deliver a model hydrophobic substance, Nile red, into B16-F10-luc-G5 melanoma cells in a time-dependent manner, with higher cellular uptake observed when using smaller chain length PEG5K and lower PEG density. The impact of the protein corona on the uptake of PEGylated zein micelles by cancer cells and immune cells was then evaluated. PEGylation was shown to confer stealth effects to the zein micelles. The presence of human plasma did not impact the uptake of the micelles by melanoma cancer cells, regardless of PEG chain length. On the other hand, it decreased the uptake by macrophages and dendritic cells. Finally, the NanoAssemblr^{TM} microfluidic system was exploited to generate zein nanoparticles. Continuous microfluidic approach was not the best option for manufacturing zein nanoparticles, as it resulted in low yield and drug entrapment. By contrast, zein nanoparticles with an appropriate size and improved encapsulation efficiency could be obtained using the conventional nanoprecipitation method. Overall, this thesis

demonstrated that PEGylated zein micelles are highly promising delivery systems that should be further investigated for use in cancer drug delivery.

CHAPTER 1

Introduction

1.1 Nanoparticles for drug delivery in cancer

Cancer is one of the leading causes of death to human life worldwide. Based on GLOBOCAN (Global Cancer Incidence, Mortality and Prevalence) estimates, 19.3 million new cancer cases were diagnosed and almost 10 million patients suffered from cancer-induced death in 2020. Moreover, cancer incidences are expected to rise by about 47% in the next two decades (Sung *et al*., 2020). Treatments against cancer include surgery, radiotherapy, drug treatments (such as chemotherapy, hormone therapy or immunotherapy), and stem cell/bone marrow transplants, depending on the type and stage of cancer (Cancer Research UK, 2021). Surgery is one of the main treatments for many types of cancer. However, it is not the best option for patients who have haematological cancers (leukaemia, lymphoma, and myeloma) or metastases. These spreading cancers require a systemic treatment, for example chemotherapy, that can reach all parts of the body through blood circulation (Dickens and Ahmed, 2018).

One of the main reasons of cancer treatment failure is the lack of selectivity of conventional chemotherapeutic agents. The systemic delivery of chemotherapeutics can cause undesirable side effects such as nausea, diarrhoea, weight loss, mouth sores, hair loss, low blood counts, and a compromised immune system, due to its effect on both cancer and normal cells (Sagnella *et al*, 2014). The solubility of anticancer drugs is another important factor limiting the therapeutic efficacy. In addition to a strong tendency to aggregate upon intravenous administration, poorly water-soluble drugs may not be soluble enough to cross the aqueous environment surrounding a cell. Thus, they may not be able to penetrate the cell membrane to reach intracellular targets (Sun *et al*., 2014). Furthermore, the overexpression of drug efflux transporters, such as P-glycoprotein (P-gp), multidrug resistance-associated protein 1 (MRP1), and breast

cancer resistance protein (BCRP), in both solid tumours and haematological malignancies causes multidrug resistance to chemotherapy, since the transporter increases its substrate efflux out of the cells, resulting in a reduced intracellular accumulation of the substrate (Sun *et al*., 2014; Blanco *et al*., 2015). Recent developments in nanotechnology have offered new hope to overcome these current limitations in cancer therapy (Jain and Stylianopoulos, 2010; Sagnella *et al.*, 2014; Wicki *et al*., 2015).

It should be noted that particle size highly affects *in vivo* biodistribution of nanomedicine. For example, small nanoparticles (less than 6 nm) are highly excreted by the kidneys, while nanoparticles of 50-100 nm in size were found to accumulate in the liver due to the discontinuous endothelium there (Alexis et al., 2008; Kobayashi *et al*., 2014; Sun *et al*., 2014). In addition, nanoparticles larger than 200 nm are recognised by the reticuloendothelial system (RES) and accumulate in the liver and spleen, resulting in rapid clearance from blood circulation (Blanco *et al*., 2015). Therefore, nanomedicines with the appropriate size (100-200 nm) have the potential to prolong circulation lifetime, due to their ability to evade renal excretion and uptake by the liver and the spleen, and achieve the preferential accumulation of drugs within solid tumours due to the enhanced permeability and retention (EPR) effect (Blanco *et al*., 2015).

The EPR effect is caused by the leakiness of tumour vasculature and a deficient lymphatic drainage system. Tumour growth induces angiogenesis, which is the formation of new blood vessels, to maintain adequate supplies of nutrients and oxygen (Kobayashi *et al*., 2014). The rapid proliferation of endothelial cells during angiogenesis leads to a reduced density of endothelial cells and thus loss of tight

junctions. The gaps of tumour vessels are significantly larger than in normal tissues (2-6 nm). They are typically 100-800 nm in size, depending on the tumour type (Nitta and Numata, 2013; Sun *et al*., 2014). The leaky tumour vasculature and the poor lymphatic drainage allow drug delivery vehicles and macromolecules smaller than approximately 400 nm to extravasate into the tumour tissue, which then retain and release the drug (**Figure 1-1**) (Yuan *et al*. 1995; Alexis *et al*., 2008; Torchillin, 2011; Kobayashi *et al*., 2014). As a result, the delivery of chemotherapeutic agents entrapped in nanomedicines is more efficient and the toxicity on normal cells can be minimised.

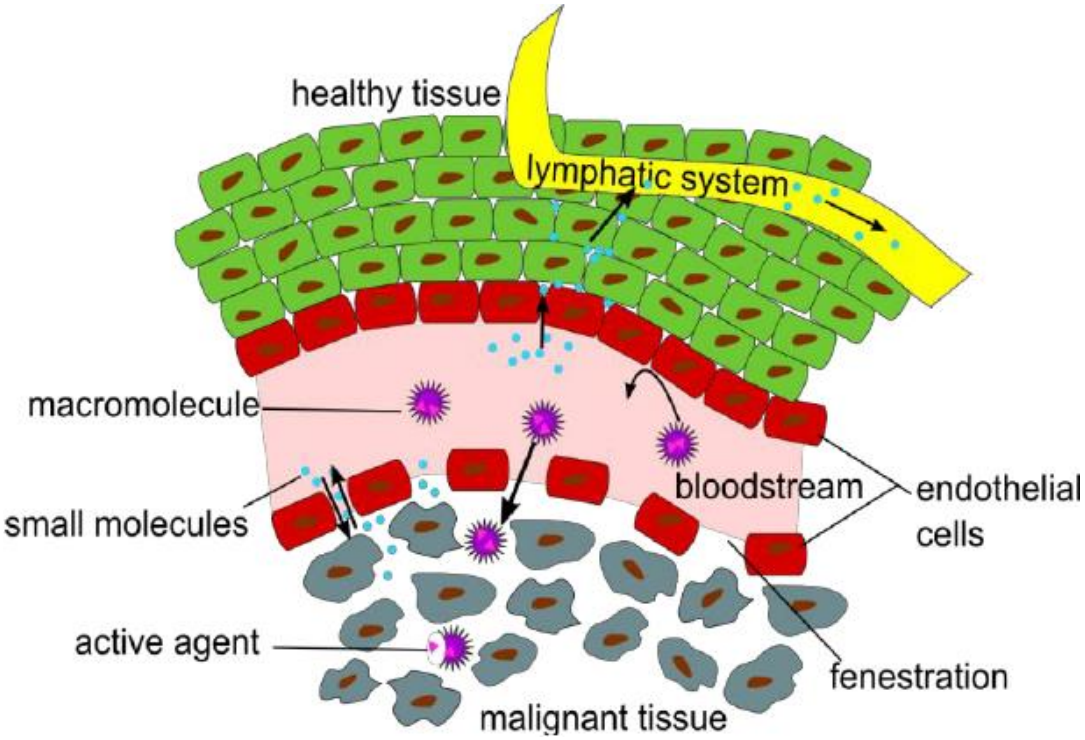

Figure 1-1. Illustration of the enhanced permeation and retention (EPR) effect of macromolecular structures as drug delivery systems and small molecules through healthy (top) and cancer (bottom) tissues (Adapted from Stockhofe *et al*., 2014).

However, while the EPR effect is widely believed to improve the delivery of nanomedicine to tumours, it actually only results in less than a 2-fold increase in nano-drug delivery when compared with major organs. This is generally insufficient for achieving therapeutic levels within the tumour, although side effects are usually significantly reduced as a result of very low accumulation within normal tissues lacking EPR. The elevated interstitial fluid pressure from constant extravasation of fluid creates intratumoral hypoxic and acidic conditions. This environment prevents the penetration of nanomedicine deep within the tumour and, therefore, contributes to tumour progression, metastasis, and drug resistance. As a result, the majority of nanomaterials designed for clinical use barely reach the stage of *in vivo* evaluation, and even fewer led to clinical trials. In practice, if nano-drugs rely on the EPR effect for delivery, their circulating half-life has to be long enough for allowing a sufficient amount of the nano-drug to reach the tumour. In general, acute and sub-acute toxicity must be assessed for at least ten half-lives, which in the case of nanomedicine is a long and costly process (Nakamura *et al*., 2016; Shi *et al*., 2020).

In addition to exploiting the EPR effect for passive accumulation within tumours, nanosized delivery systems can also increase the solubility of anti-cancer drugs by entrapping poorly water-soluble drugs in a hydrophilic nanocarrier and improve drug stability by protecting them from degradation (William *et al*., 2013; Kobayashi *et al*., 2014). Scientific evidence also demonstrated that nanocarriers such as liposomes, micelles, and polymer-lipid hybrid nanoparticles can enhance intracellular drug accumulation, increase cellular uptake, and decrease drug efflux by P-gp (Dabholkar *et al*., 2006; Wong *et al*., 2006; Riganti *et al*., 2011). Besides, nanomedicines have the potential to deliver more than one therapeutic agent for combination therapy (Jain and

Stylianopoulos, 2010). Such benefits have made the development of nanomedicines highly promising for improving cancer treatment.

1.2 Protein-based nanoparticles

Nanoparticles are generally submicron-sized materials that can be obtained from a range of synthetic and natural sources. They include viral vectors, drug conjugates, inorganic nanoparticles, and lipid- and polymer-based nanoparticles (Wicki *et al*., 2015). Among the available polymer nanocarriers used for *in vivo* applications, protein-based nanoparticles present several unique advantages in terms of biodegradability, low toxicity, low immunogenicity, and ease of availability. They also offer a wide range of surface modification and drug binding capacity. As the charge of their amino and carboxyl groups varies in response to pH, protein nanoparticles can be utilised for triggered drug release applications. (Nitta and Numata, 2013; Zaman *et al*., 2014; Tarhini *et al*., 2018; van Ballegooie *et al*., 2019). Animal proteins (i.e. gelatin, collagen, and albumin) as well as plant proteins (i.e. zein, gliadin, and soy proteins) are widely investigated for diverse biomedical purposes. Recently, plant-based proteins, particularly zein, have emerged as promising biomaterials for drug and gene delivery due to their lower risk of transmitting zoonotic disease than animal proteins. They are also less expensive and have functional groups that can be used to interact or covalently conjugate with molecules capable of modifying the targeting properties of nanoparticles (Reddy and Yang, 2011; Elzoghby *et al*., 2012; Paliwal and Palakurthi, 2014).

1.3 Zein

Zein is a water-insoluble protein extracted from corn. It accounts for about 35-60% of the total corn protein and is mostly present in the endosperm of the plant (Shukla and Cheryan, 2001; Luo and Wang, 2014). It was first discovered by Gorham in 1821 and was identified as prolamin, a major storage protein, by Osborne in 1924 (Lawton, 2002; Anderson and Lamsal, 2011). Zein was approved by the US Food and Drug Administration (FDA) in 1985 as a generally recognised as safe (GRAS) material and has been widely used for tablet coating since then (Zhang *et al*., 2016). It is, nowadays, an attractive natural material for novel applications in the fields of food science, pharmaceutics, and biomedicine, due to its ease of modification, unique solubility, excellent biocompatibility and biodegradability, as well as low toxicity (Shukla and Cheryan, 2001; Lawton, 2002; Parris et al., 2005; Fu *et al*., 2009; Lin *et al.*, 2011; Luo and Wang, 2014; Paliwal and Palakurthi, 2014; Dong *et al*., 2016; Thapa *et al*., 2017; Li and Yu, 2020).

1.3.1 Characteristics of zein

1.3.1.1 Fractions

Zein is a mixture of several fractions that vary in molecular size, charge, and solubility (Shukla and Cheryan, 2001). In general, zein comprises 4 main types, α-, β-, γ-, and δ-zein. The α-zein consists of 35% of proteins with two prominent bands of 22 and 24 kDa. β-zein (10-15% of total zein) is a polymer of 17-18 kDa, γ-zein (5-10% of total zein) consists of two parts of 27 kDa and 18 kDa, whereas δ-zein is a minor fraction of 10 kDa (Paulis and Wall, 1977; Phillips and McClure, 1985; Parris and Dickey,

2001; Sousa *et al.*, 2013). α-zein is the main type of zein that is commercially available (Luo and Wang, 2014).

Commercial zein is available in two grades: yellow and white zein. Yellow zein has approximately 88-90% purity and contains 8-9% of xanthophyll pigments, including lutein, zeaxanthin, and β-cryptoxanthin. The presence of xanthophyll lowers the solubility of zein in water, resulting in unfavourable properties of nanoparticles, such as large particle size distribution and low drug encapsulation. White zein, on the other hand, is obtained from decolourised yellow zein. As a result, it contains a very low level of xanthophylls (less than 0.001%) and is more than 96% pure (Podaralla and Perumal, 2012; Paliwal and Palakurthi, 2014).

1.3.1.2 Structure

So far, no conclusive structure of zein has been confirmed. Matsushima and colleagues previously reported that α-zein contains 9-10 helical segments arranged in an anti-parallel fashion. The helical segments are aligned to form an elongated ribbon-like shape (**Figure 1-2**). The side surfaces of the ribbon are formed by hydrophobic helices, while the top and bottom loops are connected by hydrophilic glutamine bridges (Matsushima *et al*., 1997; Zhang *et al*., 2016). Most recently, Momany *et al*. proposed a three-dimensional structure of α-zein in alcohol and water. In this revised model, α-zein has 35-60% helical character and is made up of 9 helical hydrophobic segments. Each segment consists of about 20 amino acids joined by glutamine-rich turns. The helical repeats form a triple superhelix where lutein, a natural carotenoid, is within the core to stabilise the protein (Momany *et al.*, 2006). The aforementioned models therefore explained the amphiphilic nature of zein.

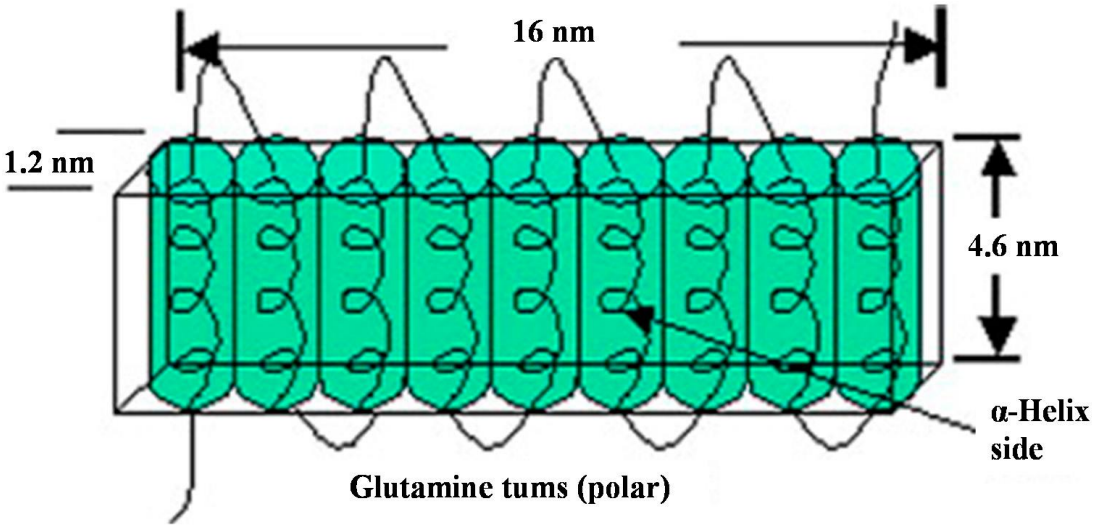

Figure 1-2. Tertiary structure model of α-zein proposed by Matsushima *et al*. (Adapted from Wang *et al.*, 2008).

1.3.1.3 Solubility

The amino acid sequence of zein consists of more than 50% non-polar amino acids, including leucine (20%), proline (10%), and alanine (10%), causing zein to be insoluble in water. Zein also has a high glutamine content (21-26%) which results in its insolubility in absolute alcohol (Gianazza *et al.*, 1977). However, it becomes soluble in the presence of aqueous alcohol, high concentrations of urea, in alkaline conditions (at pH 11 or above), or in presence of anionic surfactants (Shukla and Cheryan, 2001; Luo and Wang, 2014; Paliwal and Palakurthi, 2014). Aqueous alcohol has been used extensively for commercial zein production. At temperatures below the boiling point of ethanol, zein is soluble in 50-90% ethanol, with coacervation and precipitation taking place both above and below this range (Shukla and Cheryan, 2001).

1.3.1.4 Biocompatibility

Zein has been shown to be a promising, biocompatible biomaterial in the biomedical field, especially in tissue engineering. Zein films, for example, were reported to be compatible with HL-7702 human liver cells and NIH 3T3 murine fibroblast cells in terms of cell attachment and proliferation (Dong *et al*., 2004). Zein films are comparable with Corning culture plates and outperformed polylactic acid films and collagen in supporting cell proliferation (Dong *et al*., 2004; Sun *et al*., 2005). Zein can also be modified by cross-linking and coating to improve its compatibility with cells. Cross-linked electrospun zein fibres showed an enhanced attachment, spreading, and proliferation of fibroblast cells over unmodified fibres (Jiang *et al*., 2010). The differentiation of mesenchymal stem cells (MSCs) to osteoblasts was enhanced by coating porous zein scaffolds with hydroxyapatite (Qu *et al*., 2008). The improved proliferation of MSCs on porous zein scaffolds containing stearic acid as a plasticiser after implantation in rabbits is another evidence of good tissue compatibility (Wang *et al*., 2007).

1.3.1.5 Degradation

Zein can be degraded by many protease enzymes, such as pepsin, pancreatin, trypsin, collagenase, alcalase, papain, and thermolysin (Miyoshi *et al*., 1991; Sun *et al*., 2005; Hurtado-Lopez and Murdan, 2006; Kong and Xiong, 2006; Fu *et al*., 2009). In the absence of enzymes, zein microspheres were shown to be resistant to degradation in a number of buffers, including chloride buffer (pH 2), acetate buffer (pH 5), and phosphate buffered saline (PBS) (pH 7.4). On the other hand, they were susceptible to degradation by pepsin and pancreatin enzymes respectively found in simulated gastric

and intestinal fluids (Hurtado-Lopez and Murdan, 2006). Sun *et al*. found that zein was easily degraded by both trypsin and collagenase and its degradation products could enhance the cell viability of HL-7702 liver cells within a certain range of concentrations (Sun *et al*., 2005).

1.3.2 Zein-based carrier systems

To date, zein can form a wide range of carrier systems, such as films, fibres, gels, micro/nanocapsules, micro/nanospheres, and micelles (Fu *et al*., 2009; Zhong *et al*., 2009; Jiang *et al*., 2010; Sousa *et al*., 2010; Cao *et al*., 2012; Podaralla *et al*., 2012; Chen and Zhong, 2014; Song *et al*., 2015; Dong *et al*., 2016; Soe *et al*., 2019). Although micelles are the main focus of the thesis, zein has been extensively explored for use as drug carriers in the form of micro/nanospheres. Thus, in this thesis, only micro/nanospheres and micelles will be reviewed, with an emphasis on zein-based micro/nanospheres.

1.3.2.1 Micro/nanospheres

Spheres are matrix-type, solid colloidal particles in which drugs can be dissolved, encapsulated in, or chemically bound to the constituent polymer matrix (Letchford and Burt, 2007). Zein micro/nanospheres have been investigated as potential delivery vehicles specifically for hydrophobic compounds, including drugs, DNA, and nutrients. Several methods can be used to produce zein micro/nanospheres. The most common one is phase separation, also known as liquid-liquid dispersion, coacervation, or antisolvent precipitation (Zhang *et al*., 2016; Pascoli *et al*., 2018). In addition to phase separation, emulsification/solvent evaporation, spray-drying, and supercritical

anti-solvent have all been reported for the manufacture of zein-based particles (Zhang *et al*., 2016).

Phase separation technique is based on the differential solubility of a protein in different solvents as a function of pH, ionic strength, and electrolytes (Pascoli *et al*., 2018). In the case of zein, the process typically starts with zein and hydrophobic bioactive agents dissolved in aqueous ethanol, followed by the addition of a non-solvent, such as water. The gradual decrease in ethanol concentration below a level required for dissolving zein causes supersaturation, leading to the precipitation of the solute and the formation of zein nanoparticles (**Figure 1-3**) (Tarhini *et al*., 2018). The payload is trapped within the zein aggregates via hydrophobic interactions. As a result, hydrophobic compounds generally show higher encapsulation efficiency (EE) than hydrophilic compounds (Zhang *et al*., 2016; van Ballegooie *et al*, 2019). When using this methodology, the size, EE, drug loading, and release profiles of the resultant particles have been shown to be influenced by several parameters, including the type of solvent, zein concentration, initial alcohol concentration, shear rate, mixing method, and dilution ratio (Zhang *et al*., 2016). This technique is widely used for the preparation of zein micro/nanospheres, because it is a simple and quick process which does not require the use of surfactants for particle formation (Rao and Geckeler, 2011).

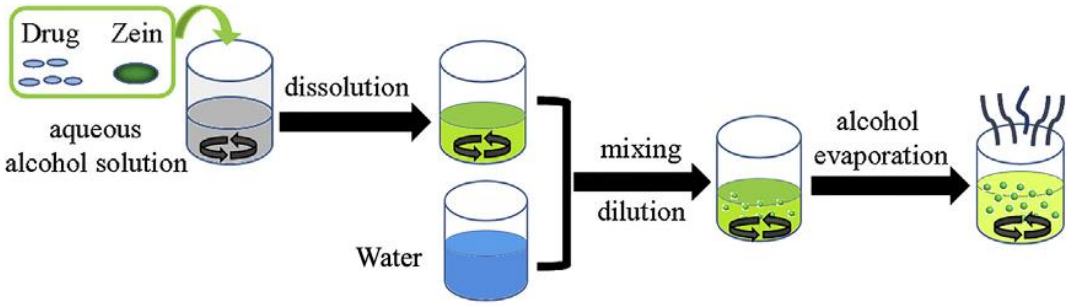

Figure 1-3. Phase separation process to fabricate zein-based micro/nanospheres (Adapted from Zhang *et al.*, 2016).

Various zein nanospheres prepared by the phase separation method have been shown to provide a sustained release of the encapsulated drugs. For instance, Dong and co-workers (2016) developed zein nanospheres encapsulating the anti-cancer drug doxorubicin (DOX) by using this method. These nanospheres were formed after rapidly pouring deionised (DI) water containing sodium caseinate as a stabiliser into zein/DOX dissolved in 80% ethanol, under vigorously vortexing. The spheres displayed a uniform size of around 200 nm, with an EE ranging from 40 to 90%. *In vitro* release studies revealed a pH-sensitive sustained release of DOX from the nanospheres. The entrapped drug was released faster at pH 5 and 6.5 than at pH 7.4. Furthermore, the drug-loaded nanospheres led to a better therapeutic effect on HeLa cancer cells *in vitro* than that observed following treatment with the drug solution at low concentrations (Dong *et al*., 2016). The production of zein nanospheres loading 5-fluorouracil (5-FU) is another example that used the phase separation technique. To this end, 5-FU and zein were ultrasonically dissolved in 70% ethanol, before being immediately added to distilled water. The formed dispersion was then allowed to evaporate at room temperature to harden the particles. This optimised formulation led

to the production of spheres bearing a diameter of approximately 110 nm and an EE of about 60%. Additionally, 5-FU-loaded zein nanospheres exhibited a controlled release profile. A larger amount of the drug was released in a pH 6.8 buffer solution than in a pH 7.4 buffer solution (Lai and Guo, 2011). Zein could also be potentially used as a gene delivery vehicle. The phase separation process was used to produce tunable-sized zein nanospheres encapsulating plasmid DNA (pDNA). To do so, zein was first dissolved in 70% ethanol. Plasmid DNA in Tris-EDTA buffer was then added to the zein solution, followed by the dropwise addition of water while vortexing. The addition of water resulted in the formation of spheres that were able to protect the encapsulated DNA against degradation by DNAse I and to release it in a sustained manner (Regier *et al*., 2012).

Emulsification/solvent evaporation is the process of forming a water-in-oil emulsion by emulsifying a drug/zein ethanolic solution into an immiscible surfactant-containing oil. The emulsion can be converted into micro/nanospheres via solvent evaporation (**Figure 1-4**) (Rao and Geckeler, 2011; Zhang *et al*., 2016). Zein microspheres encapsulating aceclofenac, a non-steroidal anti-inflammatory drug, were formed by this method for oral delivery. Zein dissolved in 90% alcohol was added to the continuous phase (sesame oil containing 0.5% span 80 as an emulsifying agent) under agitation, and the solvent was then removed by evaporation. *In vitro* studies demonstrated that these microspheres effectively retarded the release of the encapsulated aceclofenac at gastric pH, thereby minimising the risk of gastric injury (Karthikeyan *et al*., 2012).

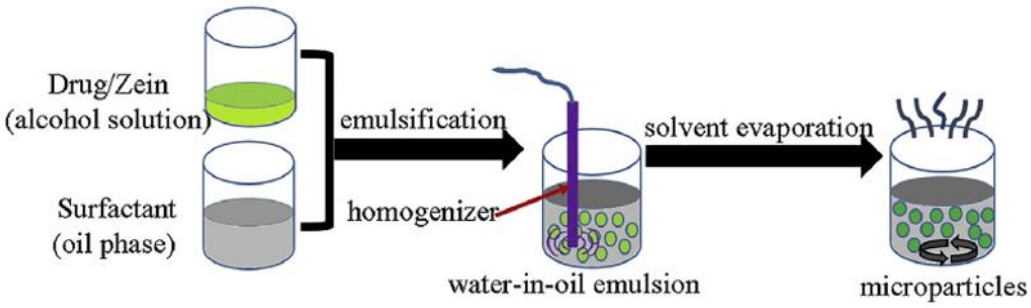

Figure 1-4. Emulsification/solvent evaporation process (Adapted from Zhang *et al.*, 2016).

Spray-drying is a simple and high throughput technique that can be used to prepare various micro/nano-sized particles. This process begins with the atomisation of the feed liquid containing zein. During atomisation, the solvent is continuously evaporating from the atomised droplets. As a result, the zein and drug gradually lose their solubility, form nuclei, and eventually solidify. As spray-drying uses a warm air stream to remove the solvent, it is not suitable for temperature-sensitive substances. To date, this process has been mostly used to produce hybrid microspheres and microcapsules in order to achieve the desired carrier microstructure and tailored drug release profiles (Freitas *et al*., 2005; Sousa *et al*., 2010; Chen and Zhong, 2014; Zhang *et al*., 2016).

Similar to spray drying, the supercritical anti-solvent process has been used to produce zein micro/nanospheres. This approach, however, uses supercritical CO_2 as an anti-solvent to facilitate an aerosol solvent extraction. The zein/drug is dissolved in a co-solvent miscible with CO_2, often an aqueous alcohol solution, then atomised into supercritical CO_2 to remove the solvent and precipitate the zein. Because the particle

formation is performed at a far lower temperature than spray drying and without oxygen, the supercritical anti-solvent technique is appropriate for encapsulating many compounds, especially heat- or oxidation-sensitive drugs (Zhong *et al*., 2008; Zhong *et al*., 2009; Zhang *et al*., 2016).

1.3.2.2 Micelles

Micelles are self-assembled colloidal delivery systems with a spherical core-shell architecture. Their formation occurs by self-association of amphiphilic molecules in aqueous solution above their critical micelle concentration (CMC) (Torchilin, 2007; Ghezzi *et al*., 2021). Drugs can be loaded into both the core and the shell, with non-polar drugs being encapsulated within the hydrophobic core, polar drugs adsorbed on the hydrophilic shell, and drugs with intermediate polarity distributed along amphiphilic molecules in intermediate positions (Sawant and Torchilin, 2010). Upon intravenous administration, micelles are often diluted below their CMC, resulting in their disassembling into free monomers and subsequent release of the loaded drugs (Torchilin, 2007; Zhang *et al*., 2016; Ghezzi *et al*., 2021). Because of their small size, micelles can easily extravasate through the leaky vasculature of the tumours and accumulate in the tumour tissue due to the EPR effect. They also allow for the engineering of the shell and/or the core to develop active targeting and stimuli-sensitive systems, and can improve the bioavailability and solubility of poorly water-soluble compounds. As a result, they have been extensively explored as potential pharmaceutical nanocarriers in cancer therapy (Torchilin, 2007; Vaze, 2016; Oprita and Sevastre, 2020).

Despite the presence of amphiphilic domains in the zein molecule, zein itself cannot form micelles due to its lack of a suitable ratio of hydrophilic and hydrophobic segments (Zhang *et al*., 2016). For this reason, conjugating a hydrophilic polyethylene glycol (PEG) to the zein molecule could produce a stable and biodegradable micelle system, with zein as its hydrophobic core and PEG as its hydrophilic shell. The resultant micelles had a low CMC and were proven to be non-immunogenic. Further investigation demonstrated that micelles could improve the solubility and stability of the hydrophobic anticancer drug curcumin, as well as providing its sustained release for an effective cellular uptake into cancer cells (Podaralla *et al*., 2012; Song *et al*., 2015). The modification of the protein core with the PEG shell therefore makes the zein micelles promising nanocarriers in biomedical applications.

1.3.3 Combination of zein with other materials

Many researchers have sought to introduce other materials, usually natural polymers, into zein-based formulations to improve colloidal stability or customise drug release profiles of zein particles (Zhang *et al*., 2016; Li and Yu, 2020).

For example, the stability of curcumin-loaded zein nanoparticles was shown to be improved by coating cationic zein with anionic pectin. The obtained nanoparticles displayed a core-shell structure, with the hydrophobic zein as the core and the hydrophilic pectin as the shell. The zein-pectin nanoparticles were approximately 250 nm in size and had high loading efficiency (higher than 86%). They could also be freeze-dried, resulting in a powder form that could be easily dispersed in water without causing particle aggregation (Hu *et al*., 2015). In another work, Lee *et al*. (2016) developed zein/alginate nanoparticles as an oral drug delivery system to carry superoxide dismutase (SOD), an antioxidant protein, for the treatment of inflammatory bowel disease induced by oxidative stress. Their findings demonstrated that zein/alginate nanoparticles could protect SOD from degradation in the harsh conditions of gastrointestinal (GI) tract and release SOD in a pH-dependent manner in the small intestine, thus lowering reactive oxygen species (Lee *et al*., 2016). Similarly, coating zein nanoparticles with chitosan was shown to protect a hydrophobic nutrient, α-tocopherol (TOC), against GI conditions and significantly improved the controlled release of the drug (Luo *et al*., 2011). In another investigation, microspheres made of poly(D-L lactide-co-glycolide) (PLGA) and zein were capable of modulating the release of amoxicillin at sufficient levels for antibacterial activity over a six-day period, which is the required interval for root canal disinfection (Sousa *et al*., 2010).

The above studies suggested that zein can be combined with additional materials to yield particles with optimised properties.

1.3.4 Zein for drug delivery applications

In addition to *in vitro* studies, zein-based micro/nanoparticles have successfully been assessed *in vivo* on animal models and in clinical settings. Zein has shown high potential in clinical applications, particularly for oral administration, due to its ability to protect its payload from GI conditions. A patented zein microsphere system for protein and peptide delivery called OraLease® is an excellent example of such potential. The system was developed to protect drugs from the harsh environment of the stomach and small intestine, extend drug residence time, and improve drug transport from the GI tract into the body. Some of the peptides and proteins that were successfully incorporated into the OraLease® system include calcitonin, erythropoietin, desmopressin, vasopressin, and insulin. According to data from Phase I clinical trial, the OraLease® formulation of desmopressin was safe, well tolerated, and physiologically effective with a dose-dependent manner (DiBiase and Morrel, 1997). In another study, a tablet system composed of compressed zein microspheres encapsulating ivermectin was clinically evaluated in dogs receiving treatment for demodicidosis, an inflammatory skin disease caused by parasitic mites. The pharmacokinetic profiles of the zein microsphere tablets produced an improved bioavailability with a delayed T_{max} (the time it takes a drug to reach the maximum concentration) and increased AUC (area under the plasma drug concentration-time curve) when compared to a commercially available formulation. Dogs receiving this treatment for 6 to 22 weeks displayed a considerable improvement in clinical signs

and a significant decrease in the number of mites on their skin, with no side effects. These results indicated that this delivery system had a high level of safety, with minimal toxicity, and led to long-term efficacy (Gong *et al*., 2011). In another work, TPGS 1000 (a non-ionic surfactant composed of d-α-tocopherol and PEG 1000 succinate)-emulsified zein nanoparticles were shown to enhance the cellular uptake and transport of daidzin, an isoflavone glycoside, in Caco-2 human epithelial cells, and improved oral bioavailability in mice (Zou and Gu, 2013).

In addition to oral delivery, zein nanocarriers have also been investigated as intravenously administered drug carriers in cancer research. For example, zein nanoparticles encapsulating 5-FU have been developed for intravenous delivery to the liver. These nanoparticles exhibited a sustained release profile *in vitro*. *In vivo,* following intravenous injection in mice, the nanoparticles predominantly accumulated in the liver and remained in the circulation for at least 24 h (Lai and Guo, 2011). In another study, Thapa *et al*. revealed that zein nanoparticles successfully delivered a combination of histone deacetylase and proteasomal inhibitor for synergistic anticancer effect in metastatic prostate cancers both *in vitro* and *in vivo* (Thapa *et al*., 2017). Recently, folate-functionalised PEGylated zein nanoparticles have been developed for active targeted delivery of paclitaxel. This nanoparticle system was able to deliver paclitaxel specifically to cancer cells via folate receptor-mediated endocytosis. *In vivo* investigation revealed the prolonged systemic circulation of these nanoparticles and their enhanced anti-tumour efficacy in folate receptor-overexpressing KB tumour-bearing mice, with minimum toxicity in healthy organs (Soe *et al*., 2019). These findings demonstrate that zein-based nanoparticles could be potentially used as delivery systems for cancer therapy.

1.4. Protein corona

The vast majority of chemotherapy is designed for parenteral administration. As a result, the blood is often the first physiological environment that nanomaterials encounter. The blood contains a complex mixture of thousand different proteins (Monopoli *et al*., 2011). Each of these proteins can potentially adsorb to the surface of nanomaterials, forming the so-called "protein corona". It is increasingly accepted that the protein corona provides the nanomaterial a new biological identity which could be substantially different from its original synthetic identity (i.e. size, shape, surface charge, and surface chemistry). These changes, in turn, play an important role in determining the biological fate of the nanomaterial in the body, including cellular uptake, biodistribution, *in vivo* clearance, and toxicity (**Figure 1-5**) (Walkey and Chan, 2012; Nguyen and Lee, 2017; Partikel *et al*., 2019). Therefore, understanding the biological identity of a nanomaterial and how it determines the physiological responses becomes crucial for the development of safe, long-circulating, and effective nanomedicines.

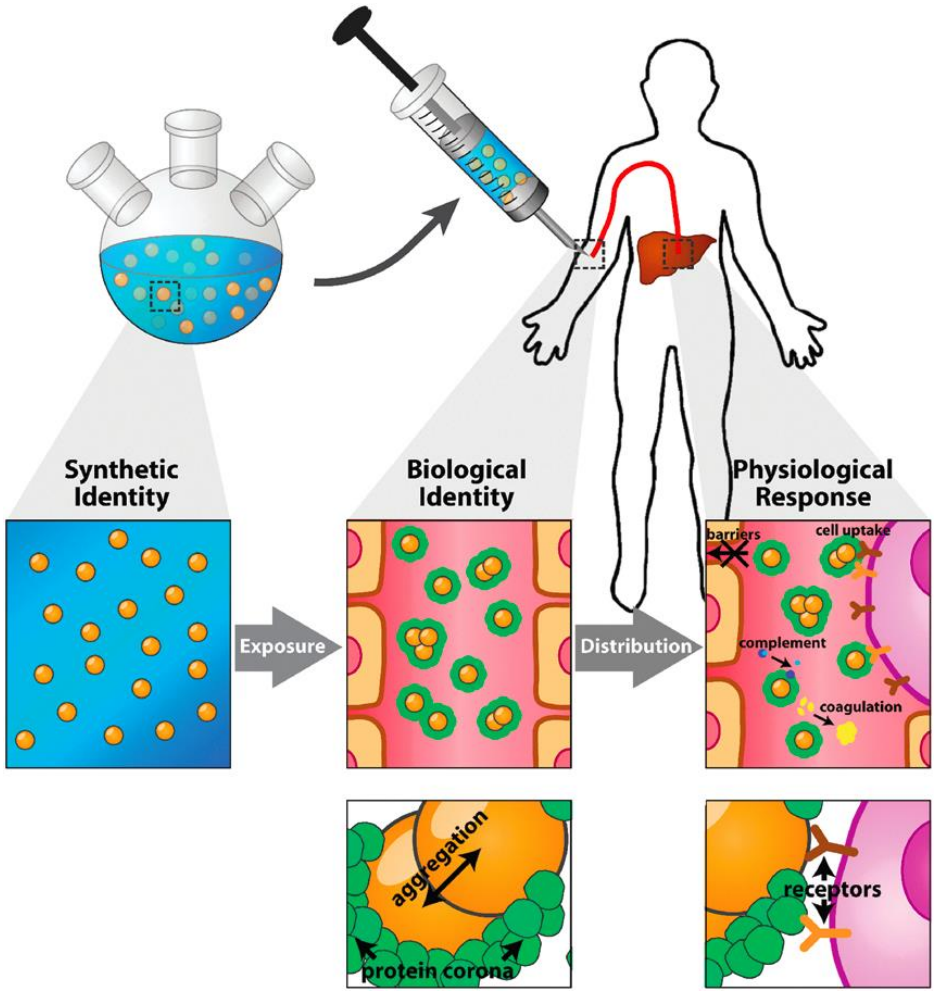

Figure 1-5. Relationship between the synthetic identity, biological identity, and physiological response. The synthetic identity corresponds to the size, shape, and surface chemistry of a nanomaterial post-synthesis. The biological identity is the size and aggregation state of the nanomaterial in a physiological environment, along with the structure and composition of the protein corona. The physiological response is the subsequent interaction of nanomaterials with biomolecules, biological barriers, and cells in the body (Adapted from Walkey and Chan, 2012).

1.4.1 Formation of protein corona

The formation of the protein corona is a dynamic, competitive, and time-dependent process (Partikel *et al.*, 2019). It can occur within a few seconds of nanomaterial exposure to a biological environment. According to the Vroman effect, the initial corona consists of highly abundant low affinity proteins (i.e. albumin, immunoglobulin G, and fibrinogen) that bind to the particle surface. However, these proteins can be replaced by higher affinity and lower abundance proteins (i.e. apolipoproteins and complement factors) over time (Vroman, 1962) (**Figure 1-6**).

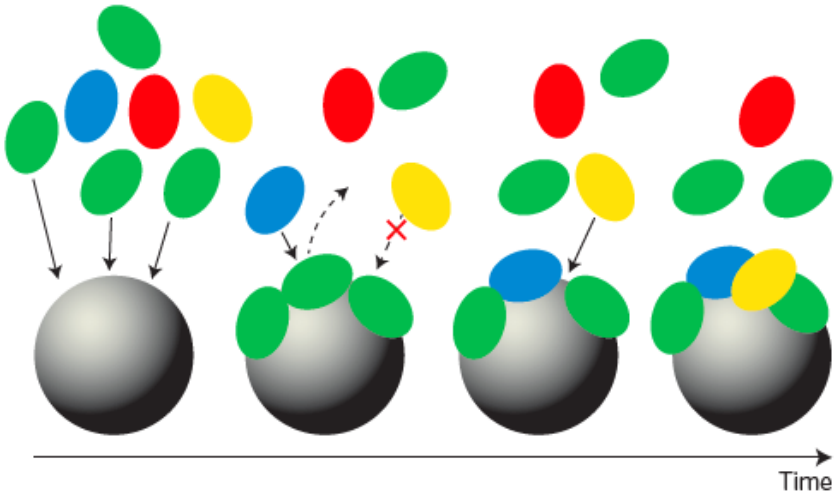

Figure 1-6. Formation of the biomolecular corona. From left to right: The biomolecules (typically highly abundant proteins) (in green) that arrive first to the surface of nanoparticles form an initial corona. Some of the initially adsorbed molecules with low affinity (in green) are subsequently displaced by molecules with a higher affinity that arrive later (in blue). Then, molecules that have a low affinity for the bare surface of nanoparticles (in yellow) can adsorb on the surface, owing to favourable interactions with the adsorbed (green and blue) biomolecules. Other biomolecules (in red) do not adsorb at all. (Adapted from Monopoli *et al.*, 2012).

The innermost layer of proteins that interact directly with the nanomaterial surface with high affinity is termed as the “hard corona”. In contrast, proteins that are loosely bound to the nanomaterial surface with low affinity constitute the “soft corona” (Walkey and Chan, 2012; Nguyen and Lee, 2017). The soft corona is thought to interact with the hard corona via weak protein-protein interactions (Walkey and Chan, 2012; Nguyen and Lee, 2017). It can undergo rapid exchange of biomolecules in short time scales (within seconds or minutes). The hard corona is more stable due to its strong association with the nanomaterials. Thus, the long-lasting hard corona plays a significant role in determining nanoparticle-cell interactions. Nevertheless, it can be exchangeable over time (in the order of several hours), but to a lesser extent after translocation of the nanomaterial to a new biological compartment (Walkey and Chan, 2012; Ahsan *et al*., 2018).

1.4.2 Impact of the protein corona on the systemic circulation time of nanoparticles

The protein corona is very complex and unique to each delivery system. The composition and quantity of the bound proteins may not correlate with their relative abundances in exposure medium (Walkey and Chan, 2012). Instead, they highly depend on both the physicochemical properties of the delivery system (i.e. size, shape, surface charge, particle base material, hydrophobicity) and the nature of the exposing environment (i.e. blood, interstitial fluid, cellular cytoplasm) (**Table 1-1**) (Aggarwal *et al*., 2009; Walkey and Chan, 2012; Nguyen and Lee, 2017; Partikel *et al*., 2019).

Table 1-1. The role of the physicochemical and environmental parameters of the nanoparticles on the protein corona.

Parameter	Observation/effect
Nanoparticles	
Surface charge	Higher opsonisation rate of charged particles than neutral particles
Hydrophobicity	Increase of the thickness of the protein corona and opsonisation rate
Starting material	Changes in the identity of adsorbed proteins
Size/morphology/shape/surface curvature	Influence on the amount, but not the identity, of bound proteins
Biological environment	
Higher protein concentration	Increase of protein corona thickness
Nature	Influence on the exchange rate and composition of the corona

(Adapted from Aggarwal *et al*., 2009; Walkey and Chan, 2012; Rahman *et al*., 2013).

In order to achieve therapeutic efficacy, nanocarriers must be present in the bloodstream long enough to reach their site of action. However, the adsorption of some blood proteins, called opsonins, on the particle surface (a process known as opsonisation) leads to the recognition and rapid elimination of nanocarriers from the systemic circulation by cells of the mononuclear phagocyte system (MPS), also known as the RES (Owens and Peppas, 2006; Walkey *et al*., 2012). The MPS consists of immune cells in the bloodstream (such as dendritic cells and monocytes) and tissue-resident macrophages in the MPS organs (i.e. liver, spleen, and lymph nodes). After opsonisation, phagocytosis can occur, which is the engulfment and eventual ingestion or removal of foreign materials from the bloodstream (Walkey *et al*., 2012). Without

the presence of adsorbed opsonin proteins, the phagocytes cannot directly recognise the particles. The most common opsonins are immunoglobulins, complement proteins, and fibrinogen (Gossmann *et al*., 2015). On the other hand, the binding of proteins such as albumin or apolipoproteins has shown to protect the nanoparticles from phagocytosis, resulting in their prolonged circulation time. These proteins are called dysopsonins (Gossmann *et al*., 2015; Nguyen and Lee, 2017). Therefore, nanoparticles should be further designed to prevent the adhesion of opsonins and assist the binding of dysopsonins in order to delay clearance by the MPS, thereby extending nanoparticle half-life for improved *in vivo* efficacy.

1.5 PEGylation and its significance

PEG, which refers to an oligomer or polymer of ethylene oxide in linear or branched structures, is the most widely used polymer in the field of advanced drug delivery due to its low toxicity and non-immunogenicity (Alexis *et al*., 2008). The modification of the surface of nanocarriers with PEG, or PEGylation, is the most common approach used for increasing the circulation time of the carriers by avoiding their clearance by the MPS (Davis and Illum 1994; Mishra *et al*., 2016; Suk *et al*., 2016).

Due to their hydrophilic characteristics, PEG chains can generate a hydrated PEG layer with a large extended volume around the surface of the nanoparticles. This protective hydrophilic layer provides steric stabilisation and confer “stealth” properties. When proteins approach the surface, the flexible PEG chains become compressed, which in turn creates a thermodynamically unfavourable situation for protein adsorption (Gref *et al*., 2000; Owens and Peppas, 2006; Behzadi *et al*., 2017). These stealth characteristics, therefore, reduce opsonisation by preventing or minimising protein

adsorption to their surface and subsequent phagocytosis, thus extending the circulation half-life of the nanoparticles from a few minutes to several hours (Gref *et al*., 2000; Alexis *et al*., 2008; Behzadi *et al*., 2017).

Having a prolonged circulation time of the nanoparticles is necessary to allow for a sufficient concentration of drug carriers to take advantage of the EPR effect and extravasate from the blood vessels at the tumour into the tumour tissue. The EPR effect enables drug accumulation in the tumour, which results in an improved anti-tumour response. For these reasons, PEGylation has been utilised for passive targeting of cancer chemotherapeutics (**Figure 1-7**) (Gabizon, 2001; Alexis *et al*., 2008; Romberg *et al*, 2008; Torchilin, 2011; Mishra *et al*., 2016; Suk *et al*., 2016).

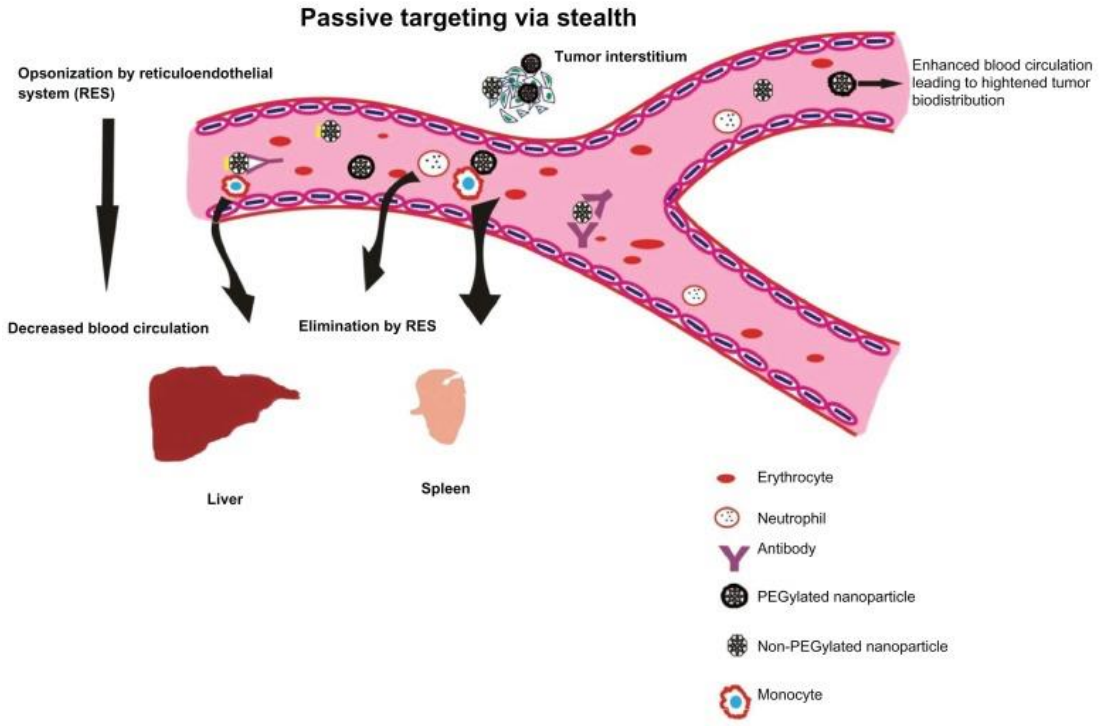

Figure 1-7. Passive targeting of nanoparticles to tumour cells with stealth characteristics. PEGylated nanoparticles are capable of evading the reticuloendothelial system (RES), thus delaying their elimination by the liver and spleen. In contrast, non-PEGylated nanoparticles are easily recognised by the immune cells, resulting in rapid clearance from blood circulation. (Adapted from Ranganathan *et al*., 2012).

One of the most successful examples of the use of PEGylation for passive targeting in cancer drug delivery is the development of Doxil®, a PEGylated liposome formulation encapsulating doxorubicin (Gabizon, 2001; Wicki *et al*., 2015). It was the first FDA-approved nanomedicine for the treatment of AIDS-related Kaposi's sarcoma, ovarian cancer, and breast cancer (Barenholz, 2012). Doxil® showed a superior efficacy in cancer therapy and lower toxicity as compared to the free drug (O'Brien *et al*., 2004; Barenholz, 2012; Mishra *et al*., 2016). The conjugation of PEG on the surface of liposomes leads to RES avoidance, thus delaying their elimination by the liver and

spleen. The PEG hydrophilic steric barrier stabilises the liposomes, preventing its opsonisation and subsequent interactions of the liposomes with macrophages (Torchilin and Trubetskoy, 1995). As a result, the circulation half-life of the liposomes was prolonged when administered parenterally, leading to higher drug accumulation at the tumour site.

1.6 Mechanisms of cellular uptake of nanoparticles

In order to exert therapeutic effects, the nanocarriers must first cross the cell membrane to deliver specific molecules (i.e. drugs, genes, proteins, or peptides) to sub-cellular targets (Chou *et al*., 2011). While small hydrophobic molecules can diffuse across phospholipid bilayers of cell membrane by passive diffusion, nanoparticles enter the cell mainly through endocytosis, an energy-dependent process (Blanco *et al.*, 2015; Behzadi *et al*., 2017; Foroozandeh and Aziz, 2018). In this process, the cell engulfs extracellular substances by invagination of the cell membrane, followed by budding off inside the cell to form membrane-bound vesicles, called endosomes (or phagosomes in case of phagocytosis). These vesicles are then transported to other intracellular compartments (Sahay *et al*., 2010; Foroozandeh and Aziz, 2018).

Endocytosis can be broadly classified into two major categories: phagocytosis (or "cell eating") and pinocytosis (or "cell drinking") (Foroozandeh and Aziz, 2018). Phagocytosis is the process by which phagocytic cells (such as macrophages, monocytes, neutrophils, and dendritic cells) engulf large particles (larger than 250 nm up to 20 μm in size), such as cell debris, bacteria, or large particulates (Sahay *et al*., 2010; Sun *et al*., 2014; Foroozandeh and Aziz, 2018). Unlike phagocytosis which takes place mainly in specialised professional phagocytes, pinocytosis can occur in most of

the cells. Pinocytosis is the process that governs the uptake of small particles including fluids, solutes, and nanoparticles. It can be sub-categorised into 1) clathrin-mediated endocytosis, 2) caveolae-mediated endocytosis, 3) clathrin- and caveolae-independent endocytosis, and 4) micropinocytosis, depending mainly on endocytic proteins involved in the process and size of the detached vesicles (**Figure 1-8**) (Nam *et al*., 2009; Sahay *et al*., 2010; Behzadi *et al*., 2017; Foroozandeh and Aziz, 2018).

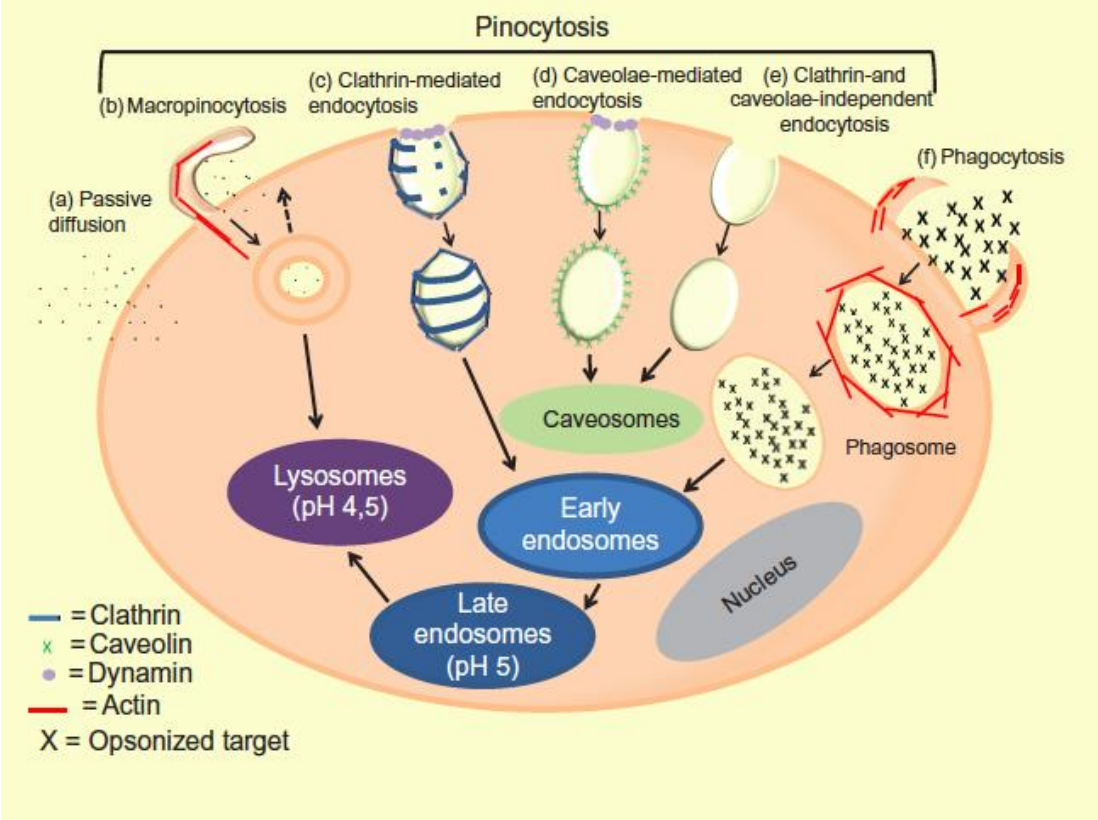

Figure 1-8. Summary of cellular uptake pathways of nanoparticles (Adapted from Panariti *et al*., 2012).

Clathrin-mediated endocytosis, also known as receptor-mediated endocytosis, is the main uptake mechanism for nanoparticles. This pathway is initiated by specific ligand-

receptor binding at regions enriched in clathrin proteins of the cell membrane. This ligand-receptor complex is then engulfed through the formation of clathrin-coated vesicles (endosomes). The endosomes will later fuse with the acidic lysosomes, resulting in sequestration followed by degradation of the cargo therapeutics by the lysosomal enzymes (Sun *et al*., 2014; Foroozandeh and Aziz, 2018).

Caveolae-mediated endocytosis is another route of cellular entry which involves flask-shaped membrane invaginations known as caveolae (or "little caves"). Caveolae are typically 50-80 nm in size and are composed of caveolin-1, a dimeric protein that confer them their flask-shaped structure. Once caveolae are detached from plasma membrane, they fuse with a cell compartment (caveosome) of neutral pH, thus bypassing lysosomes. Since caveolae-dependent mechanism is able to protect the cargo from hydrolytic enzymes and lysosomal degradation, this pathway is employed in nanomedicine for the delivery of labile materials such as nucleic acids and proteins (Behzadi *et al*., 2017; Foroozandeh and Aziz, 2018).

Clathrin- and caveolae-independent endocytosis takes place in cells without the need of clathrin and caveolin. This pathway involves cholesterol-rich micro-domains called "rafts". Few nanomaterials use this route to enter the cells. Among them, folate-modified nanoparticles have been shown to be taken up by the cells using this pathway (Sahay *et al*., 2010; Panariti *et al*., 2012; Behzadi *et al*., 2017).

Macropinocytosis is also a type of pinocytosis that takes up a large amount of extracellular fluid without the involvement of lipid rafts or pit-forming proteins. Instead, it involves the formation of macropinosomes, which are large endocytic vesicles (0.2-5 μm), as a result of actin-driven plasma membrane extensions. This

process seems to be a non-specific process for internalisation of large particles which are not possible to be taken up by other pathways (Behzadi *et al*., 2017; Foroozandeh and Aziz, 2018).

It is important to highlight that the cellular entry of nanoparticle-based therapeutics depends on many factors, including both nanoparticle characteristics (i.e. size, shape, surface charge, surface functionalisation, and composition) and cell types (Chou *et al*., 2011; Behzadi *et al*., 2017; Foroozandeh and Aziz, 2018). As mentioned earlier, the endocytosis of nanomedicine may traffic cargos to a non-target organelle. For example, the nanoparticles entrapped in intracellular vesicles (endosomes, phagosomes, macropinosomes) can fuse with lysosomes that can degrade their contents due to their highly acidic environment and lysosomal enzymes (Sriraman *et al.*, 2014; Blanco *et al.*, 2015). Therefore, understanding the uptake mechanisms of nanoparticles is important for the design of future drug delivery systems, as this will have a direct effect on their intracellular fate and on the subsequent molecular response of the cells (Chou *et al*., 2011).

1.7 Aim and objectives

Zein is biocompatible, biodegradable and confers properties that make it an attractive material as a delivery system for human use. However, its protein nature and hydrophobicity may cause immunogenicity, which could limit its use for drug delivery. To overcome this limitation, we hypothesised that conjugating zein with PEG would provide steric shielding of the delivery system, thus preventing opsonisation and providing sustained release for effective cellular uptake into cancer cells. The aim of this thesis was to develop PEGylated zein and evaluate the feasibility of using it for cancer drug delivery. To achieve this aim, the objectives of the work were:

1. to synthesise and characterise PEGylated zein micelles encapsulating a hydrophobic drug model
2. to evaluate their cellular uptake and uptake mechanisms on cancer cells *in vitro*
3. to investigate the formation of the protein corona on PEGylated zein micelles and its interaction with cells
4. to assess the potential of using microfluidics in the manufacture of zein nanoparticles

CHAPTER 2

PEGylated zein micelles for cancer therapy

2.1 Introduction

In this work, zein, a protein-based biopolymer, was used as a natural polymer for fabricating nanosized particles for drug delivery. However, because of their hydrophobicity and protein nature, zein particles can be rapidly taken up by immune cells and may cause immunogenicity, which could limit their use as drug delivery vehicles (Hurtado-Lopez and Murdan, 2006). To overcome this issue, the modification of zein by conjugation with PEG has been proposed to create a steric shielding of the delivery system, thus reducing opsonisation and providing a sustained release of the carried drug.

2.2 Aim and Objectives

The aim of the work in this chapter was to conjugate zein with PEG in order to create a steric shielding of the delivery system to prevent its opsonisation and prolong its circulation half-life. As PEG density and chain length are crucial determinants of shielding efficacy, the modification of zein with PEG of different lengths and densities requires investigation to determine optimal combination of these two materials that provides stealth efficacy for the delivery system. To achieve this aim, the objectives were:

1. to modify zein by conjugating with PEG of varying density and chain length
2. to formulate and characterise mPEG-zein micelles entrapping Nile red as the hydrophobic drug model
3. to assess the impact of PEG density and chain length on their uptake efficiency in melanoma cancer cells *in vitro*

2.3 Materials

Material	**Supplier**
Bioware® B16-F10-luc-G5 mouse melanoma cells	Caliper Life Sciences, USA
Chlorpromazine	Sigma-Aldrich, UK
Citric acid monohydrate	Sigma-Aldrich, UK
Colchicine	Sigma-Aldrich, UK
Deuterium oxide (D_2O)	Sigma-Aldrich, UK
Deuterated dimethyl sulfoxide (DMSO-d_6)	Sigma-Aldrich, UK
Dimethyl sulfoxide (DMSO)	Sigma-Aldrich, UK
Dulbecco's Modified Eagle Medium (DMEM)	Life Technologies, UK
Ethanol	Sigma-Aldrich, UK
Filipin complex from *Streptomyces filipinensis*	Life Technologies, UK
Foetal bovine serum (FBS)	Life Technologies, UK
Formalin solution, neutral buffered, 10%	Sigma-Aldrich, UK
Glucose	Sigma-Aldrich, UK
Glycine	Sigma-Aldrich, UK
Human glioblastoma (T98G)	European and American Collection of Cell Cultures (ECACC), UK
L-Glutamine	Life Technologies, UK
Methanol	Sigma-Aldrich, UK
Methoxy PEG succinimidyl carboxymethyl (SCM) ester, MW 5 kDa (M-SCM-5000)	JenKem Technology, USA

Methoxy PEG succinimidyl carboxymethyl (SCM) ester, MW 10 kDa (M-SCM-10K)	JenKem Technology, USA
Nile red	Sigma-Aldrich, UK
Penicillin-Streptomycin	Life Technologies, UK
Phosphate buffered saline (PBS) tablets	Sigma-Aldrich, UK
Roswell Park Memorial Institute (RPMI) 1640 medium	Life Technologies, UK
Sodium hydroxide (NaOH)	Sigma-Aldrich, UK
Trisodium citrate dihydrate	Sigma-Aldrich, UK
Triton X-100	Sigma-Aldrich, UK
TrypLE® Express	Life Technologies, UK
Vectashield® mounting medium containing 4',6-diamidino-2-phenylindole (DAPI)	Vector Laboratories, UK
Yellow zein	Sigma-Aldrich, UK
3-(4,5-dimethylthiazol-2-yl)-2,5-diphenyl-tetrazolium bromide (MTT)	Sigma-Aldrich, UK

2.4 Methods

2.4.1 PEGylation of zein

The synthesis of PEGylated zein was adapted from a method described by Podaralla and colleagues (Podaralla *et al*., 2012). In this study, mPEG-succinimidyl carboxymethyl (mPEG-SCM) was used to conjugate with yellow zein (a mixture of α, β, γ, and δ-zein, containing 8-9% of xanthophyll pigments, including lutein, zeaxanthin, and β-cryptoxanthin). The molecular weight (MW) of mPEG-SCM (5 and 10 kDa) and PEG to zein ratio were also varied, as summarised in **Table 2-1**.

Table 2-1. Composition of the three mPEG-zein synthesised in the study.

	Composition	**Weight ratio**	**Molar ratio**
mPEG5K-zein (0.5:1)	mPEG5K:zein	0.5:1	2.3:1
mPEG5K-zein (1:1)	mPEG5K:zein	1:1	4.6:1
mPEG10K-zein	mPEG10K:zein	1:1	2.3:1

mPEG-zein was prepared in a single step reaction. Briefly, yellow zein (0.1 g) was dissolved in 4 mL of ethanol (90% v/v). Various amounts of mPEG-SCM (0.05 g of mPEG-SCM (5 kDa) for mPEG5K-zein (0.5:1); 0.1 g of mPEG-SCM (5 kDa) for mPEG5K-zein (1:1); 0.1 g of mPEG-SCM (10 kDa) for mPEG10K-zein) were dissolved in 1 mL of ethanol (90% v/v). PEG solution was added to zein solution and the mixture was stirred for 3 h under magnetic stirring (100 rpm) at 25°C. One mL of glycine solution (1 M) (1.50 g of glycine in 20 mL of distilled water) was then added to stop the reaction and quench the excess PEG ester. The mixture was then diluted

with 5 mL citrate buffer (pH 7.4) to precipitate the PEGylated zein and dialysed (using dialysis tubing with a MW cut-off of 12-14 kDa) against distilled water (2.5 L) under stirring (120 rpm) at 25°C for 48 h to remove the free PEG and ethanol. The distilled water was changed 3 times during the dialysis process. The resulting product was then freeze-dried using a Christ Epsilon 2-4 LSC® freeze dryer (Osterode am Harz, Germany). The obtained mPEG-zein conjugates were stored at -20°C for long-term storage.

Citrate buffer (pH 7.4) was prepared using the following protocol. Firstly, a citric acid solution (0.1 M) was prepared by dissolving citric acid monohydrate (0.42 g) in distilled water (20 mL). Secondly, a trisodium citrate solution (0.1 M) was prepared by dissolving trisodium citrate dihydrate (2.94 g) in distilled water (100 mL). Then, 0.8 mL citric acid solution (0.1 M) was added to 9.2 mL trisodium citrate solution (0.1 M). Distilled water was added to adjust the volume up to 100 mL. The mixture was gently mixed under stirring at 25°C for 5 min. The pH of the citrate buffer was adjusted to pH 7.4 using NaOH solution (1 M).

2.4.2 Attenuated Total Reflection - Fourier Transform Infrared spectroscopy (ATR-FTIR) analysis

To confirm the PEGylation of zein, samples were directly analysed by ATR-FTIR without the need for any further sample preparation. The ATR-FTIR spectra of zein, mPEG, mPEG-zein conjugates, and physical mixtures of mPEG with zein were taken with a Bruker Tensor II-FTIR® spectrophotometer (Billerica, MA), using 100 scans with 2 cm^{-1} resolution. Data was collected within a range of 400-4000 cm^{-1} at 20°C.

2.4.3 Proton Nuclear Magnetic Resonance (^{1}H NMR) analysis

^{1}H NMR analysis was used to characterise the core-shell structure of mPEG-zein micelles. The samples (zein, mPEG, and mPEG-zein) were prepared in deuterium oxide (D_2O) and deuterated dimethyl sulfoxide (DMSO-d_6) at a concentration of 5 mg/mL. ^{1}H NMR spectra were recorded at 500 MHz using a Bruker Avance® III HD500 NMR spectrometer (Billerica, MA). The core-shell structure of mPEG-zein micelles was confirmed by comparing the ^{1}H NMR spectra in DMSO-d_6 and in D_2O.

2.4.4 Determination of Critical Micelle Concentration (CMC)

The ability of mPEG-zein to self-assemble into micelles was evaluated by steady-state fluorescence technique using Nile red as a hydrophobic fluorescent probe. Briefly, 32 µL Nile red stock solution (1 mg/mL in methanol) was added to 5-mL plastic vials. Following the complete evaporation of methanol after 5-6 h, 1 mL of mPEG5K-zein (0.5:1), mPEG5K-zein (1:1), and mPEG10K-zein (at concentrations ranging from 0.001 to 1 mg/mL in glucose solution (5% w/v)) was added to the vials, making the final concentration of Nile red in each vial 100 µM. Each sample was vortexed and incubated overnight at 25°C, protected from light, before measurement. Fluorescence intensity was measured with a Varian Cary Eclipse® spectrofluorometer (Palo Alto, CA) (λ_{exc}: 550 nm; λ_{em}: 570-800 nm; excitation and emission slits at 5 nm and 20 nm, respectively). The ratio of Nile red emission intensity at the wavelength of maximum emission (λ_{max}) in the presence of mPEG-zein (I) over the fluorescence in its absence (I_0, in glucose solution (5% w/v)) was plotted as a function of mPEG-zein concentration. The CMC value was obtained from the intersection of the tangents to

the two linear portions of the graph of the fluorescence intensity as a function of mPEG-zein concentration.

2.4.5 Preparation of Nile red-loaded mPEG-zein micelles

Nile red (0.25 mg) and mPEG-zein (50 mg) were dissolved in 10 mL of ethanol (90% v/v). The mixture was stirred (100 rpm) at 37°C overnight to allow partitioning of the Nile red into mPEG-zein micelles. Free Nile red and ethanol were removed by dialysis (MW cut-off: 12-14 kDa) against distilled water (2.5 L) under continuous stirring (120 rpm) at 25°C for 48 h. The distilled water was changed 3 times during the dialysis process. The resulting products were then freeze-dried using a Christ Epsilon 2-4 LSC® freeze dryer (Osterode am Harz, Germany) and stored at -20°C until further use.

2.4.6 Transmission electron microscopy (TEM)

The morphology of mPEG-zein micelles (0.4 mg/mL in distilled water) was observed by TEM using a JEOL JEM-1200EX® transmission electron microscope (Jeol, Tokyo, Japan), operating at an accelerating voltage of 80 kV. Each sample (3 μL) was drop cast onto a carbon-coated copper grid (400 mesh size) and was air-dried overnight before imaging.

2.4.7 Size and zeta potential measurement

The size and zeta potential of empty and Nile red-loaded mPEG5K-zein (0.5:1), mPEG5K-zein (1:1), and mPEG10K-zein micelles were respectively measured by photon correlation spectroscopy and laser Doppler electrophoresis, using a Malvern Zetasizer Nano-ZS® at 37°C (Malvern Instruments Ltd, Malvern, UK). All samples

were freshly prepared and diluted to the concentration of 0.2 mg/mL in glucose solution (5% w/v). The samples were vortexed before being transferred to a cuvette for measurement.

2.4.8 Determination of Nile red encapsulation efficiency

Nile red-loaded mPEG-zein micelles (1 mg) were dispersed in 1 mL distilled water and centrifuged at 5000 g for 14 min at 25°C using an IEC Micromax® centrifuge (Thermo Scientific, Loughborough, UK). After centrifugation, the supernatant was discarded and the pellet was dissolved in 1 mL methanol. An aliquot was further diluted with methanol to the desired concentration range to determine the encapsulated Nile red. The amount of Nile red encapsulated in the micelles was quantified by spectrofluorometry (λ_{exc}: 550 nm, λ_{em}: 638 nm, slit widths: 5 nm), using a Varian Cary Eclipse® spectrofluorometer (Agilent Technologies, Santa Clara, CA). A standard calibration line was generated from Nile red solutions (10-100 ng/mL) in methanol. The amount of Nile red loaded in the micelles was calculated by correlating the fluorescence intensity with the standard calibration curve. The encapsulation efficiency (EE) was calculated as follows:

$$\text{EE (\%)} = \frac{\text{Amount of Nile red loaded in micelles} \times 100}{\text{Amount of Nile red used in the formulation}}$$

2.4.9 *In vitro* evaluation

2.4.9.1 Cell culture

B16-F10-luc-G5 mouse melanoma and T98G human glioblastoma cell lines were cultivated in either RPMI 1640 (for B16-F10-luc-G5 cells) or in DMEM (for T98G

cells) media supplemented with 10% v/v FBS, 1% v/v L-glutamine, and 0.5% v/v penicillin-streptomycin. Cultures were maintained at 37°C in a 5% CO_2 atmosphere.

2.4.9.2 *In vitro* cytotoxicity

The toxicity of mPEG-zein micelles was assessed using a standard 3-(4,5-dimethylthiazol-2-yl)-2,5-diphenyltetrazolium bromide (MTT) assay. B16-F10-luc-G5 and T98G cancer cells were seeded into 96-well plates at a density of 1.5 x 10^4 cells/well for 24 h. Next, the medium was removed and the cells were treated with fresh medium containing empty mPEG-zein micelles (concentration range 2-512 µg/mL (2-fold dilution)) for 72 h. Untreated cells were used as controls. Following treatment, 50 µL of MTT solution (5 mg/mL in PBS) was added into each well, and the cells were incubated with the solution for an additional 4 h. The MTT reagent was removed and the formazan crystals were dissolved in 200 µL DMSO. The absorbance was measured at 570 nm using a Multiskan Ascent® plate reader (Thermo Scientific, Waltham, MA). Cell viability was calculated as the percentage of relative change of absorbance compared with the control (untreated cells).

2.4.9.3 Cellular uptake

2.4.9.3.1 Qualitative analysis

The cellular uptake of Nile red-loaded mPEG-zein micelles was qualitatively investigated using confocal microscopy. B16-F10-luc-G5 cells were seeded on coverslips in 6-well plates (1 x 10^5 cells/well) and allowed to adhere overnight. On the following day, the medium was removed and replaced with a fresh medium containing free Nile red or equivalent amount of Nile red loaded in mPEG-zein micelles (844 ng

Nile red per well) at 37°C for 2 h. After 2 h incubation, the cells were then washed twice with 3 mL PBS before being fixed with 2 mL formaldehyde solution (4%) for 10 min. The imaging of the cellular uptake was conducted using a Leica SP5® confocal microscope (Wetzlar, Germany). Nile red was excited with the 543 nm laser line, detected at 615-660 nm. Cell nuclei were stained with Vectashield® mounting medium containing DAPI, which was excited with the 405 nm laser line and detected at 415-491 nm.

2.4.9.3.2 Quantitative analysis

B16-F10-luc-G5 and T98G cells were seeded into 6-well plates at a density of 2 x 10^5 cells/well and allowed to grow for 24 h. The cellular uptake was studied by incubating cells with Nile red encapsulated in mPEG-zein micelles or free in solution, as described for confocal microscopy. After a 2-h incubation, adherent cells were washed and detached (using 250 µL TrypLE® Express and 500 µL medium per well), followed by analysis on a FACSCanto® flow cytometer using FACSDiva® software (BD, Franklin Lakes, NJ). At least 10,000 cells were analysed for each sample.

2.4.9.3.3 Mechanisms of cellular uptake

To investigate the mechanisms responsible for the endocytosis-mediated cellular uptake, B16-F10-luc-G5 cells were seeded using the same protocol as detailed in 2.4.9.3.2. After 24 h, the medium was removed and the cells were pre-treated with the endocytosis inhibitors chlorpromazine (20 µg/mL), filipin (5 µg/mL), and colchicine (40 µg/mL) at 37°C for 30 min. Afterwards, the treatments were removed and replaced with co-incubation of Nile red-encapsulated mPEG-zein micelles (844 ng Nile red per

well) with the inhibitors (chlorpromazine (5 µg/mL), filipin (3 µg/mL), and colchicine (40 µg/mL)) for another 2 h. The cells were then processed for flow cytometry analysis as described above.

2.4.10 Statistical analysis

Results are represented as means ± standard error of the mean (SEM) unless stated otherwise. Statistical significance was assessed by one-way analysis of variance and Tukey multiple comparison post-test (Minitab® software, State College, PE). Differences were considered statistically significant for $P < 0.05$.

2.5 Results

2.5.1 ATR-FTIR analysis

mPEG-zein was synthesised by the formation of an amide bond between the terminal amino group of glutamine present in zein and mPEG-SCM (MW 5 and 10 kDa). The proposed chemical reaction is shown in **Figure 2-1**.

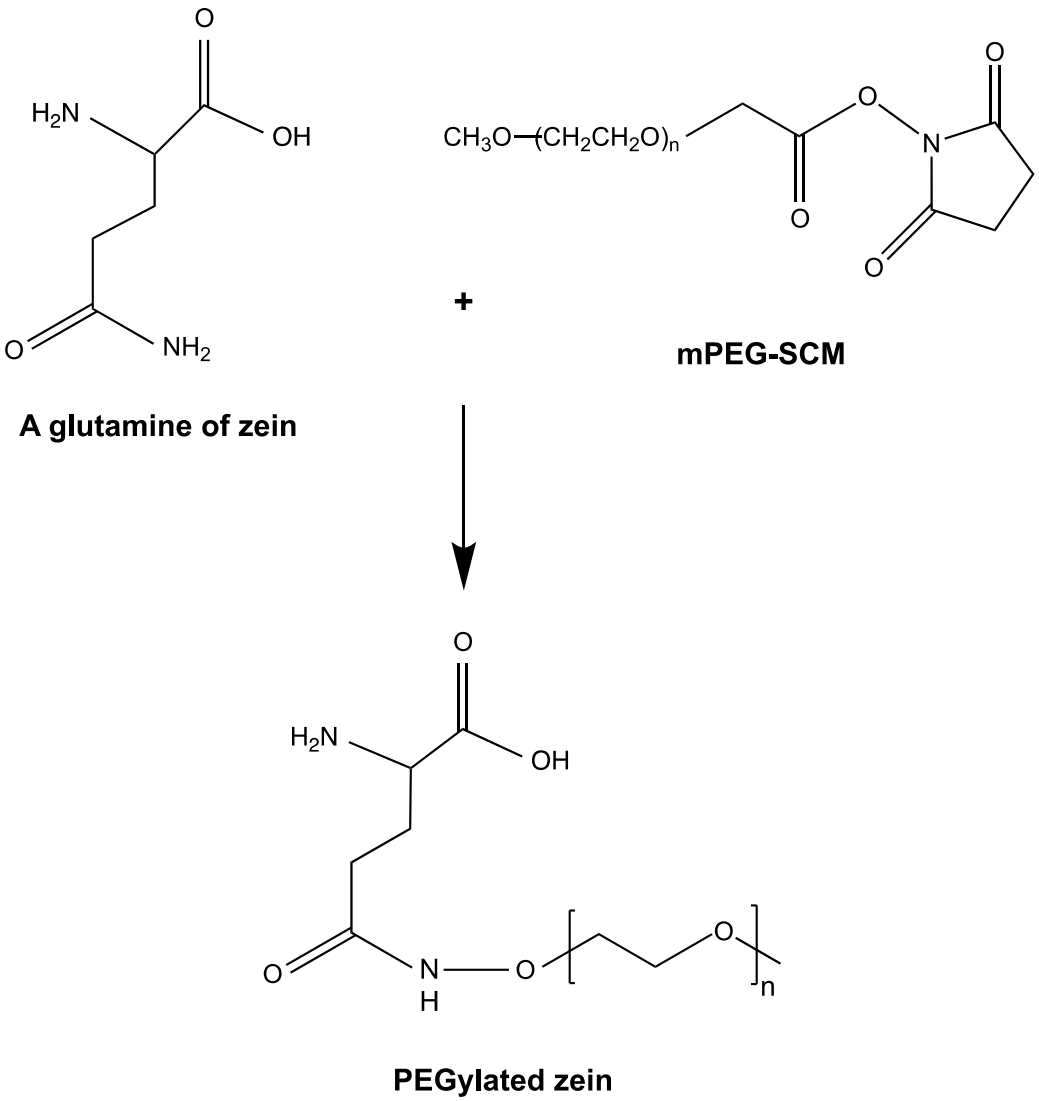

Figure 2-1. Schematic reaction of the PEGylation of zein.

The FTIR spectra of zein, mPEG, mPEG-zein conjugates, and physical mixtures of mPEG with zein confirmed that PEGylation was achieved (**Figure 2-2**). Amide I and II protein peaks of zein were observed at 1643 and 1516 cm^{-1}, respectively, on the FTIR spectrum of mPEG-zein. The stretching vibration of the C-C and C-O in CH_2CH_2O groups of PEG at 840-960 cm^{-1} and 1150 cm^{-1}, respectively, and the methylene group at 2742 cm^{-1} appeared in the spectra of three mPEG-zein conjugates. Furthermore, the N-hydroxysuccinimide (NHS) ester peak of PEG at 1741 cm^{-1} disappeared after conjugation with zein. These indicate that the PEGylation of zein was successful (Podaralla *et al.*, 2012; Song *et al.*, 2015).

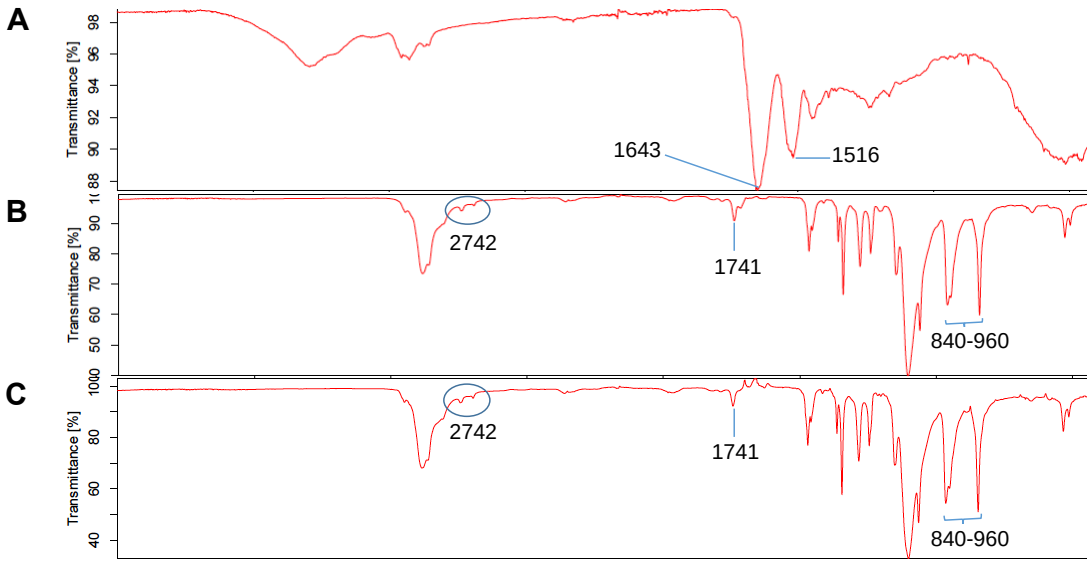

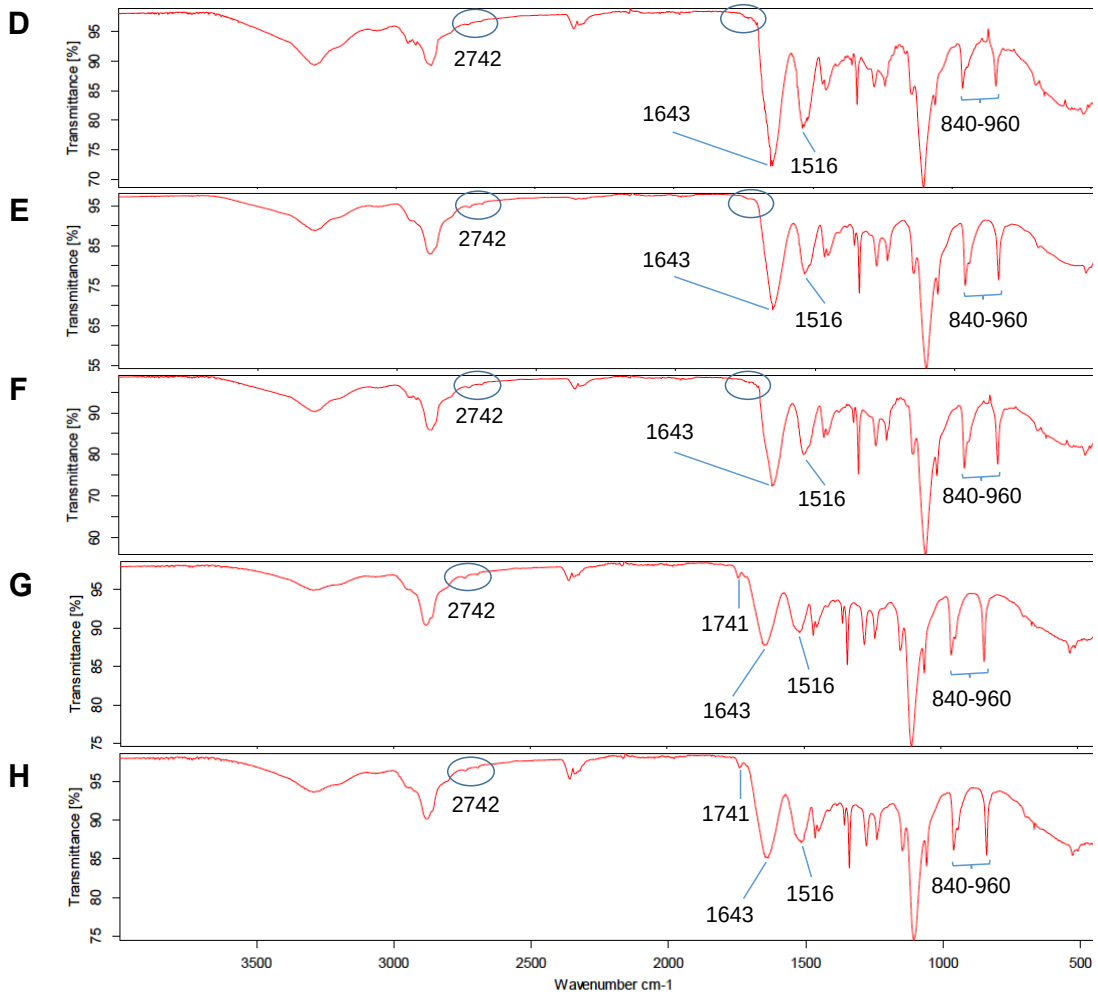

Figure 2-2. FTIR spectra of A) zein, B) mPEG5K, C) mPEG10K, D) mPEG5K-zein conjugate (0.5:1), E) mPEG5K-zein conjugate (1:1), F) mPEG10K-zein conjugate, G) physical mixture of mPEG5K with zein, and H) physical mixture of mPEG10K with zein.

2.5.2 ^{1}H NMR analysis

The core-shell structure of mPEG-zein micelles was confirmed by comparing the ^{1}H NMR spectra in DMSO-d_6 and D_2O (**Figure 2-3**). As the micelles were not formed in organic solvent, both the ethylene protons of PEG (3.5 ppm) and the amide protons of zein (3.3 ppm) could be observed in the spectra obtained in DMSO-d_6. On the contrary,

only the ethylene protons of PEG (3.6 ppm) were visible in the D_2O, while the zein peak disappeared. The changes in ^1H NMR spectra suggest that mPEG-zein could self-assemble into micelles in water, with hydrophilic mPEG in the outer shell and the hydrophobic zein in the core.

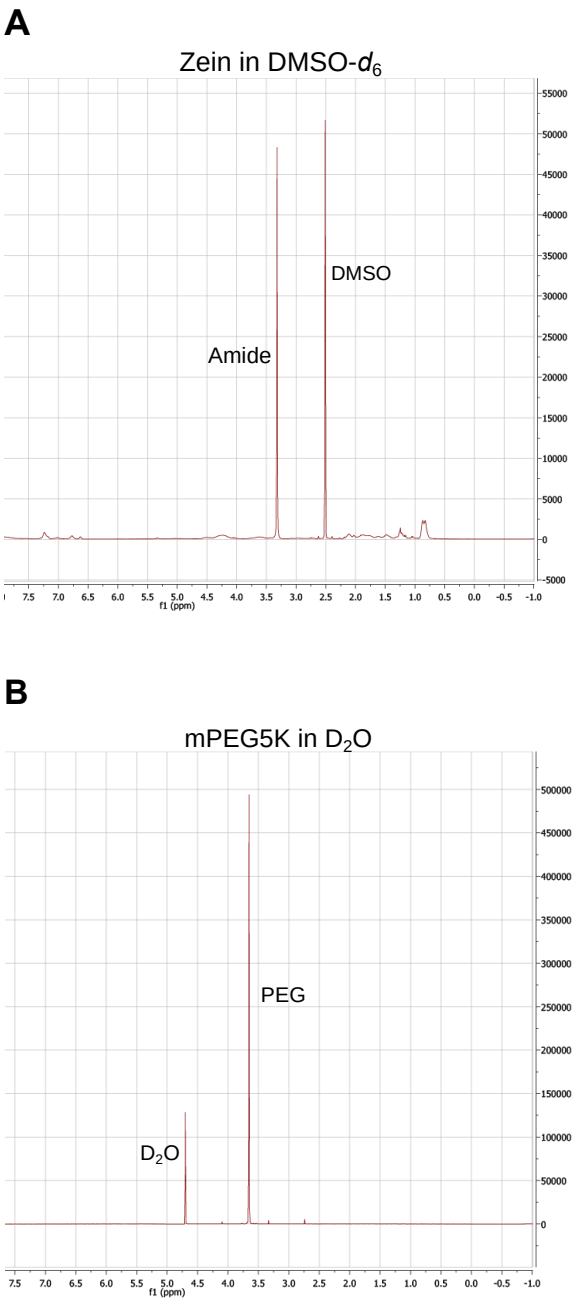

C

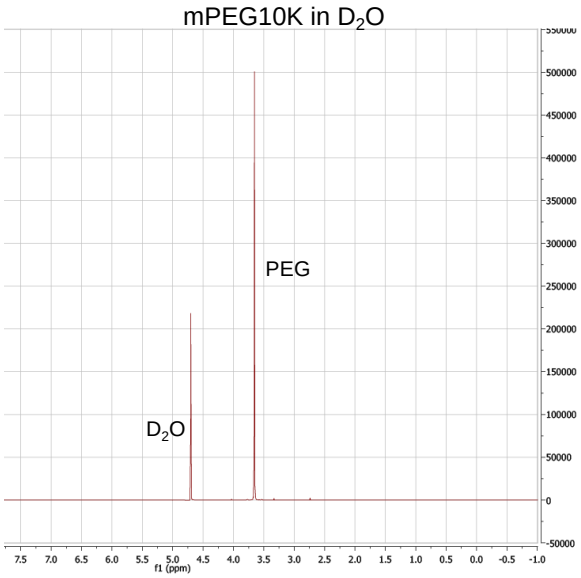
mPEG10K in D_2O
PEG
D_2O
f1 (ppm)

D

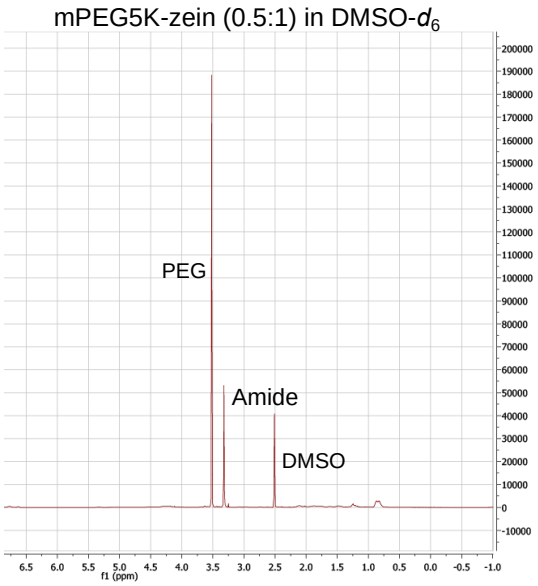
mPEG5K-zein (0.5:1) in DMSO-d_6
PEG
Amide
DMSO
f1 (ppm)

E

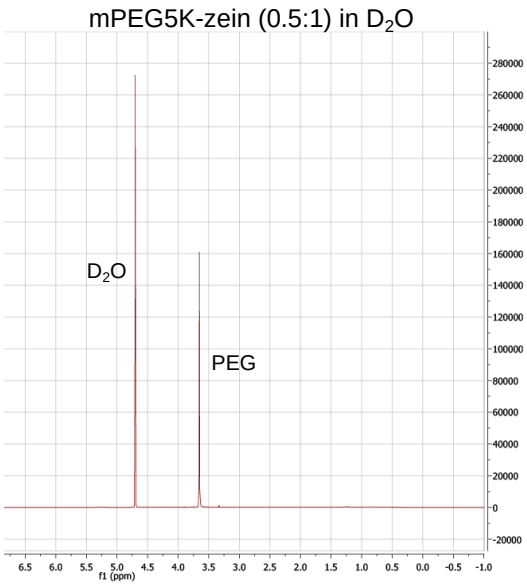
mPEG5K-zein (0.5:1) in D_2O
D_2O
PEG
f1 (ppm)

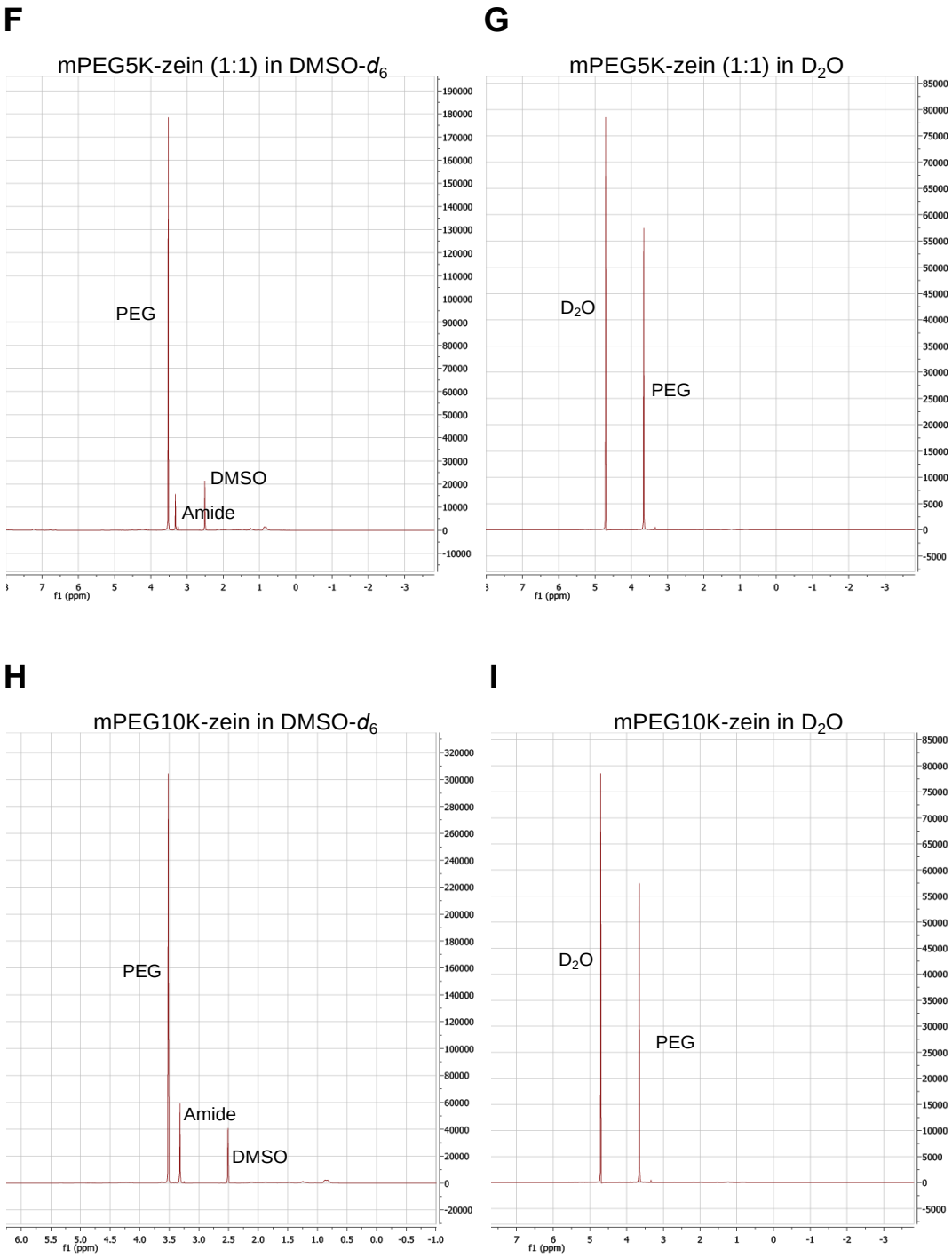

Figure 2-3. ^{1}H NMR spectra of A) zein in DMSO-d_6, B) mPEG5K in D_2O, C) mPEG10K in D_2O, D) mPEG5K-zein (0.5:1) in DMSO-d_6, E) mPEG5K-zein (0.5:1) in D_2O, F) mPEG5K-zein (1:1) in DMSO-d_6, G) mPEG5K-zein (1:1) in D_2O, H) mPEG10K-zein in DMSO-d_6, and I) mPEG10K-zein in D_2O.

2.5.3 Determination of the CMC

The CMC of mPEG-zein was determined using Nile red as a hydrophobic fluorescent probe. Nile red is weakly fluorescent in water. However, its fluorescence intensity increased with increasing mPEG-zein concentrations, as it is solubilised within the hydrophobic core of the micelles (Laskar *et al*., 2018). The CMC values of mPEG5K-zein (0.5:1), mPEG5K-zein (1:1), and mPEG10K-zein micelles were 82 ± 10, 90 ± 5, and 88 ± 3 µg/mL, respectively (**Figure 2-4**).

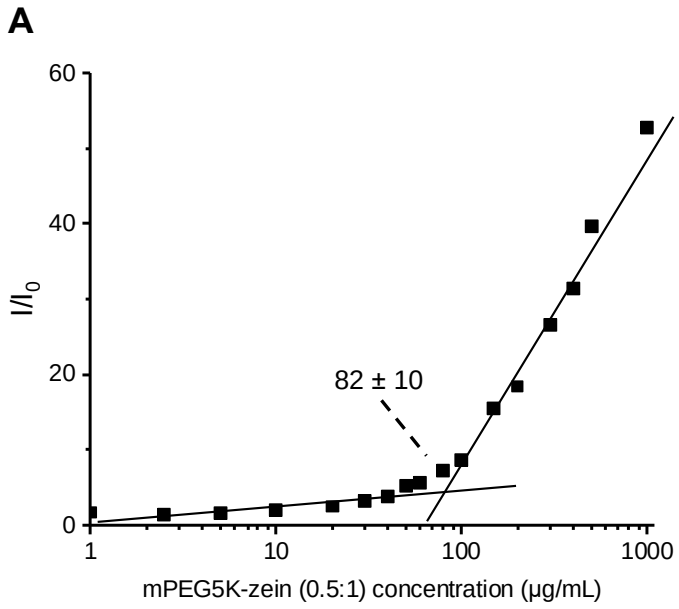

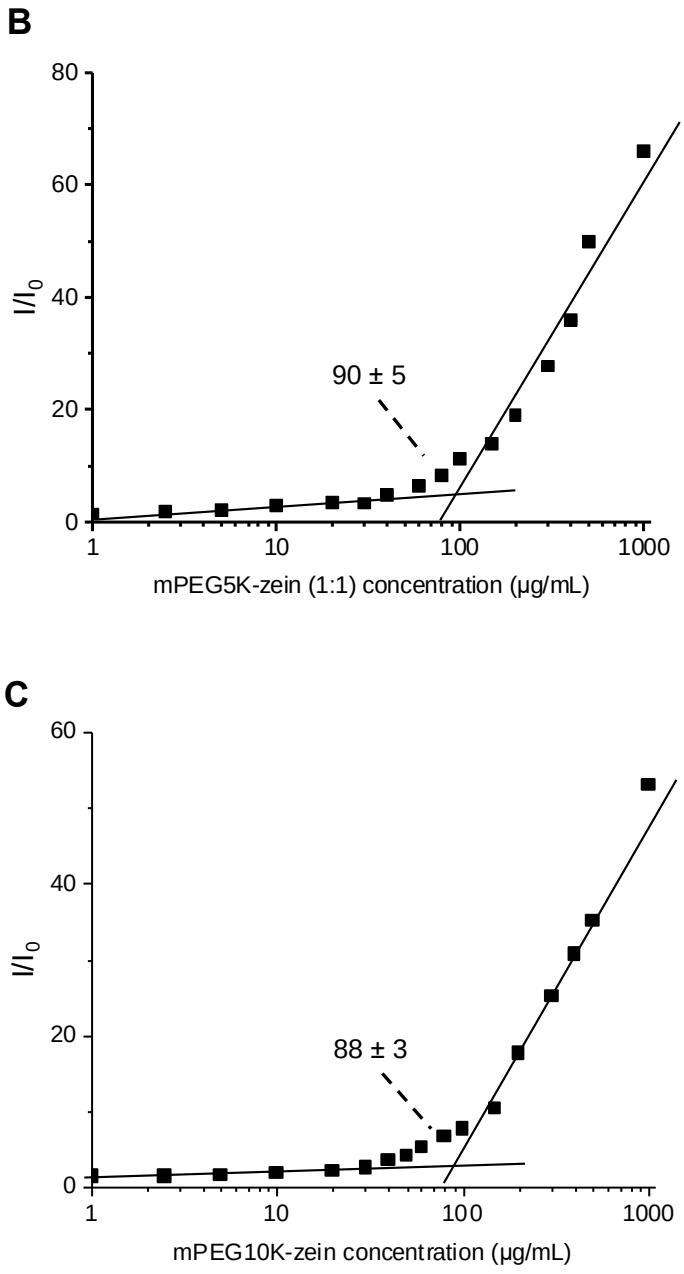

Figure 2-4. Relative fluorescence intensity (I/I_0) of Nile Red in the function of the concentration of mPEG5K-zein (0.5:1) (A), mPEG5K-zein (1:1) (B), and mPEG10K-zein (C). Results represent the mean ± standard deviation (SD) of 3 mPEG-zein batches.

2.5.4 Characterisation of mPEG-zein micelles

TEM images revealed that the obtained micelles had a spherical shape (**Figure 2-5**). The difference in size of the 3 mPEG-zein micellar formulations was further confirmed by dynamic light scattering (DLS) measurements (**Table 2-2**).

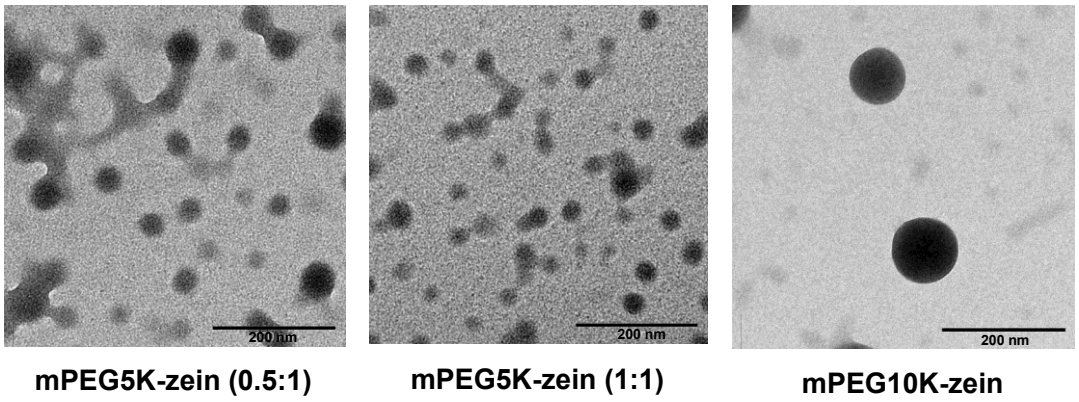

Figure 2-5. TEM images of mPEG-zein micelles (scale bar: 200 nm).

At constant PEG to zein molar ratio, the MW of PEG which is used to conjugate with zein had an influence on particle diameter, as the size of mPEG5K-zein micelles (134.79 ± 1.63 nm) are statistically significantly smaller than that of their 10K counterpart (166.32 ± 2.15 nm). PEG density also resulted in the change in particle size of the micelles as the particle diameter decreased from 134.79 ± 1.63 nm to 96.39 ± 1.94 nm when double the amount of PEG was used in the conjugation. All empty micelle formulations showed low polydispersity (≤ 0.2), indicating a narrow size distribution. A similar size trend was observed in Nile red-loaded mPEG-zein micelles. The encapsulation of Nile red into the micelles led to a small increase in particle diameter, except in the case of mPEG10K-zein, where the size increased almost twice

(from 166.32 ± 2.15 nm to 280.06 ± 42.93 nm) with a poor size distribution (PDI = 0.43).

Table 2-2. Particle size and zeta potential of empty and Nile red-loaded mPEG-zein micelles. Results represent mean ± SEM of 4 samples.

Formulation	Particle size (nm)	Polydispersity index (PDI)	Zeta potential (mV)
Empty mPEG-zein micelles			
mPEG5K-zein (0.5:1)	134.79 ± 1.63	0.23 ± 0.02	25.55 ± 1.15
mPEG5K-zein (1:1)	96.39 ± 1.94	0.24 ± 0.01	21.18 ± 2.18
mPEG10K-zein	166.32 ± 2.15	0.09 ± 0.02	23.55 ± 2.49
Nile red-loaded mPEG-zein micelles			
mPEG5K-zein (0.5:1)	147.13 ± 3.48	0.25 ± 0.04	24.30 ± 1.91
mPEG5K-zein (1:1)	116.77 ± 10.96	0.26 ± 0.04	21.40 ± 0.28
mPEG10K-zein	280.06 ± 42.93	0.43 ± 0.12	22.70 ± 0.44

The zeta potential of the empty micelles was positive in all formulations (25.55 ± 1.15 mV for mPEG5K-zein (0.5:1), 21.18 ± 2.18 for mPEG5K-zein (1:1), and 23.55 ± 2.49 mV for mPEG10K-zein). These results suggest that the MW and the ratio of PEG used for the conjugation had minimal effect on particle surface charge. The entrapment of Nile red did not alter the surface charge of the micelles, as similar zeta potential values were observed (24.30 ± 1.91 mV for mPEG5K-zein (0.5:1), 21.40 ± 0.28 for mPEG5K-zein (1:1), and 22.70 ± 0.44 mV for mPEG10K-zein). These positive zeta

potential values confirmed that Nile red was entrapped in the hydrophobic inner core of the micelles.

2.5.5 Determination of Nile red encapsulation efficiency

To determine the encapsulation efficiency (EE) and loading capacity of the micelles, a standard calibration curve was designed across a concentration range of 10-100 ng/mL using 6 different concentrations of Nile red in methanol. The quantification of Nile red was performed at the excitation wavelength of 550 nm and the emission wavelength of 638 nm. The fluorescence intensities were plotted against known concentrations to determine the equation of the straight line and regression coefficient (R^2). As shown in **Figure 2-6**, a linear relationship between the fluorescence intensity and Nile red concentration was observed, which could be described by the regression equation: $y = 1.1641x - 4.9097$ ($R^2 > 0.99$).

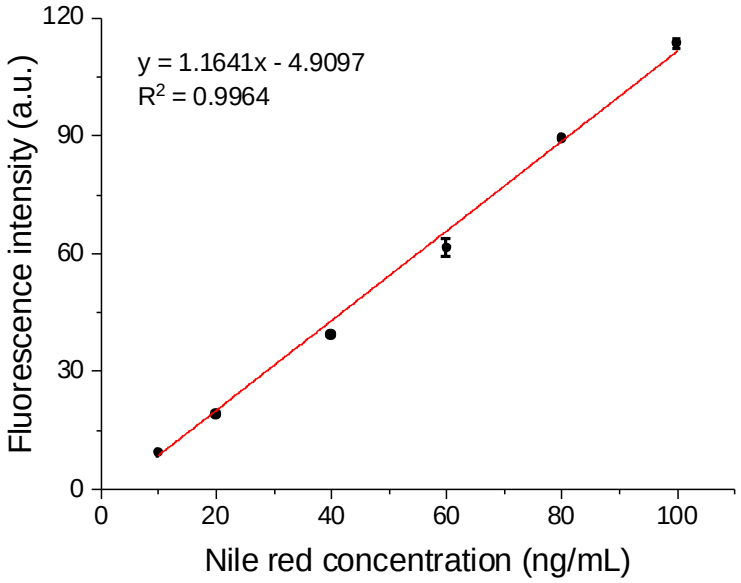

Figure 2-6. Standard calibration curve of Nile red in methanol for quantification determination of one assay (n = 5). Error bars are smaller than the symbols when not visible.

The pellet obtained after centrifugation of each micelle formulation was dissolved in methanol and quantified by spectrofluorometry. The amount of encapsulated Nile red was calculated by correlating to Nile red standard curve of each assay. The Nile red EE of each mPEG-zein is shown in **Table 2-3**. The EE of mPEG5K-zein (0.5:1) and mPEG5K-zein (1:1) was comparable (~70% and ~74%, respectively), while mPEG10K-zein demonstrated higher EE among all formulations (~85%).

Table 2-3. Encapsulation efficiency of Nile red in mPEG-zein formulations. Results represent mean ± SEM of 4 samples.

mPEG-zein types	Encapsulation efficiency (%)
mPEG5K-zein (0.5:1)	70.47 ± 3.77
mPEG5K-zein (1:1)	73.70 ± 4.10
mPEG10K-zein	84.74 ± 2.90

The amount of Nile red per mg mPEG-zein in all PEGylation types was also calculated. The Nile red encapsulation values normalised for the total amount of mPEG-zein were used to calculate the amount of mPEG-zein and the corresponding Nile red for *in vitro* studies. **Table 2-4** shows that loading content of Nile red in each type of mPEG-zein was within a narrow range (3.5-4.2 µg Nile red per mg mPEG-zein).

Table 2-4. Amount of Nile red per mg of mPEG-zein in three micelle formulations. Results represent mean ± SEM of 4 samples.

mPEG-zein types	Nile red (µg)/mPEG-zein (mg)
mPEG5K-zein (0.5:1)	3.51 ± 0.19
mPEG5K-zein (1:1)	3.67 ± 0.20
mPEG10K-zein	4.22 ± 0.14

2.5.6 *In vitro* cytotoxicity

The absence of toxicity is an essential property for any drug delivery system. The cell viability of B16-F10-luc-G5 and T98G cells was assessed after 72 h exposure to mPEG-zein micelles at concentrations ranging from 2 to 512 µg/mL **(Figure 2-7)**. The half-maximal inhibitory concentration (IC_{50}) in both cell lines was higher than 512 µg/mL for all three formulations. As shown in **Figure 2-7A,** the PEGylated zein micelles were not toxic to B16-F10-luc-G5 cells at concentrations below the CMC (2-64 µg/mL), as cell viability above 80% was considered to be non-toxic to the cells in this study. At concentrations higher than 64 µg/mL, the cell viability dropped with increasing micelle concentration until it fell below 80% for all formulations at a concentration of 512 µg/mL. Overall, all three micelle types displayed good biocompatibility in B16-F10-luc-G5 cells up to a concentration of 64 µg/mL. The cell viability of B16-F10-luc-G5 cells was concentration-dependent, whereas T98G cell viability was not. Nevertheless, these micelles were safe to T98G cells, as a cell viability higher than 80% was observed across all the concentrations used **(Figure 2-7B)**.

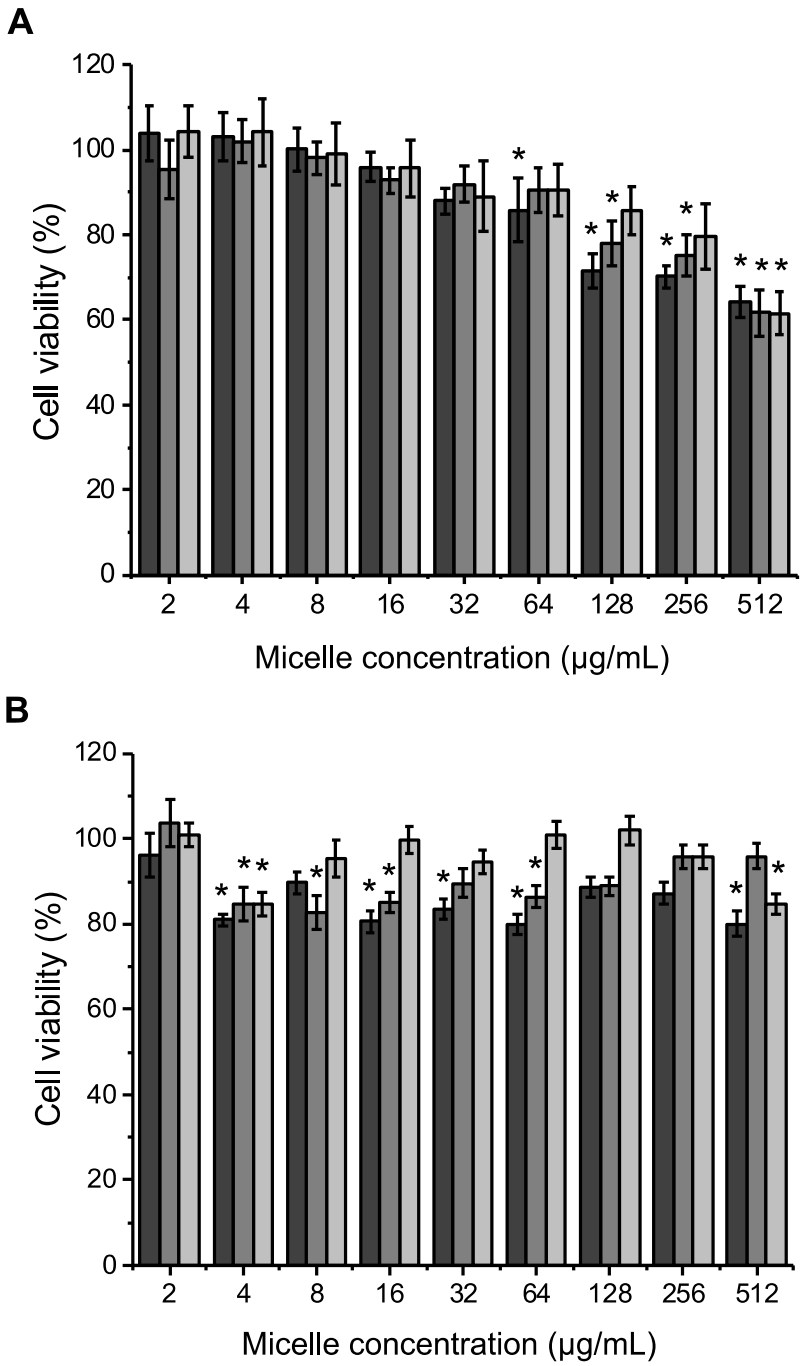

Figure 2-7. Cell viability of B16-F10-luc-G5 (A) and T98G (B) cells treated with empty mPEG5K-zein (0.5:1) (dark grey), mPEG5K-zein (1:1) (grey), or mPEG10K-zein (light grey) micelles for 72 hours (*: $P < 0.05$, compared with control of each group). Results represent mean ± SEM of 3 independent experiments.

2.5.7 Cellular uptake

2.5.7.1 Qualitative analysis

The uptake of mPEG-zein micelles by B16-F10-luc-G5 melanoma cancer cells was qualitatively evaluated using confocal microscopy (**Figure 2-8**). After 2-h incubation, all mPEG-zein micelles could deliver Nile red into the cells. mPEG5K-zein (0.5:1) led to a higher uptake of Nile red than mPEG5K-zein (1:1) and mPEG10K-zein. Fluorescent Nile red, predominantly located in the cytoplasm, was found to be co-localised in the nuclei following treatment with mPEG5K-zein (0.5:1) micelles while the other 2 formulations showed weak red fluorescence signals within the nucleus. The highest Nile red accumulation in the cells was observed as a result of treatment with Nile red solution.

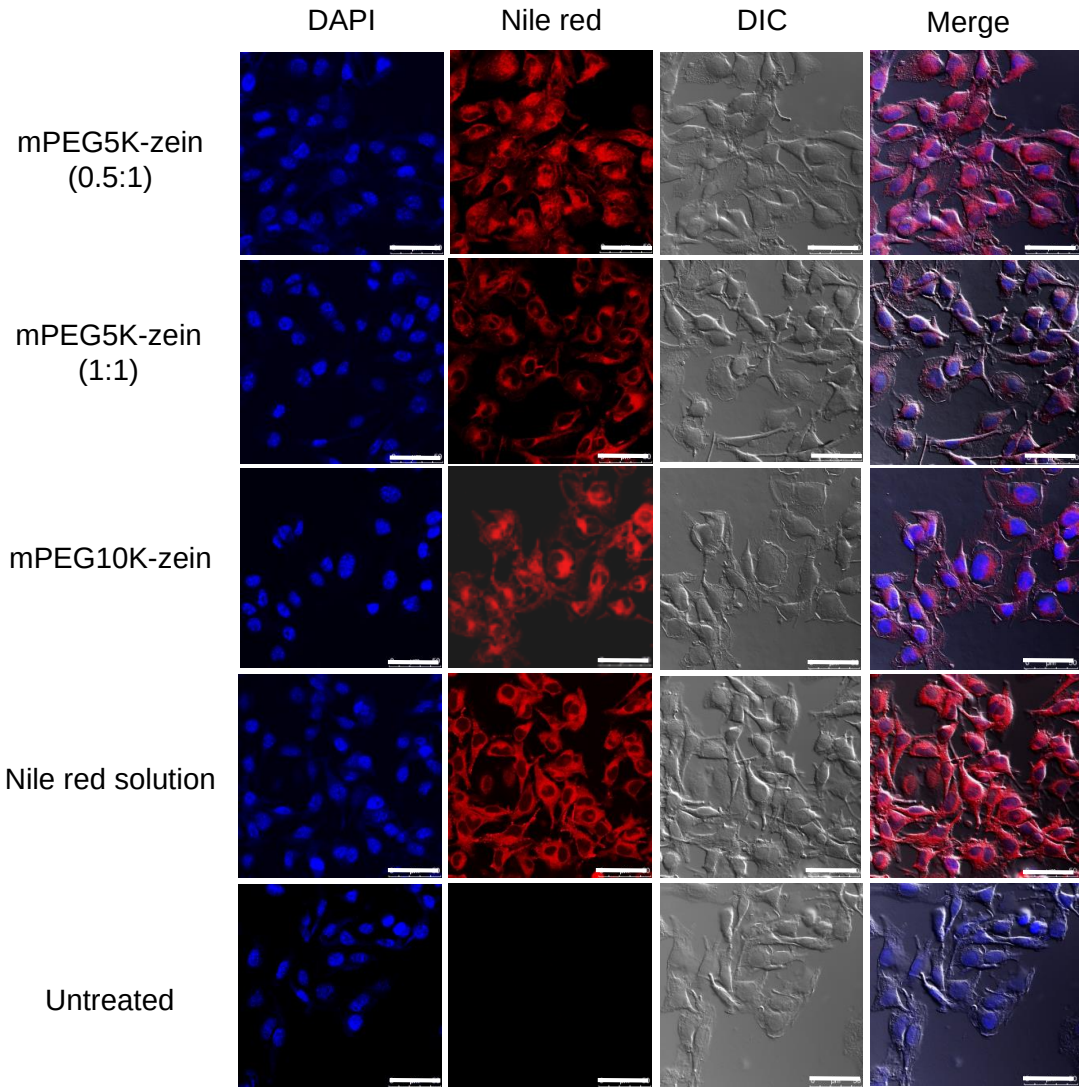

Figure 2-8. Confocal images of B16-F10-luc-G5 cells after incubation with Nile red loaded in mPEG-zein micelles or as a solution (DIC: Differential Interference Contrast) (scale bar: 50 μm).

2.5.7.2 Quantitative analysis

The cellular uptake of mPEG-zein micelles was further confirmed by flow cytometry. The mean fluorescence intensity (MFI) of cells incubated with Nile red solution was at least 3-fold higher than that of mPEG-zein micelles (**Figure 2-9**), which correlated well with the observation from confocal microscopy. Among the 3 micelle

formulations, mPEG5K-zein (0.5:1) micelles were the most efficient in delivering Nile red into the cells, by at least 1.7-fold improvement of Nile red internalisation in comparison with the other 2 formulations. mPEG5K-zein (1:1) and mPEG10K-zein displayed similar uptake levels. The higher cell-associated fluorescence intensity found in the cells incubated with mPEG5K-zein (0.5:1) micelles suggests that PEGylation with a shorter PEG chain length (5K) and less PEG content (0.5:1 PEG to zein weight ratio) could improve the cellular uptake efficacy of the zein micelles.

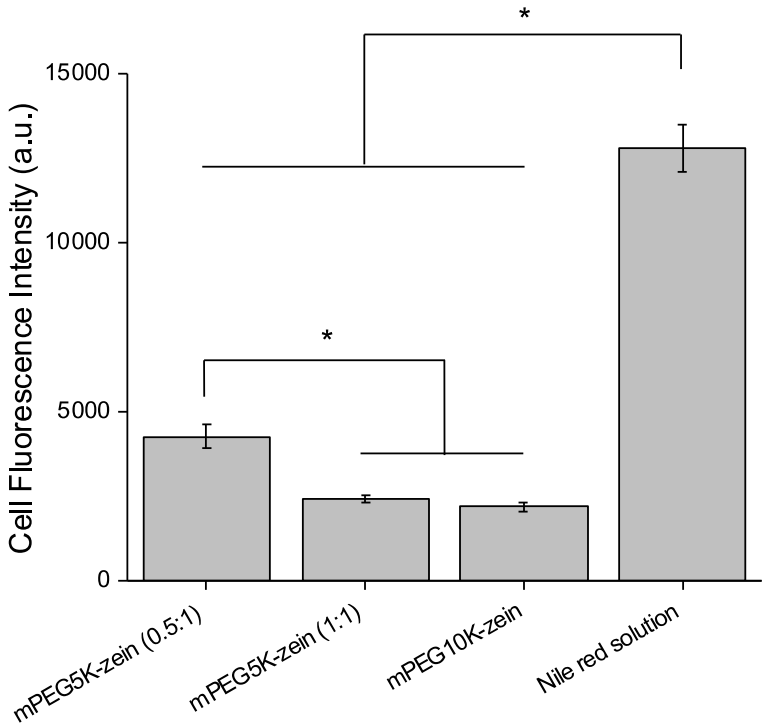

Figure 2-9. Flow cytometry analysis of the cellular uptake of Nile red loaded in mPEG-zein micelles or as a solution, in B16-F10-luc-G5 cells (a.u.: arbitrary units) (*: $P < 0.05$). Results represent mean ± SEM of 3 independent experiments.

2.5.7.3 Mechanisms of cellular uptake

To investigate the endocytosis pathways of mPEG-zein micelles entering B16-F10-luc-G5 cells, various pathway-specific inhibitors were used: chlorpromazine as the inhibitor of clathrin-mediated endocytosis, filipin as the inhibitor of caveolae-mediated endocytosis, and colchicine as the inhibitor of macropinocytosis (Cheng *et al*., 2014). The uptake of all mPEG-zein micelle formulations was significantly inhibited by chlorpromazine by about 20% (**Figure 2-10**), indicating that these micelles were mainly internalised by clathrin-mediated endocytosis. The uptake of mPEG5K-zein (1:1) micelles was partially inhibited by filipin (~10% inhibition), suggesting that mPEG5K-zein (1:1) micelles were also taken up by caveolae-mediated endocytosis through caveosomes. Macropinocytosis, however, did not participate in the uptake of these micelle systems, as colchicine did not result in a drop in the intracellular Nile red level.

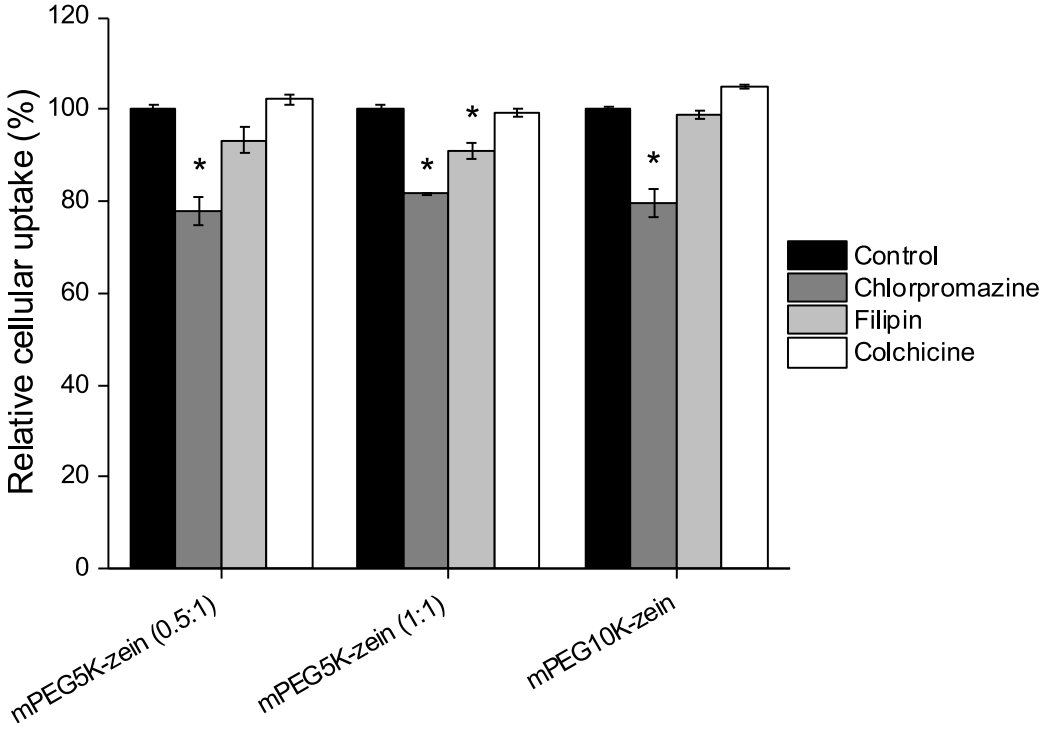

Figure 2-10. Effects of endocytosis inhibitors on the uptake of Nile red loaded in mPEG-zein micelles by B16-F10-luc-G5 cells (*: $P < 0.05$, compared with control). Results represent mean ± SEM of 3 independent experiments.

2.6 Discussion

Due to the protein origin and hydrophobicity of zein, the immunogenicity of zein-based particles had raised concerns about their potential application as drug and vaccine delivery vehicles (Hurtado-Lopez and Murdan, 2006). To date, one of the most effective strategies to make nanoparticles long circulating is to graft PEG molecules on their surface, a process known as PEGylation, to create a hydrophilic steric stabilisation that improves colloidal stability and protects the particles from non-specific protein adsorption, and therefore reducing opsonisation and subsequent phagocytosis (Torchilin and Trubetskoy, 1995, Romberg *et al*., 2008, Cruz *et al*., 2011).

Podaralla group successfully grafted mPEG-succinimidyl succinate on white zein (Podaralla *et al*., 2012). So far, there have been no reports of PEGylation utilising mPEG-SCM and yellow zein (a mixture of α, β, γ, and δ-zein). As a result, in this study, mPEG-zein was synthesised by the formation of an amide bond between the terminal amino group of glutamine present in yellow zein and mPEG-SCM using dialysis method through solvent exchange. As PEG density and chain length are major determinants of shielding efficacy, investigating the appropriate PEG conjugating to zein that provides stealth efficacy for the delivery system was necessary. Firstly, to evaluate the effect of the PEG chain length, nanoparticles were produced from mPEG-zein conjugate where the molar ratio of PEG to zein was kept constant and the MW of the PEG was increased from 5 kDa (mPEG5K-zein (0.5:1)) to 10 kDa (mPEG10K-zein). Secondly, to study the influence of PEG density, nanoparticles were made from mPEG5K-zein conjugate with doubled PEG content (mPEG5K-zein (0.5:1) and mPEG5K-zein (1:1)).

The PEGylation of zein was confirmed by ATR-FTIR analysis. The disappearance of the NHS ester peak after conjugation demonstrated that the conjugation was successful. The self-assembly of mPEG-zein into micelles in water was analysed by ^{1}H NMR spectra in DMSO-d_6 and D_2O. The disappearance of the zein peak in the D_2O confirmed the amphiphilic nature of the mPEG-zein conjugate, able to self-assemble in water with the hydrophilic mPEG in the outer shell and the hydrophobic zein in the core (**Figure 2-11**).

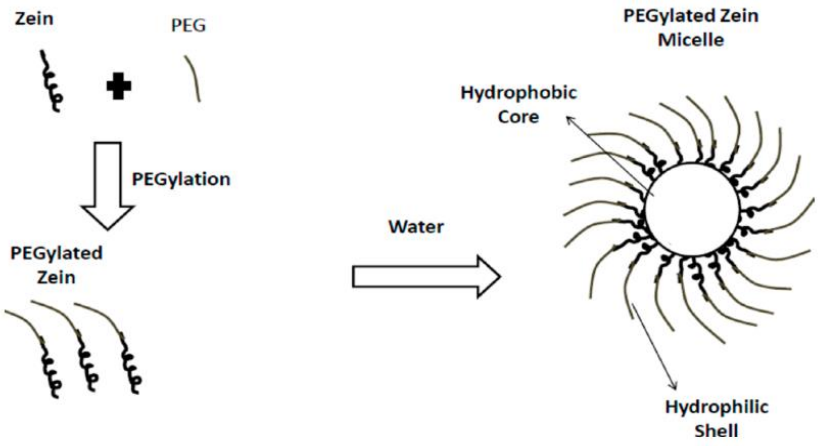

Figure 2-11. Schematic mPEG-zein micelle formation (Adapted from Podaralla *et al.*, 2011).

The self-assembly behaviour of mPEG-zein was further studied by a steady-state fluorescence technique using Nile red as a hydrophobic fluorescent probe. The CMC values of the three formulations were not statistically different, suggesting that the MW of PEG and PEG density had no effect on the CMC. As expected, the CMC value obtained for our mPEG5K-zein (1:1) micelles was relatively higher than that previously published (55 and 20 µg/mL in Podaralla *et al*. and Song *et al*.,

respectively), when using pyrene as a fluorescence probe (Podaralla *et al.*, 2012; Song *et al.*, 2015). This difference could be mostly related to the properties of different types of zein used as a starting material. Podaralla *et al*. used white zein, Song *et al*. used purified α-zein, while yellow zein was chosen in our study (Podaralla *et al.*, 2012; Song *et al.*, 2015). The yellow zein contains xanthophyll, which is responsible for a number of unwanted properties such as affecting the solubility of zein, large particle size distribution, and low drug encapsulation (Podaralla and Perumal, 2012; Paliwal and Palakurthi, 2014). It was possible that xanthophylls were removed during the synthesis of mPEG-zein since the yellow zein turned to white micelle dispersion after dialysis. However, the presence of xanthophyll in the starting yellow zein could decrease the solubility of zein from the start of the reaction, affecting the self-assembly property of the micelles in aqueous solution and resulting in a higher CMC.

Additionally, the higher CMC obtained could be partly due to the different hydrophobic probe used. Because of limitation in measuring fluorescence intensity for pyrene by the spectrofluorometer used in the present study, Nile red was chosen as the fluorescence probe for CMC determination instead. Chan and co-workers previously demonstrated that the CMC value for diblock copolymer micelles characterised using pyrene was lower than that using Nile red (15.1 mg/mL by pyrene versus 19.5 mg/mL by Nile red) (Chan *et al*., 2017). Nevertheless, the CMC values obtained in our study were still lower than the commercial polyethylene oxide polypropylene oxide block copolymer (Pluronics) (Xiong *et al*., 2015), indicating the thermodynamic stability of the mPEG-zein micelles.

mPEG-zein was able to encapsulate a hydrophobic drug model, Nile red, resulting in spherical-shape micelles as demonstrated by TEM. The difference in size of 3 mPEG-

zein micelles correlated well with the size obtained from the DLS. Their sizes, however, were larger than the corresponding sizes measured by TEM, as TEM imaging involves drying of the samples before measurement, unlike DLS, where hydrodynamic sizes are measured. Loading Nile red led to a slight increase in particle size. The size of Nile red-loaded mPEG-zein micelles ranged from 100 to 300 nm, depending on the MW of PEG used and PEG to zein ratio. However, these micelles should achieve passive accumulation within solid tumours due to the EPR effect, as their sizes were smaller than the cut-off size for extravasation (400 nm) (Yuan *et al*., 1995).

All three types of self-assembled micelles bore similar positive zeta potential, suggesting that the MW of PEG used for the conjugation had no substantial effect on particle surface charge. The entrapment of Nile red did not alter the surface charge of the micelles, as similar zeta potential values were observed for Nile red-loaded mPEG-zein micelles, thus further confirming that Nile red was entrapped in the inner core of the micelles. The positive net surface charge of mPEG5K-zein micelles was in agreement with that presented by Song *et al.* when using α-zein in their micelle formulation (39 mV) (Song *et al*., 2015).

The EE of Nile red in three mPEG-zein formulations was in the range of 70-85%, which was lower than that reported for the loading of curcumin in mPEG5K-zein micelles (~95% curcumin EE) (Podaralla *et al*., 2012; Song *et al*., 2015). This might be due to the difference in micelle compositions, since yellow zein, which contains xanthophyll, was used to conjugate with mPEG in this study. The presence of xanthophyll bound to zein was reported to highly decrease the solubility of zein, resulting in lower EE (Paliwal and Palakurthi, 2014). Thus, the presence of xanthophylls and their impact on Nile red loading should be explored further.

The EE of Nile red in mPEG5K-zein (0.5:1) and mPEG5K-zein (1:1) was comparable. The modulation of the MW of PEG conjugated to zein had an impact on the entrapment of Nile red in the micelles, which increased when using larger MW PEG. The increased entrapment with the higher PEG MW was also reported in PEG-coated fluconazole nanoparticles (Abdellatif *et al*., 2019). However, in some delivery systems such as PEG-PLGA and chitosan nanoparticles, the EE was independent of the PEG MW (Cruz *et al*., 2011; Bachir *et al*., 2018). The EE was even found to be decreased with increasing PEG MW, for example in the case of cholesterol-bearing PEGylated polymeric micelles, due to the overall low cholesterol content in the copolymer chain for polymers with higher MW PEG, making these micelles less favourable for drug encapsulation (Laskar *et al*., 2014).

The nanosize range of PEGylated zein micelles is expected to achieve the passive accumulation of nanoparticles within solid tumours due to the EPR effect, which is facilitated by the leakiness of tumour vasculature and the lack of lymphatic drainage (Torchilin, 2011; Maeda, 2015). We therefore evaluated the cellular uptake of mPEG-zein micelles in B16-F10-luc-G5 melanoma cancer cells. A higher Nile red uptake was observed from Nile red solution over mPEG-zein micelles. This could be explained by the different cellular uptake mechanisms used by Nile red solution and the micelles: passive diffusion of Nile red solution to the cells, while the micelles are taken up by endocytosis. Podaralla and colleagues, however, found that mPEG-zein micelles could enhance curcumin delivery (by 2-3-fold) into NCI/ADR-RES drug-resistant ovarian human cancer cells, compared to free curcumin (Podaralla *et al*., 2012). The discrepancy seen might be attributed to the difference in micelle compositions, model substances, as well as cell types.

Among the three studied micelle formulations, mPEG5K-zein (0.5:1) micelles were the most efficient in delivering Nile red into the cells, therefore demonstrating that PEGylation with shorter PEG chain length and less PEG density could improve the cellular uptake efficacy of the zein micelles. Our result was consistent with several types of PEGylated nanocarriers. For instance, the increase in PEG MW led to the reduced uptake of the chitosan nanoparticles by macrophages (Bachir *et al*., 2018). Similar finding was also reported using PEGylated cationic liposomes as PEGylation with shorter PEG chain length resulted in higher uptake in PC3 prostate cancer cells, when compared to its longer chain counterparts (Pozzi *et al*., 2014). Furthermore, grafting gold nanoparticles with longer chain PEG at higher density resulted in less nanoparticle internalisation in HeLa, MDA-MB-231, and MCF-7 cancer cell lines (Cruje and Chithrani, 2014). Increasing PEG MW and density was shown to hinder nanoparticle-cell interactions, as higher MW PEG grafting with high density led to a larger surface shielding of the micelles (Du *et al*., 1997; Suk *et al*., 2016). As a result, a decreased uptake of the mPEG5K-zein (1:1) and mPEG10K-zein formulations compared to the mPEG5K-zein (0.5:1) in cancer cells could be explained by a decrease in cell adhesion. Hence, modifying micelles with shorter PEG chains with a low coverage density would be sufficient to enhance cellular internalisation while also conferring stealth effects, i.e. improving micelle stability, reducing opsonisation and phagocytosis, and therefore extending the circulation time.

All three micelle formulations were mainly internalised into the cells via clathrin-mediated endocytosis, which is the main route by which nanocarriers enter cells (Cheng *et al*., 2014). However, it is unclear whether 20% inhibition is enough to confirm a dominant mechanism of uptake. To reach a firm conclusion on their

internalisation pathways, the cell uptake mechanisms of mPEG-zein micelles should be further elucidated by including controls of each specific pathway. The cellular uptake of other zein-based delivery systems via energy-dependent endocytosis was also previously reported, however involving different endocytosis pathways. Doxorubicin-loaded zein nanoparticles and caseinate-zein nanoparticles involved macropinocytosis instead of caveolin-mediated or clathrin-mediated pathways (Luo *et al*., 2013; Dong *et al*., 2016).

Despite the amount of research on polymeric micelles, data regarding the uptake mechanisms and intracellular trafficking of these micelles remains limited. Endocytosis, which involves micelle interaction with the cellular membrane, followed by the uptake in cell cytoplasm, has been reported as the main mechanism for micelle internalisation. However, in a few cases, polymeric micelles are internalised in their contact form: most of the time they disassociate in the plasma membrane or are degraded in lysosomes. Besides, micelles can enter cells as such, but they can release the drug outside the cells or be taken up as free monomers, leading to the accumulation of the drug in various subcellular compartments (Nelemans and Gurevich, 2020; Ghezzi *et al*., 2021).

CHAPTER 3

Impact of protein corona on PEGylated zein micelles

3.1 Introduction

Many physicochemical properties of delivery systems, such as their size, shape, charge, and surface chemistry, have been shown to strongly influence their cellular interactions (Albanese *et al*., 2012). However, when exposed to biological fluids, a layer of proteins is formed on the surface of delivery vehicles to form a so-called "protein corona". Protein corona can be classified into "hard corona" and "soft corona". The hard corona corresponds to proteins that are adsorbed to the delivery system with high affinity and do not readily desorb, whereas loosely bound proteins that adsorb with low affinity to the delivery system form a soft corona. Hard and soft coronas can also be defined based on the time required for the exchange of the adsorbed proteins. Hard corona usually shows a much higher exchange time (in the order of several hours), while soft corona undergoes rapid exchange of biomolecules (within seconds or minutes) (Corbo *et al*., 2016; Nguyen and Lee, 2017). The formation of the protein corona significantly alters the properties of the nanocarrier, giving it a new biological identity that impacts its biological responses within the body, such as circulation time, cellular uptake, kinetics, and toxicity (Monopoli *et al*., 2012; Nguyen and Lee, 2017).

Adsorption of opsonin proteins on the particle surface is the key factor in inducing phagocytosis, and eventually the removal of nanocarriers from blood circulation. PEGylation is often used to shield the nanoparticles from opsonisation and subsequent phagocytosis, because it creates high level of hydration of the hydrophilic polyether backbone, known as the "stealth" effect, hence preventing protein adsorption by means of steric stabilisation. This approach, therefore, allows the particle to circulate in the blood for extended periods of time to reach its therapeutic site of action (Gref *et al*.,

2000; Owens and Peppas, 2006; Walkey *et al*., 2012; Partikel *et al*., 2019). Yet, little is known about the impact of the protein corona on PEGylated zein micelles and their interactions with cells, or about the PEG chain length required to obtain stealth zein micelles.

3.2 Aim and Objectives

The aims of the work in this chapter were therefore 1) to assess the formation of a protein corona surrounding these PEGylated zein micelles upon contact with various biological fluids and 2) to evaluate their cellular uptake *in vitro* on cancer cells, macrophages, and dendritic cells.

3.3 Materials

Material	Supplier
Albumin, bovine serum	Sigma-Aldrich, UK
Bioware® B16-F10-luc-G5 mouse melanoma cells	Caliper Life Sciences, USA
Dimethyl sulfoxide (DMSO)	Sigma-Aldrich, UK
Dulbecco's Modified Eagle Medium (DMEM)	Life Technologies, UK
Foetal bovine serum (FBS)	Life Technologies, UK
Human glioblastoma (T98G)	European and American Collection of Cell Cultures (ECACC), UK
L-Glutamine	Life Technologies, UK
Methanol	Sigma-Aldrich, UK
Penicillin-Streptomycin	Life Technologies, UK
Phosphate buffered saline (PBS) tablets	Sigma-Aldrich, UK
Plasma (human)	Sigma-Aldrich, UK
Roswell Park Memorial Institute (RPMI) 1640 medium	Life Technologies, UK
Silver Stain Plus® Kit	Bio-Rad, UK
TrypLE® Express	Life Technologies, UK
3-(4,5-dimethylthiazol-2-yl)-2,5-diphenyl-tetrazolium bromide (MTT)	Sigma-Aldrich, UK
2x Laemmli sample buffer	Bio-Rad, UK
4-20% Mini-PROTEAN TGX® gels	Bio-Rad, UK

10x TGS buffer, Precision Plus Protein® Dual Color Standards	Bio-Rad, UK

3.4 Methods

3.4.1 Stability of mPEG-zein micelles in the presence of proteins

3.4.1.1 Proteins from FBS

The size measurement of empty mPEG5K-zein (0.5:1) and mPEG10K-zein micelles (1 mg/mL) was carried out in complete DMEM (cDMEM, containing 10% v/v FBS) and serum-free (sfDMEM) medium, at 0, 2, 6, and 24 h in triplicates. It should be noted that FBS used throughout the thesis was not heat-inactivated. All measurements were performed at 37°C on a Malvern Zetasizer Nano-ZS®, using a high-resolution model. Samples were vortexed at the start of the experiment and were further incubated at 37°C for subsequent measurements at the indicated times without being vortexed.

3.4.1.2 Proteins from human plasma (HP)

The size of the micelles in cell culture medium with 10% v/v HP (sfRPMI + HP) or without HP (sfRPMI) was also measured by DLS as described above.

3.4.2 Cell culture

B16-F10-luc-G5 mouse melanoma and T98G human glioblastoma cell lines were cultured as described in Chapter 2. Bone marrow-derived (BMD) macrophages and dendritic cells were kindly obtained from Professor Craig Roberts' laboratory. They were derived from tibia and femur of 6- to 8-week-old mice. Briefly, bone marrow was flushed with DMEM medium, to obtain BMD precursor cells which were resuspended in DMEM supplemented with 10% v/v FBS, 30% v/v L929-conditioned medium, 2% v/v L-glutamine, 2% v/v penicillin-streptomycin and seeded into Petri dishes. After 10 days at 37°C and 5% CO_2, adherent macrophages were harvested, washed and

resuspended in RPMI containing 10% v/v FBS, 2% v/v L-glutamine, 1% v/v penicillin-streptomycin.

Dendritic cells were cultured by flushing tibia and femur of mice with RPMI medium. Precursor cells were resuspended in RPMI supplemented with 10% v/v FBS, 2% v/v L-glutamine, 1% v/v penicillin-streptomycin, and 10% v/v granulocyte-monocyte colony stimulating factor conditioned medium (X63). Non-adherent cells were harvested at Day 7, washed and resuspended in RPMI containing 10% v/v FBS, 2% v/v L-glutamine, 1% v/v penicillin-streptomycin. The cells were maintained at 37°C in a humidified CO_2 incubator and used within 4 days after collection.

3.4.3 Effect of the protein corona on the cellular uptake of mPEG-zein micelles

3.4.3.1 Proteins from FBS

The effect of FBS on mPEG-zein micelle uptake by cancer cells, macrophages, and dendritic cells was examined by flow cytometry.

B16-F10-luc-G5 and T98G cancer cells were seeded into 6-well plates at a density of 2 x 10^5 cells/well and grown at 37°C for 24 h. Nile red-loaded mPEG5K-zein (0.5:1) and mPEG10K-zein micelles were pre-incubated in complete medium or in serum-free medium (presence or absence of FBS) at 37°C for 1 h, before being added to the cells (844 ng Nile red per well, in a volume of 3 mL). To investigate the kinetics of uptake of mPEG-zein micelles in cancer cell lines, the cells were incubated with the treatments for 15 min, 30 min, 1 h, 2 h, or 4 h, before being collected and analysed by flow cytometry as described in Chapter 2.

Murine BMD macrophages and dendritic cells were seeded and treated with the mPEG-zein micelles as described above. Because the difference in cellular uptake of the micelles in the presence and absence of serum protein could be seen within 2 h in previous studies, a 2-h incubation with the treatment was chosen for this and subsequent experiments. After 2-h treatment time, 500 µL cRPMI was added to each well. Single cell suspensions were obtained by scraping after the addition of 500 µL medium per well.

3.4.3.2 Proteins from HP

B16-F10-luc-G5, macrophages, and dendritic cells were seeded into 6-well plates at a density of 2 x 10^5 cells/well and allowed to settle for 24 h. Then, the grown cells were incubated in sfRPMI for 1 h, before treatment. Nile red-loaded mPEG-zein micelles (20 mg/mL in water) were pre-incubated in HP or glucose solution (5% w/v) (in presence or absence of HP) at a volume ratio of 1:1 at 37°C for 1 h and were added to the cells at a concentration of 844 ng Nile red per well in serum-free medium. After a 2-h incubation with the treatment, all three cell types were processed for flow cytometry analysis as described above.

3.4.4 Evaluation of cell viability

B16-F10-luc-G5, T98G, macrophages, and dendritic cells were seeded into 96-well plates at a density of 1.5 x 10^4 cells/well for 24 h. Next, the cells were incubated for either 2 h (for macrophages and dendritic cells) or 4 h (for B16-F10-luc-G5 and T98G cancer cells) with Nile red loaded in mPEG5K-zein (0.5:1) and mPEG10K-zein

micelles (56 ng Nile red per well), using untreated cells as controls. Following treatment, the cells were processed and analysed as described in 2.4.9.2.

3.4.5 Preparation of hard corona samples

3.4.5.1 Hard corona from FBS

mPEG-zein micelles (mPEG5K-zein (0.5:1) and mPEG10K-zein) were incubated in cDMEM or sfDMEM (3 mg/3 mL) at 37°C for 1 h. The micelle dispersion was then centrifuged at 4696 g for 10 min at 4°C, using a Heraeus Megafuge® 16R centrifuge (Thermo Scientific, Loughborough, UK) to remove loosely bound and excess proteins. The pellet was then re-dispersed with 3 mL ultrapure water, followed by a second centrifugation step (4696 g, 4°C, 10 min) in order to only obtain hard corona proteins. After centrifugation, the pellet was resuspended with 100 µL ultrapure water and kept at -20°C for further study.

3.4.5.2 Hard corona from HP

HP stock solution (0.5 mL) was diluted with 2.5 mL ultrapure water. mPEG-zein micelles (3 mg) were incubated with the diluted HP (3 mL) at 37°C for 1 h, followed by 2-step centrifugation (as described above) to obtain hard corona pellets.

3.4.6 Analysis of protein corona

3.4.6.1 Sodium dodecyl sulphate polyacrylamide gel electrophoresis (SDS-PAGE)

The protein samples were diluted with 2x Laemmli sample buffer containing 2-mercaptoethanol (5% v/v) as a reducing agent at the volume ratio of 1:1. The samples (20 µL, 5 µg protein) were reduced at 90°C for 5 min and loaded onto a 4-20% Mini-

PROTEAN® TGX™ gel. The gel was run with Tris/glycine/SDS buffer at 120 V for 1 h with Precision Plus Protein™ Dual Color Standards as a molecular standard. The gel was then stained with a Silver Stain Plus™ kit according to the kit's instruction manual.

Briefly, after gel electrophoresis, the gel was placed in the fixative enhancer solution (200 mL), with gentle agitation for 20 min. The fixative enhancer solution was decanted and the gel was rinsed twice with DI water (10 min each). Next, the gel was stained with 100 mL staining solution, for approximately 20 min. After the desired staining was reached, the staining reaction was stopped by placing the gel in acetic acid solution (5% v/v) for 15 min. Lastly, the gel was rinsed with DI water for 5 min before imaging.

3.4.6.2 Liquid chromatography-mass spectrometry (LC-MS) analysis

The protein samples (30 µL) were processed by filter-aided sample preparation to remove PEG before protein digestion by trypsin, used with an enzyme:protein ratio of 1:100. Trypsinised peptide samples were analysed using nanoscale liquid chromatography coupled to electrospray ionisation tandem mass spectrometry (nLC-ESI-MS/MS). Dry peptides were solubilised in 20 µL acetonitrile (5% v/v) with formic acid (0.5% v/v) and fractionated using the auto-sampler of a nanoflow uHPLC system (Thermo Scientific RSLCnano, Loughborough, UK). Peptide ions were detected by electrospray ionisation mass spectrometry using an Orbitrap Elite™ MS (Thermo Scientific, Loughborough, UK). The ionisation of LC eluent was performed by interfacing the LC coupling device to a TriVersa NanoMate® (Advion Biosciences, Ithaca, NY) with an electrospray voltage of 1.7 kV. Prior to analysis on the Orbitrap

Elite^{TM} MS, peptides were desalted and concentrated for 12 min on a trap column (0.3 × 5 mm) using a flow rate of 25 μL/min with acetonitrile (1% v/v) and formic acid (0.1% v/v). Peptides were separated on a Pepmap^{TM} C18 reversed phase column (length: 50 cm, diameter size: 75 μm, particle size: 3 μm, pore size: 100 Å) (Thermo Scientific, Loughborough, UK). Samples were processed with mobile phase A consisting of formic acid in water (0.1% v/v) and mobile phase B consisting of formic acid (0.08% v/v) in a mixture of acetonitrile (80% v/v) and water (20% v/v). The separation was performed at a fixed solvent flow rate of 0.3 μL/min, using a gradient of 4-100% mobile phase B over 120 min. The Orbitrap Elite^{TM} MS acquired full-scan spectra in the mass range of m/z 300-2000 Da for a high-resolution precursor scan at a set mass resolving power of 60,000 (at 400 m/z). Collision-induced dissociation was performed in the linear ion trap with the 20 most abundant precursors using rapid scan mode. Singly charged ions were excluded from selection, while selected precursors were added to a dynamic exclusion list for 180 s.

3.4.6.3 Protein identification

Data were analysed using the Mascot search engine (v2.6.2, Matrix Science) against the NCBIprot database using the *Homo Sapiens* taxonomy. A mass tolerance of 10 ppm for the precursor and 0.3 Da MS/MS was used for peptide matching.

3.4.7 Statistical Analysis

All data were reported as means ± SEM unless stated otherwise. Statistical analysis was performed by ANOVA followed by Tukey multiple comparison post-test and

unpaired *t*-test was performed for paired comparisons (Minitab® software, State College, PE) at a significance level of 0.05.

3.5 Results

3.5.1 Stability of mPEG-zein micelles in the presence of proteins

The stability of mPEG5K-zein (0.5:1) and mPEG10K-zein micelles in cell culture medium in the presence or absence of FBS (10% v/v) was determined by measuring their size at various times by DLS (**Figure 3-1A**). In the presence of FBS, the size of mPEG5K-zein (0.5:1) micelles slightly increased over 24 h by 16% (from 83.45 ± 0.86 nm to 97.44 ± 1.36 nm), significantly higher than that observed without FBS at 24 h (83.43 ± 1.62 nm). The size of mPEG10K-zein micelles did not significantly vary in the presence or absence of FBS, slightly increasing with time by 3%, from 128.03 ± 0.21 nm after mixing to 132.50 ± 0.87 nm after 24 h in the presence of FBS.

The stability of the micelles in the presence of HP was also investigated (**Figure 3-1B**). The size of mPEG5K-zein (0.5:1) micelles stayed the same over 24 h, independently of the presence or absence of HP (from 135.43 ± 1.44 nm to 130.87 ± 4.48 nm after 24 h). Likewise, mPEG10K-zein micelles displayed a similar size over 24 h. The presence of HP led to a slight decrease of the micelle size (212.13 ± 0.93 nm and 225.87 ± 5.98 nm respectively with and without HP after 24-h incubation). Although these micelles did not exhibit an increase of their size following incubation with HP, a decrease of their zeta potential was observed (from 28.57 ± 1.01 mV to 20.30 ± 2.70 mV for mPEG5K-zein (0.5:1) and from 30.90 ± 0.44 mV to 23.03 ± 0.78 mV for mPEG10K-zein).

Furthermore, the very limited size change indicated that both micelles were stable over 24 h under all the applied conditions.

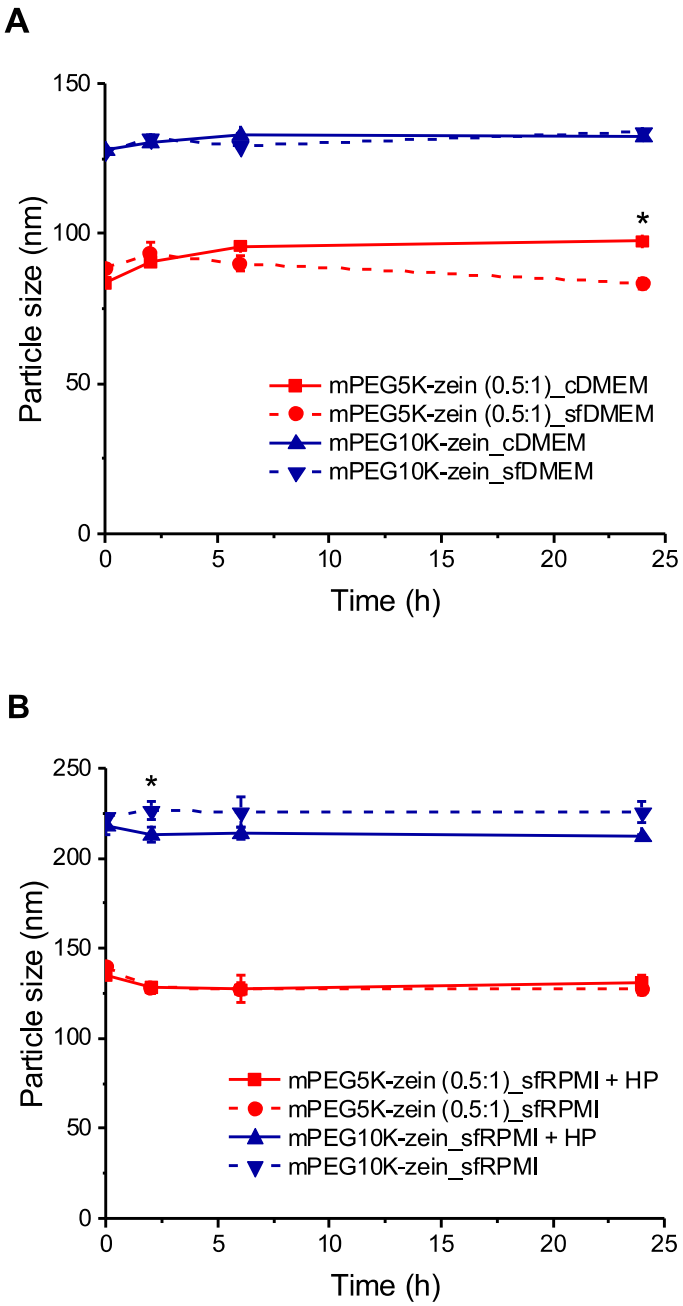

Figure 3-1. Stability of mPEG5K-zein (0.5:1) and mPEG10K-zein micelles in the presence or absence of 10% v/v FBS (A) or HP (B) (cDMEM: complete DMEM medium, sfDMEM: serum-free DMEM medium, sfRPMI: serum-free RPMI medium, sfRPMI + HP: serum-free RPMI medium + 10% v/v HP) (*: $P < 0.05$, compared with

its serum-free counterpart at the same incubation time). Results represents mean ± SD of one sample, triplicate readings.

3.5.2 Effect of protein corona on the cellular uptake of mPEG-zein micelles

3.5.2.1 Proteins from FBS

To evaluate the effect of FBS on the cellular uptake of PEGylated zein micelles, Nile red-loaded mPEG5K-zein (0.5:1) and mPEG10K-zein micelles were pre-incubated in either complete media or in serum-free media at 37°C for 1 h, to allow protein adsorption on the surface of the micelles. The cellular uptake of the pre-formed corona micelles in complete media or in serum-free media was carried out at various durations in B16-F10-luc-G5 and T98G cancer cells. Flow cytometry analysis revealed that mPEG-zein micelles could deliver Nile red into both cancer cell lines in a time-dependent manner (**Figure 3-2**).

The presence of FBS on the surface of the micelles slightly decreased the uptake of Nile red by B16-F10-luc-G5 cells, over 4 h, compared to that observed with micelles in serum-free conditions (**Figure 3-2A**). For mPEG5K-zein (0.5:1) micelles, the cellular uptake was significantly reduced by 26% and 19% following a 15-min and 30-min treatments, and then was similar to that observed with micelles without a protein corona after 1 h. It was higher than that observed with mPEG10K-zein micelles, confirming that smaller PEG5K chains facilitate cellular uptake compared to higher PEG10K chains within a delivery system. The cellular uptake of Nile red following treatment with mPEG10K-zein micelles in the presence of FBS was initially similar to that observed in serum-free condition for the first 30 min, then became markedly reduced by 26%, 22%, and 19% after 60, 120, and 240 min, respectively.

The cellular uptake observed for T98G cells was fairly similar, but the effect of protein corona was more profound in the case of mPEG5K-zein (0.5:1) micelles. As shown in **Figure 3-2B**, a significant decrease of the micelle uptake in the presence of FBS was observed (37-41% uptake reduction after 30-120 min treatment and 23% uptake reduction after 4-h treatment). FBS had no significant effect on cellular uptake efficiency of mPEG10K-zein micelles during a short incubation period. Although it exhibited a similar trend at longer exposure durations (28% and 18% uptake reduction following a 2-h and 4-h incubation in serum-supplemented conditions), these differences were not statistically significant.

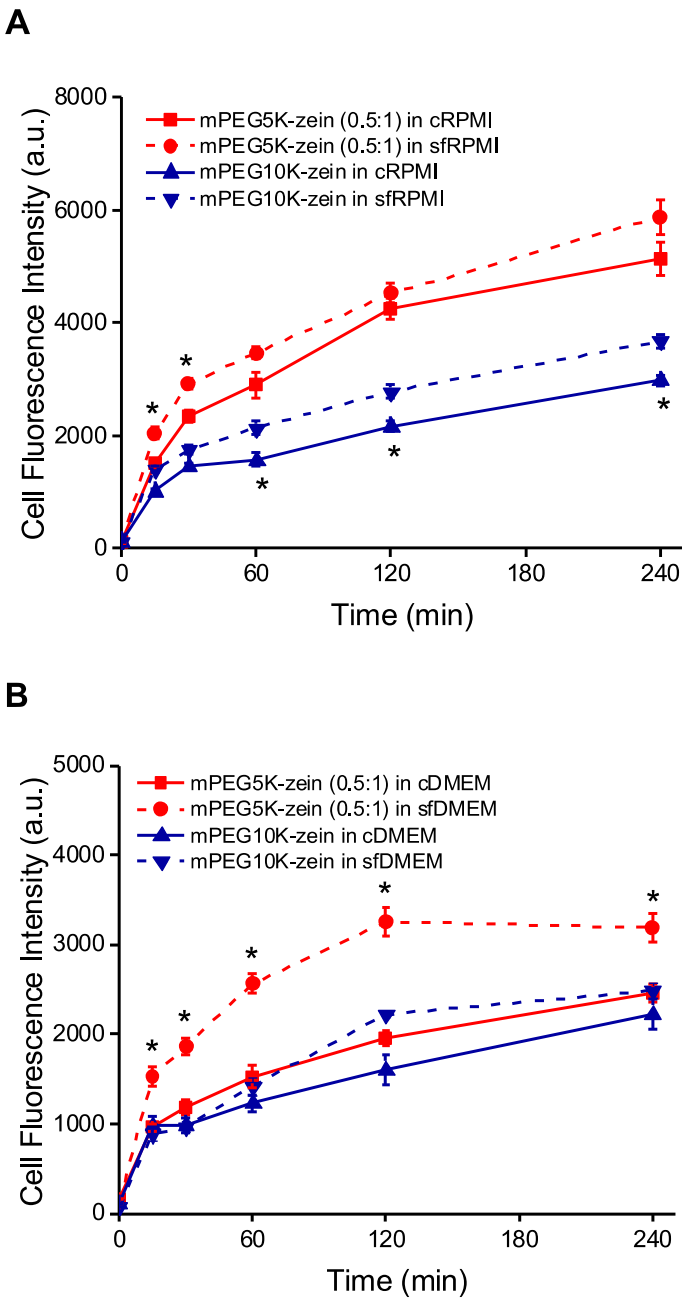

Figure 3-2. Time-dependent uptake of pre-formed corona mPEG5K-zein (0.5:1) and mPEG10K-zein micelles in complete and serum-free media by B16-F10-luc-G5 cells (A) and T98G (B) (cRPMI: complete RPMI medium, sfRPMI: serum-free RPMI medium, cDMEM: complete DMEM medium, sfDMEM: serum-free DMEM medium) (*: $P < 0.05$, compared between serum-free condition and its serum-

containing counterpart at the same treatment time). Results represent mean ± SEM of 3 independent experiments.

Although higher uptake levels in serum-free conditions were observed for both cancer cell lines, our particles may behave differently in different cell systems. Following intravenous administration, nanomaterials are often covered by corona proteins. Some of them can act as opsonins to influence the recognition and clearance of the particles by cells of the MPS, predominantly dendritic cells in the bloodstream and macrophages at tissues, and thus potentially prevent the particles to reach their target tumours (Walkey *et al*., 2012; Mo *et al*., 2018). Therefore, the effect of FBS on the uptake of mPEG-zein micelles by bone marrow-derived macrophages and dendritic cells was also investigated.

Similar results were obtained for the macrophages and the dendritic cells treated with the pre-formed corona micelles in medium with or without FBS (**Figure 3-3**). The results showed that the uptake of the micelles was partially inhibited in the presence of FBS (~20% uptake reduction for both micelle formulations on macrophages and ~28% and ~33% respectively for mPEG5K-zein (0.5:1) and mPEG10K-zein micelles on dendritic cells). The presence of the protein corona on the micelles therefore decreased the cellular uptake of Nile red by the macrophages and the dendritic cells compared to the micelles without protein corona, regardless of the MW of PEG used in the micelle formulations.

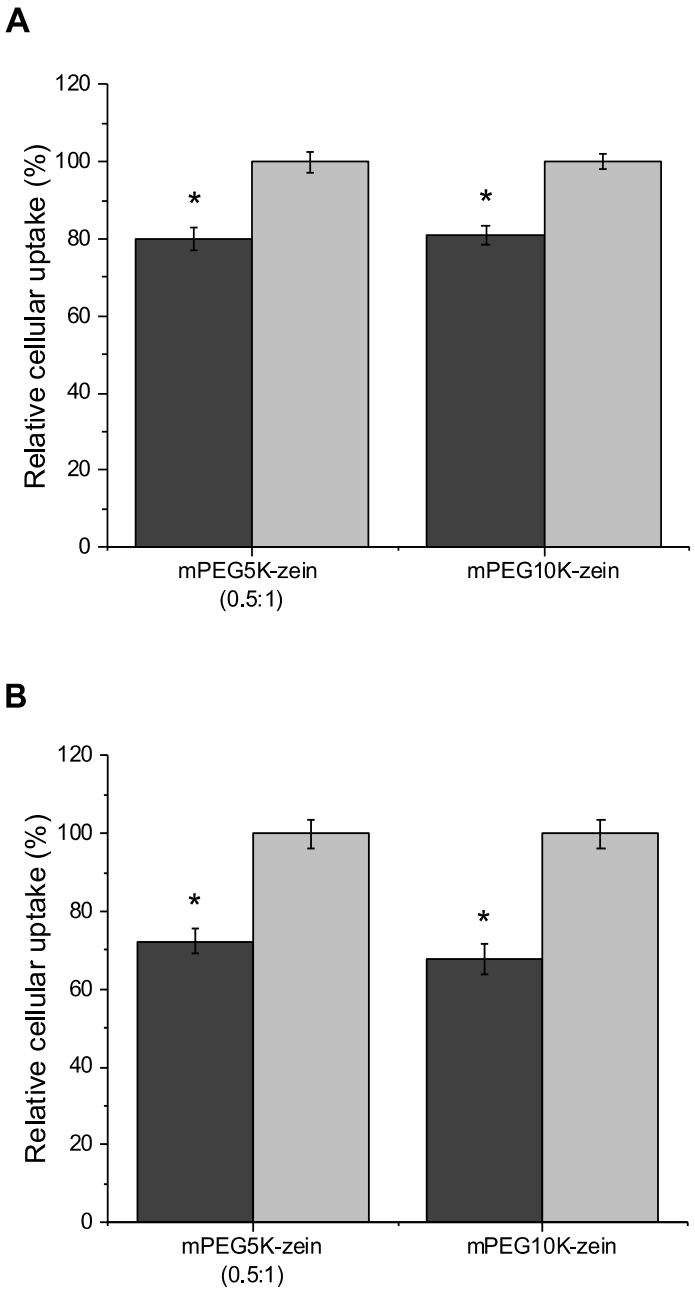

Figure 3-3. Uptake of the pre-formed corona micelles in cRPMI (dark grey) or sfRPMI (light grey) by macrophages (A) and dendritic cells (B) (*: $P < 0.05$, compared with sfRPMI). Results represent mean ± SEM of 3 independent experiments.

3.5.2.2 Proteins from HP

To investigate the impact of protein corona on drug delivery vehicles in contact with physiological fluids, HP was used to prepare pre-formed corona micelles. In this study, Nile red-loaded mPEG5K-zein (0.5:1) and mPEG10K-zein micelles were pre-incubated in HP or in glucose solution (5% w/v) at 37°C for 1 h. They were then added to B16-F10-luc-G5, macrophages, and dendritic cells in serum-free medium for 2 h, to determine the effect of a pre-formed corona on cellular uptake levels. Flow cytometry analysis revealed that pre-coating the micelles with HP had no substantial effect on the uptake of Nile red by the cancer cells, independently on the PEG chain length used in the formulations (**Figure 3-4A**). On the other hand, pre-coating the micelles with HP resulted in a decreased uptake by macrophages (9% uptake reduction for mPEG5K-zein (0.5:1) and 18% uptake reduction for mPEG10K-zein) (**Figure 3-4B**). Also, the uptake of mPEG5K-zein (0.5:1) and mPEG10K-zein micelles by dendritic cells was reduced by 22% and 19%, respectively after pre-incubation with HP (**Figure 3-4C**).

A

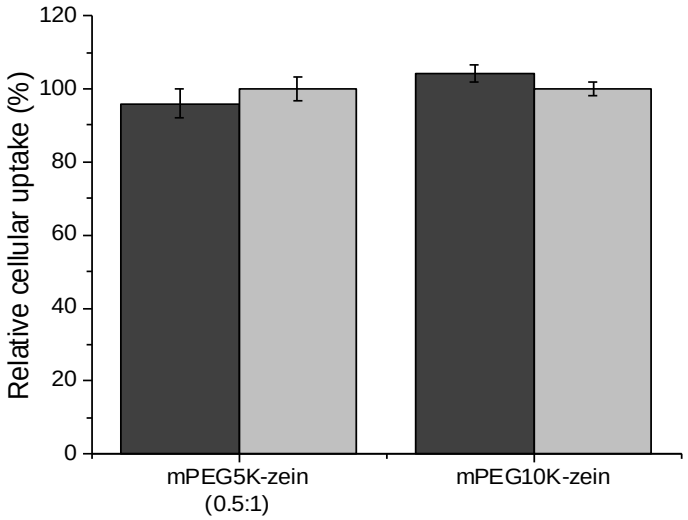
120
100
80
60
40
20
0
Relative cellular uptake (%)
mPEG5K-zein
(0.5:1)
mPEG10K-zein

B

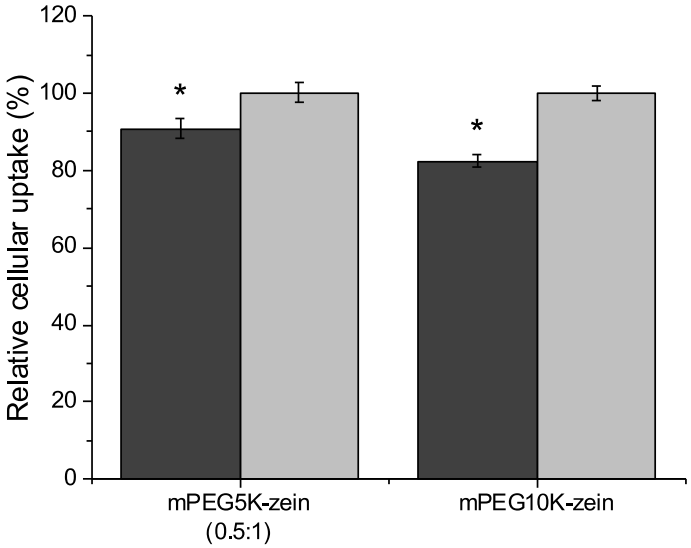
120
100
80
60
40
20
0
Relative cellular uptake (%)
*
*
mPEG5K-zein
(0.5:1)
mPEG10K-zein

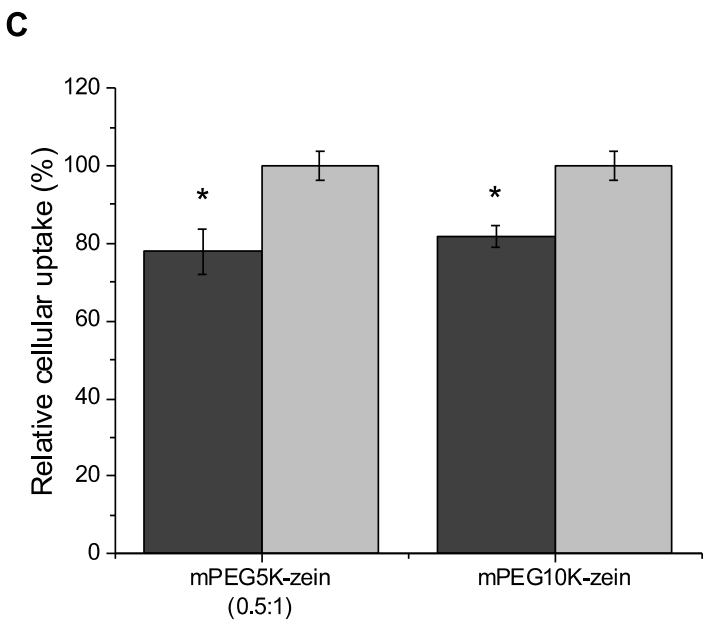

Figure 3-4. Cellular uptake of Nile red-loaded in mPEG5K-zein (0.5:1) and mPEG10K-zein micelles pre-coated with HP (dark grey) or glucose 5% w/v solution as control (light grey), by B16-F10-luc-G5 cancer cells (A), macrophages (B), and dendritic cells (C) (*: $P < 0.05$, compared with controls without protein corona). Results represent mean ± SEM of 3 independent experiments.

The adsorption of HP on the micelle surface, therefore, had a positive impact on the uptake of the formulations by all three cell types. It did not have any impact on the uptake of PEGylated zein micelles by the melanoma cancer cells, regardless of the PEG MW used in the formulations. It decreased the uptake of the micelles by macrophages, with a higher decrease observed with mPEG10K-zein micelles, and by dendritic cells for both micelle formulations.

3.5.3 Evaluation of cell viability

The viability of B16-F10-luc-G5 and T98G cancer cells, macrophages, and dendritic cells was assessed following treatment with Nile red-loaded mPEG-zein micelles at the experimental conditions used in the cellular uptake experiments (same concentration, treatment for 4 h for the cancer cells and 2 h for the macrophages and dendritic cells). The viability of the 4 cell types was higher than 80% following treatment with both mPEG5K-zein (0.5:1) and mPEG10K-zein micelles, suggesting that the micelles were not toxic to the cells at these experimental conditions. It was not significantly different from that observed with untreated cells (**Figure 3-5**). This confirmed that the differences in the cellular uptake analysis were not resulting from the toxicity of the micelles.

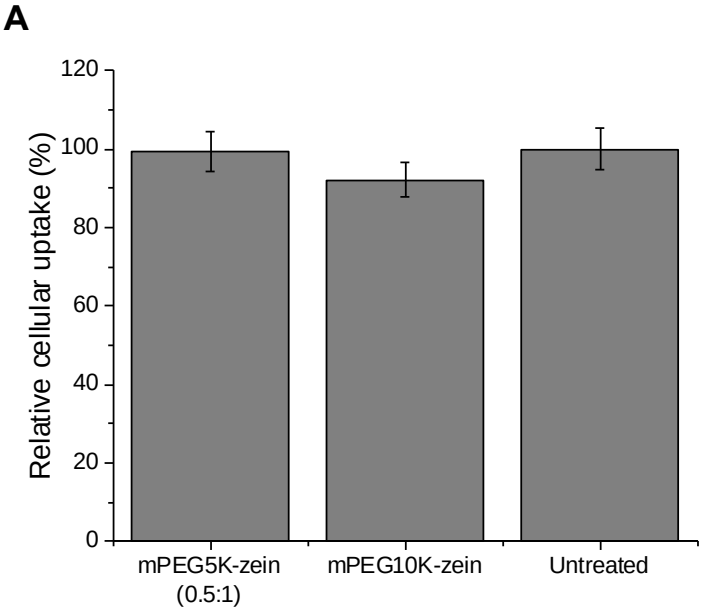

B

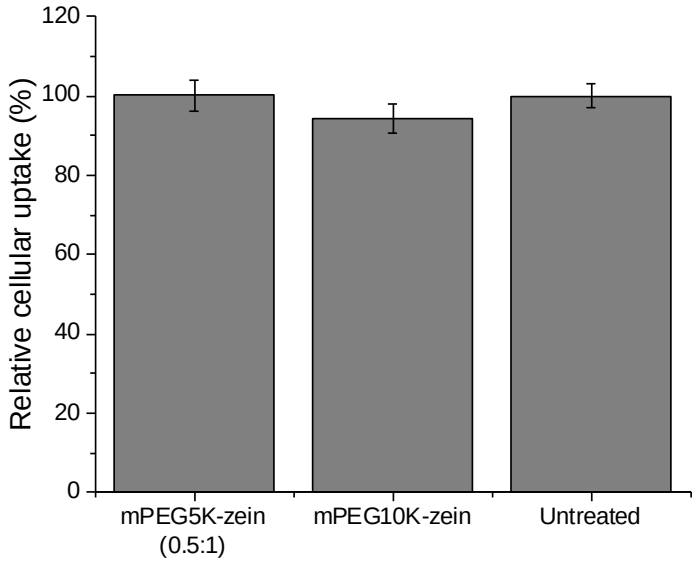
Relative cellular uptake (%)
120
100
80
60
40
20
0
mPEG5K-zein
(0.5:1)
mPEG10K-zein
Untreated

C

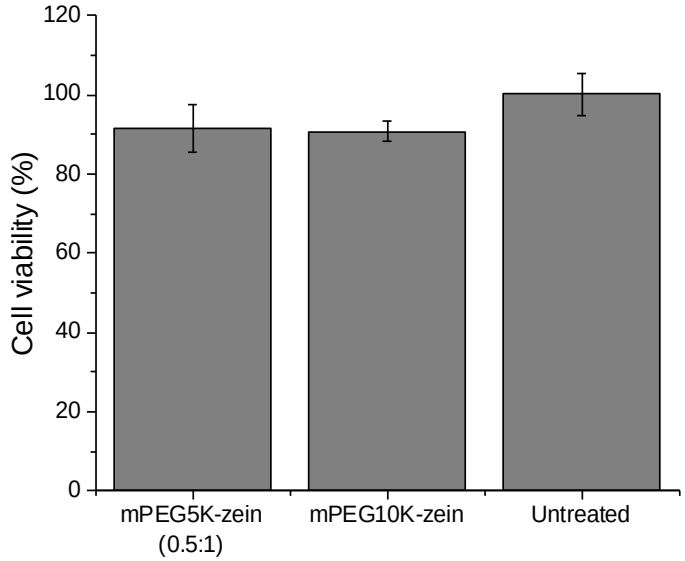
Cell viability (%)
120
100
80
60
40
20
0
mPEG5K-zein
(0.5:1)
mPEG10K-zein
Untreated

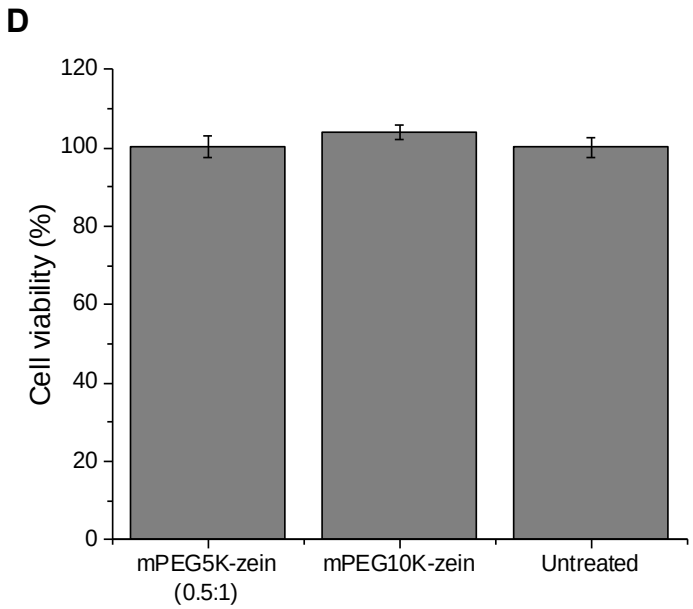

Figure 3-5. Viability of B16-F10-luc-G5 (A) and T98G (B) cancer cells, macrophages (C), and dendritic cells (D) treated with Nile red-loaded mPEG-zein micelles for 4 h (cancer cells) or 2 h (macrophages, dendritic cells). Results represent mean ± SEM of 3 independent experiments. There was no statistical difference between the treatments.

3.5.4 Analysis of the protein corona

3.5.4.1 SDS-PAGE

The hard corona proteins were obtained after 1-h incubation of mPEG5K-zein (0.5:1) and mPEG10K-zein micelles in various media, followed by 2-step centrifugation. They were then separated according to their MW using SDS-PAGE and visualised by silver staining. As shown in **Figure 3-6**, the protein profiles observed for mPEG5K-zein (0.5:1) and mPEG10K-zein micelles were almost identical. The corona of the micelles exposed to either cDMEM or HP was composed of a number of proteins. Both micelles were mainly covered by serum albumin (band at ~62 kDa) which is the protein with the highest concentration in FBS and human blood plasma (Righetti *et*

al., 2005; Gossmann *et al*., 2015). Protein bands at ~22-24 kDa correspond to α-zein. Other zein fractions were also detected from micelles that have been incubated with sfDMEM. However, the intensities of these bands were considerably low.

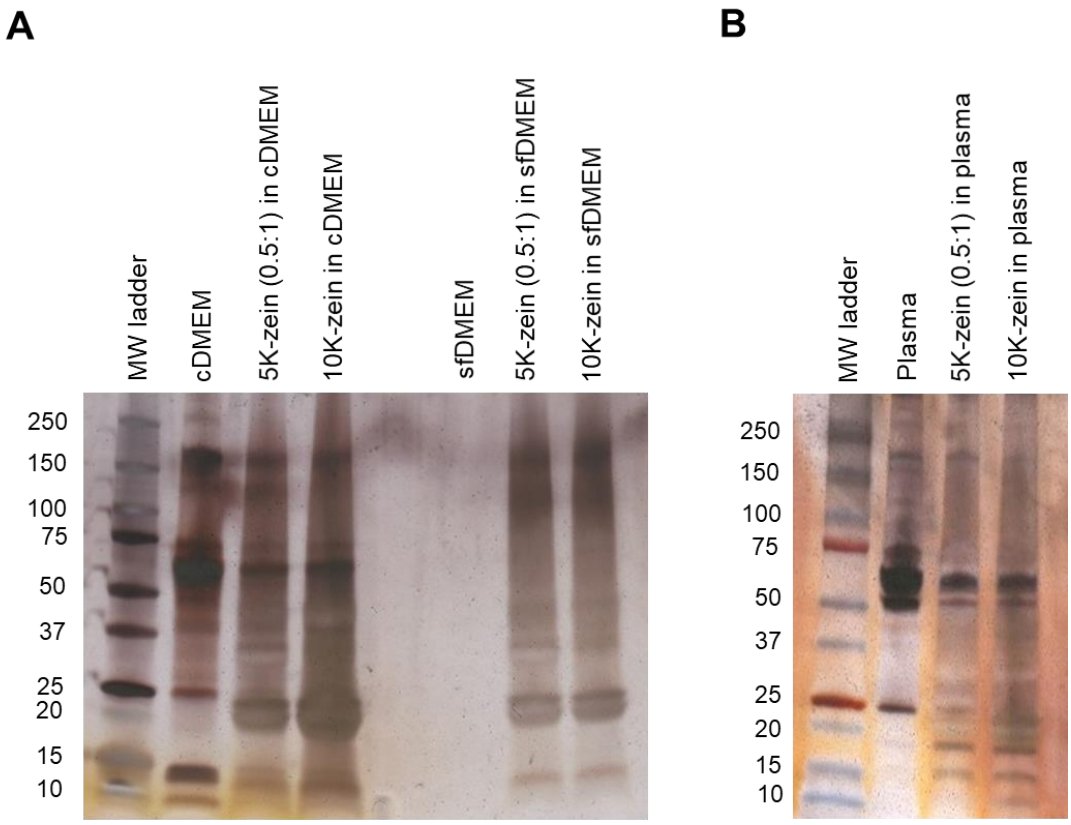

Figure 3-6. SDS-PAGE gels of protein corona surrounding mPEG-zein micelles following incubation in cDMEM, sfDMEM (A) and HP (B) at 37°C for 1 h. The analysis was performed in duplicate – for clarity only one replicate is shown.

3.5.4.2 LC-MS analysis

The composition of the proteins bound onto mPEG-zein micelles was identified using nLC-ESI-MS/MS. A total of 132 and 109 proteins were identified from the protein

coronas recovered from mPEG5K-zein (0.5:1) and mPEG10K-zein samples, respectively. Among these proteins, 48 proteins appeared on both types of micelles. All the identified proteins with different MW, molecular weight search (MOWSE) score, and exponentially modified protein abundance index (emPAI) are presented in **Appendix Table A-1**. The emPAI was used to estimate the absolute protein amounts in the sample (Ishihama *et al*., 2005; Yan *et al*., 2013). Grouping the proteins according to their MW showed that low MW proteins (< 25 kDa) were predominantly found on mPEG5K-zein (0.5:1) micelles, while proteins with medium size (25-100 kDa) were significantly enriched on mPEG10K-zein micelles (**Figure 3-7B**). We also detected a very low level of high MW proteins (> 100 kDa) on the surface of both micelles. This result therefore demonstrated the presence of a distinct protein binding pattern on each micelle type.

The bound proteins were further classified according to their functions (**Figure 3-7A**). Both micelle types were mainly covered by immunoglobulins, lipoproteins, the proteins involved in tissue leakage, and other plasma components. We found a significant enrichment of immunoglobulins (49%) on the surface of mPEG5K-zein (0.5:1) micelles. The most abundant protein from the corona recovered from mPEG5K-zein (0.5:1) micelles was the immunoglobulin light chain (13%), followed by albumin (10%). In contrast, proteins that preferentially bound to mPEG10K-zein micelles were other plasma components (33%). Lipoproteins and immunoglobulins constituted up to 40% of the protein corona (~20% from each group). The highest enrichment of proteins on the surface of mPEG10K-zein micelles was albumin (27%) and the next most abundant protein was apolipoprotein A-I (14%) (**Figure 3-7C**).

Our results suggested that plasma protein adsorption was influenced by PEG MW, since different protein compositions and contents were detected from the corona of both micelle types.

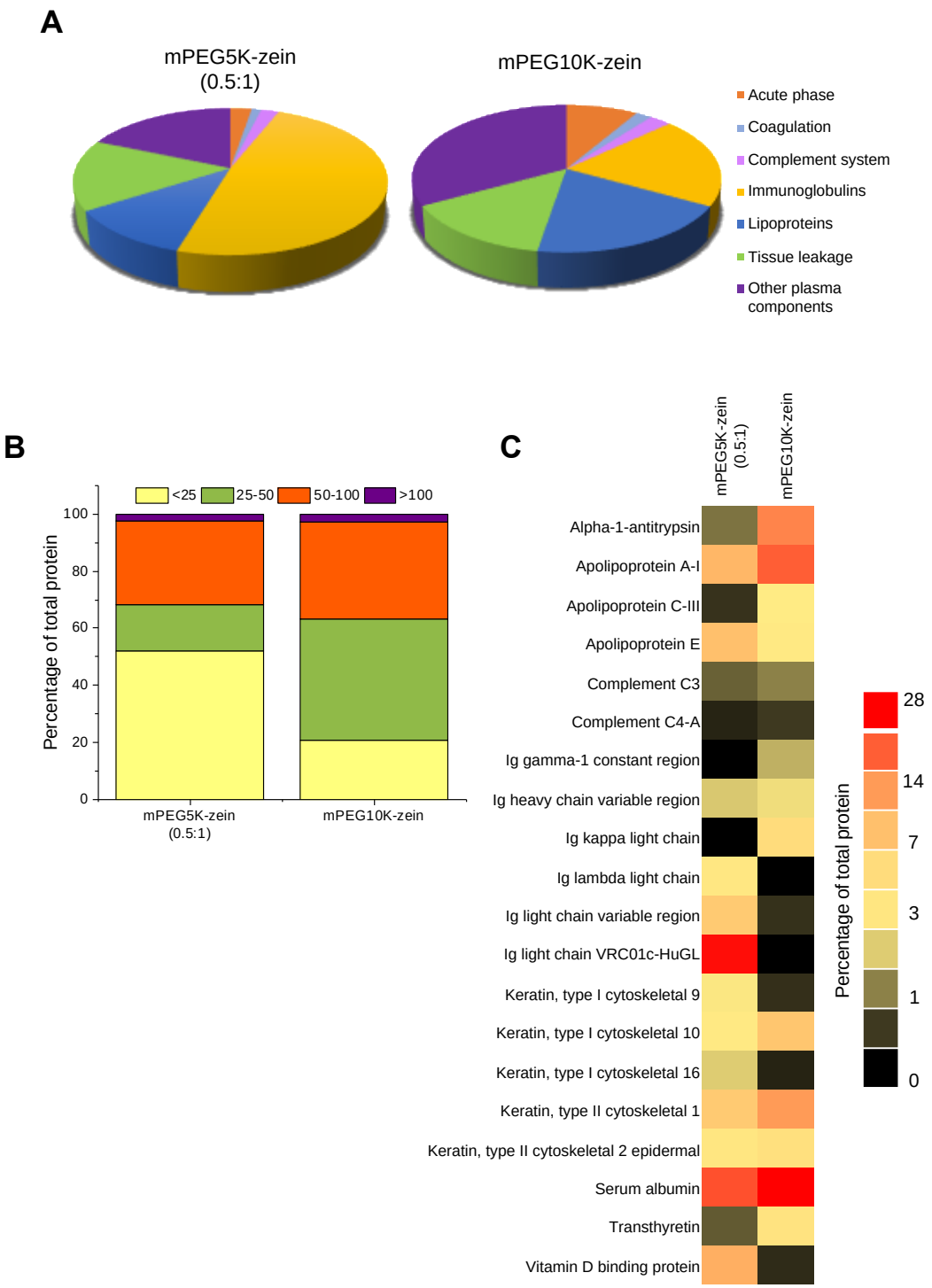

Figure 3-7. Proteomic analysis of the protein corona surrounding mPEG5K-zein (0.5:1) and mPEG10K-zein micelles. Proteins were classified by function (A) and weight (kDa) (B). The 20 most abundant proteins in the corona of mPEG-zein micelles were used to create the heat map (C).

3.6 Discussion

It has been recently established that nanoparticles, once entering in biological environment, are immediately covered by a layer of serum proteins, known as the protein corona. The protein corona alters the properties of the pristine surface of nanoparticles, giving them a new biological identity which subsequently impacts their interactions with cells (Monopoli *et al*., 2012; Nguyen and Lee, 2017). This makes the correlation of *in vitro* and *in vivo* experiments difficult, as the biological impact of the nanoparticles in a physiological system cannot simply be linked to the nature of the particles alone. Therefore, for continued development of PEGylated zein micelles in biomedicine, studies on interactions of micelle-corona complexes and their influence on cancer cells and immune cells are of interest. However, due to the limitation of the speed of the centrifuge used at the time conducting this study, no hard corona sample of mPEG5K-zein (1:1) micelles could be obtained. Thus, all of the work that was described in this chapter was performed with two micelle formulations: mPEG5K-zein (0.5:1) and mPEG10K-zein.

Generally, the proteins adsorbed to nanoparticles can be determined indirectly via *in situ* size measurements. The larger the amount of proteins attached, the larger its hydrodynamic radius will become (del Pino *et al*., 2014). Hence, DLS was employed for investigation of the thickness of the corona layer in this study by determining the overall size of protein-nanoparticle complexes. Typically, DLS does not require separation of unbound excess proteins, and thus this technique is most relevant to *in vivo* environments, as it measures the protein corona while the nanoparticle is dispersed in a physiological environment.

The size of both micelles slightly increased in the presence of FBS. This small size enlargement (~14 nm (16%) for mPEG5K-zein (0.5:1) and ~4 nm (3%) for mPEG10K-zein) might be due to the formation of the protein corona on the surface of the micelles, as previously reported for various delivery systems. However, the magnitude of the size change can vary depending on the delivery systems. Lesniak and colleagues observed an increased size of silica nanoparticles by 114% (from 49 nm in water to 105 nm in DMEM) (Lesniak *et al*., 2012). The size of nanoporous polymeric nanoparticles increased by about 30%, from ~500 nm to ~650 nm in the presence of 10% v/v FBS (Yan *et al*., 2013). Also, Pozzi and co-workers demonstrated that multi-component cationic liposome-HP complexes were about 50 nm larger than that of their counterparts in the absence of the protein corona (from 86 to ~140 nm) (Pozzi *et al*., 2014). Furthermore, the average size of black phosphorus nanosheets-corona complexes increased by 8% (from 338.4 ± 2.3 nm to 365.3 ± 5.9 nm), while the diameter of black phosphorus quantum dots unexpectedly increased over 6000% (from 5.6 ± 1.4 nm to 362.5 ± 5.6 nm) after the protein corona was formed (Mo *et al*., 2018).

When mPEG-zein micelles were allowed to interact with HP, such an increase in size was not observed. Unexpectedly, the particle size of mPEG10K-zein micelles decreased slightly. In general, proteins interact with nanoparticles by forming a corona around their surface, resulting in a thickening of the nanoparticle surface and a subsequent increase in their size. However, they may lead to a size reduction due to osmotically driven shrinkage (Gräfe *et al*., 2016). For our delivery systems, the latter effect may be predominant, particularly for the mPEG10K formulation. Repulsive forces of mPEG10K-zein micelles against HP could prevent the formation of a dense protein corona. Instead, proteins that are impermeable to the micelles might induce

osmotic pressure, which caused water to escape from the micelle and the micelle to shrink.

Although these micelles did not exhibit an increase in their size following incubation with HP, a drop in zeta potential values by about 8 mV was detected. This might be due to the binding of negatively charged proteins on the micelle surface. The neutralisation of the particle surface charge resulting from the binding of proteins with opposite charges on nanoparticle surface was in accordance with data published by several groups for other delivery systems. For example, polyethyleneimine-coated magnetic nanoparticles showed a zeta potential of 48.4 ± 7.8 mV. It decreased to negative values with increasing concentrations of foetal calf serum in RPMI medium (Gräfe *et al*., 2016). The zeta potential of multi-component cationic liposomes and their PEGylated counterparts was found to be negative after incubation with HP (Pozzi *et al*., 2014). The neutralisation of the particle surface charge was also observed in negatively charged nanomaterials. For instance, nanoporous polymer particles displayed a change in zeta potential from -39 ± 5 mV in sfRPMI to -25 ± 4 mV and -26 ± 5 mV upon protein adsorption in cRPMI and FBS media, respectively (Yan *et al*., 2013). Also, the zeta potential values of black phosphorus nanosheets and black phosphorus quantum dots increased from -18.1 to -8.4 mV and -20.6 to -6.4 mV, respectively after the protein corona was formed on their surfaces (Mo *et al*., 2018).

Surface modification of delivery systems with PEG has been reported to prevent non-specific interactions with proteins, as hydrophilic PEG chains become compressed when proteins approach the surface, thus creating a thermodynamic barrier to protein adsorption (Gref *et al*., 2000; Walkey *et al*., 2012; Dai *et al*., 2014; Partikel *et al*., 2019). The presence of FBS or HP in the medium surrounding the micelles led to

minimal changes in hydrodynamic diameter, indicating limited micelle-protein interactions. Our results suggest that both mPEG5K-zein (0.5:1) and mPEG10K-zein micelles exhibited stealth properties regardless of PEG chain length.

After determining changes in the size and zeta potential, *in vitro* experiments have shown that the presence of FBS slightly decreased the uptake of both micelle systems by all 4 cell types: B16-F10-luc-G5 and T98G cancer cells, macrophages, and dendritic cells. Pre-coating the micelles with HP had no significant influence on the uptake of Nile red by B16-F10-luc-G5 cancer cells, independently on the PEG chain length used in the formulations. It decreased the uptake of the micelles by macrophages, with a higher decrease observed with mPEG10K-zein micelles, and by dendritic cells for both micelle formulations. The limited effect of the protein corona on the cellular uptake of our mPEG-zein micelles could be explained by a decreased protein binding resulting from the stealth properties of PEG (Otsuku *et al*., 2012; Cruje and Chithrani 2014). Furthermore, the cellular uptake of our mPEG-zein micelles in the presence of protein corona was still high and greater than that usually observed with many PEGylated systems. Pozzi *et al*. (2014) reported that multi-component cationic liposomes with intermediate PEGylation (PEG2K) showed high cellular uptake efficiency in PC3 human prostate cancer cells both in the absence and presence of the protein corona: 80% uptake in the absence of HP and 50% uptake after incubation with HP (Pozzi *et al*., 2014). In another study, the uptake of PEGylated polystyrene nanocarriers by RAW264.7 murine macrophage-like cells was almost completely inhibited after incubation with plasma (relative fluorescence intensity decreased from ~1000 to less than 100 when the nanocarriers were previously incubated with water and plasma, respectively) (Schöttler *et al*., 2016).

The decrease in the cellular uptake of pre-treated micelles (human plasma) by macrophages and dendritic cells could be explained by the lowered micelle-cell membrane adhesion caused by the adsorption of proteins around the micelle surface. The small decrease in cellular uptake is probably due to the decreased protein binding resulting from the stealth properties of PEG. Furthermore, PEGylation could not inhibit serum protein adsorption completely, even at high grafting density, but it could selectively suppress the adsorption of specific proteins, such as opsonins (Walkey *et al*., 2012). Taken together, these two factors might be the reason of a decrease uptake by macrophages and dendritic cells.

The relationship between the protein corona and nanoparticle uptake efficiency has previously been investigated in several nanomaterials. Lesniak and colleagues, for instance, demonstrated a significant inhibition of the uptake of silica nanoparticles in the presence of serum by A549 human lung cancer cells (1,500,000 a.u. in serum-free versus 10,500 a.u. in complete medium, after 2-h incubation) (Lesniak *et al*., 2012). As nanoparticle uptake involves cell membrane adsorption followed by subsequent internalisation via energy-dependent endocytosis (Wilhelm *et al*., 2002), the lowered particle-cell membrane adhesion due to the adsorption of serum proteins on the nanoparticle surface thereby caused a reduction in internalisation efficiency (Lesniak *et al*., 2013). Nevertheless, a protein corona could affect nanoparticle uptake efficiency with different outcomes. Yan *et al.* reported that the adsorption of FBS on disulphide-stabilised poly-(methacrylic acid) nanoporous polymer particles significantly decreased the cellular uptake in monocytes by at least 50%. In contrast, it did not affect the uptake level in macrophages (Yan *et al*., 2013). Pozzi and colleagues also demonstrated that the cell internalisation of PEGylated multi-component cationic

liposomes in PC3 prostate cancer cells decreased after incubation with HP, but the cellular uptake of non-PEGylated liposome-HP complexes increased with respect to their counterparts in the absence of the corona (Pozzi *et al*., 2014).

SDS-PAGE was performed to gain an overview about the protein signature of hard corona proteins of mPEG-zein micelles following incubation with HP. The protein pattern of both micelles, fairly similar, was dominated by serum albumin, which is the most abundant protein in blood (Righetti *et al*., 2005). However, it is well accepted that numerous proteins which exhibit a low abundance in blood are also highly enriched on particle surface (Gossmann *et al*., 2015; Schöttler *et al*., 2016; Partikel *et al*., 2019). Therefore, nLC-ESI-MS/MS was applied for the identification and the relative quantification of the hard corona composition which allowed for more detailed insights about the protein adsorption behaviour.

Our results suggested that plasma protein adsorption was influenced by PEG MW, since different protein compositions and contents were detected from the corona of both micelle types. These results were supported by several publications. Apart from PEG chain length, Gref and co-workers revealed that the type and amount of the corona proteins were also determined by PEG density at the particle surface as well as the nature of the core material (Gref *et al*., 2000). Walkey *et al*. reported that PEGylation could not inhibit serum protein adsorption completely even at high grafting density, but selectively suppressed the adsorption of specific serum proteins, leading to a decreased macrophage uptake (Walkey *et al*., 2012). In a recent study, Partikel and colleagues observed a significant depletion of bound proteins that are involved in immunoregulatory processes, in terms of amount and number, due to PEGylation on PLGA nanoparticles (Partikel *et al*., 2019). These proteins are known

as opsonins. The adsorption of opsonins, such as immunoglobulins and complement factors, onto nanoparticle surface is thought to promote phagocytosis and clearance of the particles by cells of the MPS. These particles tend to deposit and concentrate in the organs of the RES, namely liver and spleen, and are eventually cleared from the body.

By contrast, the binding of dysopsonins, such as albumin, has been shown to prolong blood circulation lifetime. Ogawara and team reported that pre-coating polystyrene nanoparticles with albumin could suppress the association of serum proteins with opsonic activity, resulting in prolonged blood circulation after intravenous injection in rats (Ogawara *et al*., 2004). Instead of albumin, Schöttler and colleagues identified clusterin (also known as apolipoprotein J) as another protein with dysopsonic properties. They found that the presence of clusterin on PEG and poly(ethyl ethylene phosphate)-functionalised polystyrene nanoparticles was necessary to prevent macrophage uptake (Schöttler *et al*., 2016). Clusterin was also detected in our hard corona proteins, but at very low levels (less than 1% in both micelle systems). However, we found albumin and various apolipoproteins, mainly apolipoproteins A-I and E, to be prominent in the protein corona recovered from both micelles. Apolipoproteins, which are responsible for lipid transport and metabolism, generally exhibit dysopsonic function, as reported previously (Partikel *et al*., 2019; Schöttler *et al*., 2016).

In summary, even though immune relevant proteins such as immunoglobulins were present in high percentage in the hard corona recovered from our micelles, in particular in the case of PEG5K, we also found an enrichment of dysopsonins such as albumin and apolipoproteins. The presence of dysopsonins might antagonise the biological

effects of micelle-bound opsonins (Tenzer *et al*., 2011), leading to a limited decrease in cellular uptake by macrophages and dendritic cells.

Though this chapter provides the first investigation of the impact of the protein corona on mPEG-zein micelle uptake by cancer cells and immune cells, there are some limitations and challenges of the methodology used. Due to the limitation of the speed of the centrifuge used at the time conducting this study, no hard corona sample of mPEG5K-zein (1:1) micelles could be obtained. As a result, all of the work that was described in this chapter was performed with two micelle formulations: mPEG5K-zein (0.5:1) and mPEG10K-zein. In fact, this study should be tested on all three formulations in order to gain a better understanding of the protein adsorbed on the micelles with low and high PEG densities and their correlation with the interaction with cells. Besides, the non-PEGylated system should also be used as the control group to confirm the effect of PEGylation in minimising the corona formation.

CHAPTER 4

Microfluidic versus manual manufacturing of zein-based nanoparticles

4.1 Introduction

Zein has an amphiphilic molecular structure that makes it soluble in 50-90% v/v aqueous ethanol. It is insoluble in water due to its large fraction of non-polar amino acids, whereas its high glutamine content makes it insoluble in absolute alcohol (Gianazza *et al.*, 1977). By taking advantage of its different solubilities in ethanol and water, zein was shown to be able to form nanoparticles suitable for use as carrier systems for the delivery of essential oils, drugs, and DNA (Parris *et al*., 2005; Regier *et al*., 2012; Dong *et al*., 2016; Thapa *et al*., 2017).

Zein nanoparticles can be produced by several preparation methods, the most common one is a simple benchtop process called nanoprecipitation. This method involves mixing a zein ethanolic solution with water to cause the nanoprecipitation of zein and the formation of zein nanoparticles. The payload is trapped within the matrix of the particles as it forms (Olenskyj *et al*., 2017; Tarhini *et al*., 2018; van Ballegooie *et al*., 2019). The particle size depends on parameters such as mixing process, rate of injection of one phase into another phase, agitation speed, pH of the solution, and the volume ratio of aqueous to organic phase (Pascoli *et al*., 2018; Tarhini *et al*., 2018). Due to variation of shear force and spatial shear intensity within the solution, particle sizes can vary from batch to batch, especially at larger scales (Olenskyj *et al*., 2017; van Ballegooie *et al*., 2019). Hence, new methods that can optimise process control and enhance zein nanoparticle quality and consistency are needed.

Over the past decade, microfluidic-based manufacturing systems have been successfully used for obtaining high quality nanoparticles that can be applied for drug delivery. Microfluidic approach allows experimental parameters such as temperature,

flow rate, and reagent concentration to be varied and controlled in a rapid, reproducible, and precise manner (deMello and deMello, 2004). Aqueous and organic phases are still used in the same way to precipitate nanoparticles, but microfluidic systems offer rapid and consistent mixing at the junction where two solvent streams meet using hydrodynamic flow focusing, allowing better control of nanoparticle properties such as size, surface characteristics, and drug loading over the process of nanoprecipitation (Karnik *et al*., 2008; van Ballegooie *et al*., 2019). Despite the advantages of microfluidics, only two research groups have exploited this technology to generate zein nanoparticles (Olenskyj *et al*., 2017; van Ballegooie *et al*., 2019). They demonstrated that rapid and tunable microfluidic mixing can be used to reproducibly synthesise small and homogeneous zein nanoparticles. They also revealed key parameters, including zein concentration, solvent type and concentration, flow rate ratio, relative flow rate of the aqueous and organic phase, and chip configuration, that influence nanoparticle size and polydispersity. However, the applicability of this technology for encapsulating drugs or other materials in zein nanoparticles has not been addressed.

4.2 Aim and Objectives

The aims of the work in this chapter were therefore 1) to assess the potential of using microfluidics to synthesise zein nanoparticles encapsulating coumarin-6 (CR6) as a lipophilic drug model and 2) to investigate the influence of PEG density and chain length on zein nanoparticle characteristics, coupled with preliminary *in vitro* studies.

4.3 Materials

Material	**Supplier**
Albumin, bovine serum	Sigma-Aldrich, UK
Bioware® B16-F10-luc-G5 mouse melanoma cells	Caliper Life Sciences, USA
Chlorpromazine	Sigma-Aldrich, UK
Colchicine	Sigma-Aldrich, UK
Coumarin 6	Sigma-Aldrich, UK
Copper (II) sulphate pentahydrate ($CuSO_4 \bullet 5H_2O$)	Sigma-Aldrich, UK
Dimethyl sulfoxide (DMSO)	Sigma-Aldrich, UK
Ethanol	Sigma-Aldrich, UK
Filipin complex from *Streptomyces filipinensis*	Life Technologies, UK
Foetal bovine serum (FBS)	Life Technologies, UK
Folin & Ciocalteu's phenol reagent	Sigma-Aldrich, UK
Formalin solution, neutral buffered, 10%	Sigma-Aldrich, UK
L-Glutamine	Life Technologies, UK
Methanol	Sigma-Aldrich, UK
Penicillin-Streptomycin	Life Technologies, UK
Phosphate buffered saline (PBS) tablets	Sigma-Aldrich, UK
Potassium sodium tartrate ($C_4H_4KNaO_6$)	Sigma-Aldrich, UK
Roswell Park Memorial Institute (RPMI) 1640 medium	Life Technologies, UK
Sodium carbonate (anhydrous) (Na_2CO_3)	Sigma-Aldrich, UK
Sodium hydroxide (NaOH)	Sigma-Aldrich, UK

Triton X-100	Sigma-Aldrich, UK
TrypLE® Express	Life Technologies, UK
Vectashield® mounting medium containing 4',6-diamidino-2-phenylindole (DAPI)	Vector Laboratories, UK
Yellow zein	Sigma-Aldrich, UK
3-(4,5-dimethylthiazol-2-yl)-2,5-diphenyl-tetrazolium bromide (MTT)	Sigma-Aldrich, UK

4.4 Methods

4.4.1 Optimisation of production parameters

4.4.1.1 Microfluidic system

The preparation of zein nanoparticles using microfluidic mixing on a NanoAssemblr™ Benchtop (Precision NanoSystems Inc., Vancouver, Canada) was adapted from van Ballegooie *et al*. (2019) with some modifications. Briefly, zein (5-30 mg) was dissolved in 1 mL of ethanol (80% v/v) (forming 0.5-3% w/v solution) and stirred at 700 rpm overnight at 25ºC. The zein solution was filtered through a 13-mm syringe filter (0.8 µm) to remove any large particulates. Subsequently, CR6 (0.02-0.1% w/w of zein) was added to the filtered zein solution and the mixture was stirred at 400 rpm for 1 h at 37ºC. The mixing process took place in a microfluidic cartridge with staggered herringbone structures, which has two inlets: one for the organic phase and the other for the aqueous phase. The CR6-zein solution was loaded into a syringe (1 mL) as the organic phase in the right inlet channel, while the aqueous phase (Milli-Q® water) was loaded into a 3 mL syringe in the left inlet channel (**Figure 4-1**). The samples were run at various total flow rates (TFR) (0.5, 2, and 6 mL/min) and flow rate ratios (FRR) between the water and the zein phase (1:1, 3:1, and 5:1). The mixing process was carried out at room temperature. The nanoparticles were collected at the microfluidic chip's outlet channel. Each run was programmed to discard the first 0.35 mL and the last 0.05 mL of the sample to ensure that the variability in fluid dynamics at the start and end of the synthesis run did not affect the sample. The collected samples were placed in a 50ºC room to anneal for 1.5 h to enable CR6 loading into the nanoparticles. Samples (1 mL) were then transferred to 1.5 mL Eppendorf tubes and purified by one cycle of centrifugation (1000 g, 10 min, 25ºC) to remove ethanol and

free CR6. Pellets were resuspended in 1 mL Milli-Q® water and were left to settle at room temperature (20ºC) for 1 h before analysis.

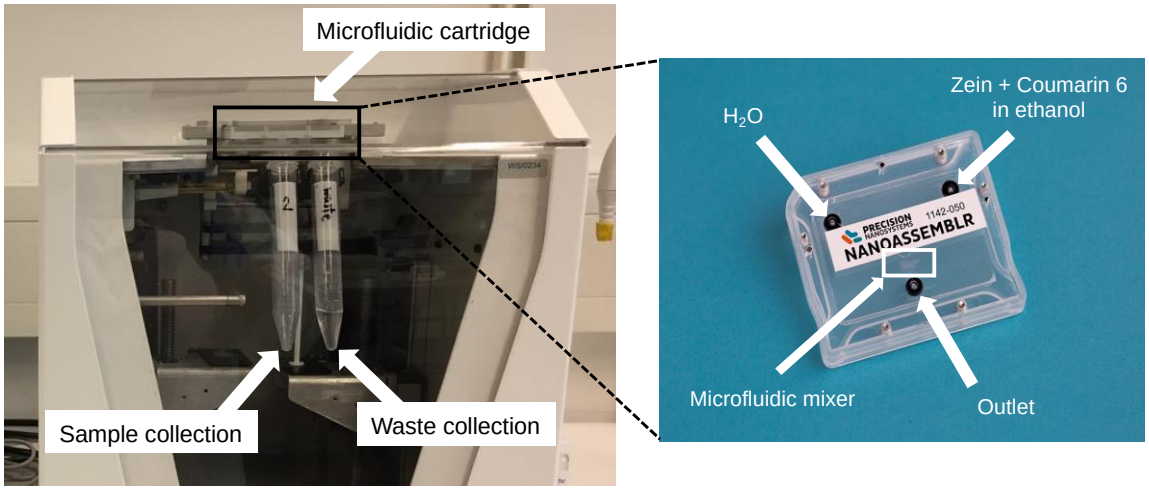

Figure 4-1. Zein nanoparticles manufacture using a microfluidic cartridge coupled with a NanoAssemblr™ device.

4.4.1.2 Nanoprecipitation method

Zein (10 mg) was dissolved in 2 mL of ethanol (80% v/v) (forming 0.5% w/v solution) and stirred at 700 rpm at 25ºC overnight. The zein solution was filtered through a 13-mm syringe filter (0.8 µm). Next, 0.01 mg CR6 (5 µL from CR6 stock solution (2 mg/mL in DMSO)) was added to the solution (making CR6 loading at 0.1% w/w of zein) and the mixture was stirred at 400 rpm for 1 h at 37ºC. Zein nanoparticles were then formed either 1) by dropwise addition of organic phase (zein + CR6 solution) to aqueous phase (Milli-Q® water) (**Method 1**) or 2) by dropwise addition of aqueous phase (Milli-Q® water) to organic phase (zein + CR6 solution) (**Method 2**) (**Figure 4-2**). The addition of one phase to the other was carried out under stirring at 700 rpm. The volume ratio of aqueous to organic phase was varied from 1:1 to 5:1. The

nanoparticles were placed at 50°C to anneal for 1.5 h and were then pelleted by one cycle of centrifugation at 1000 g for 10 min at 25ºC. Pellets were resuspended in 1 mL Milli-Q® water and were left to settle at room temperature for 1 h before analysis.

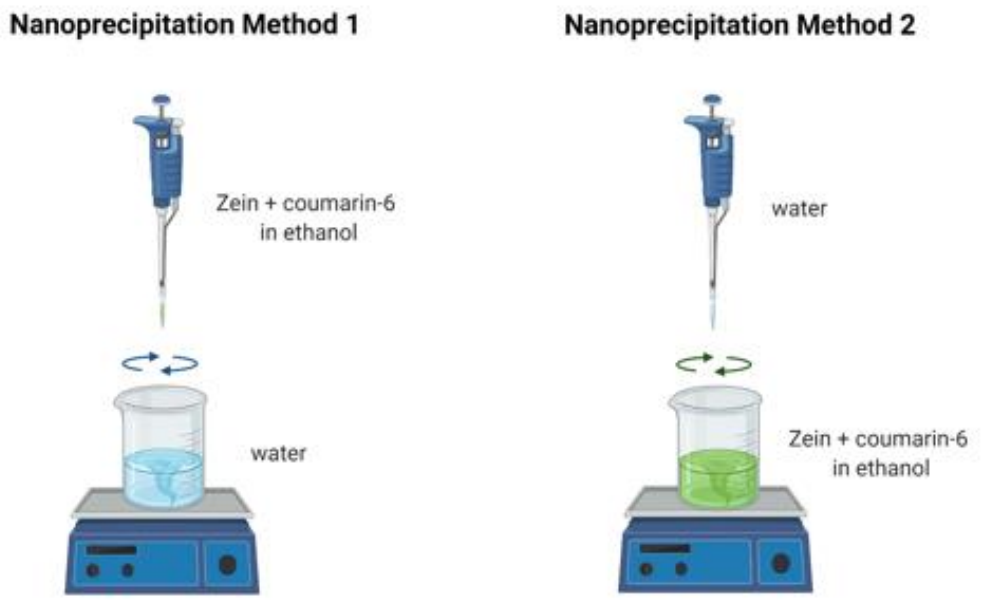

Figure 4-2. Nanoprecipitation methods used to prepare zein nanoparticles. Nanoparticles were formed either by addition of the organic phase to the aqueous phase (**Method 1**) or by addition of the aqueous phase to the organic phase (**Method 2**). This figure was created with Biorender.com.

4.4.2 Preparation of zein nanoparticles

4.4.2.1 Microfluidics

Zein solution (0.5% w/v in 80% ethanol) was stirred at 400 rpm at 25ºC overnight before being filtered through a 13-mm syringe filter (0.8 µm). Subsequently, CR6 (0.1% w/w of zein) was added and the mixture was stirred at 200 rpm for 3 h at 37ºC. The FRR between the water and the zein phases was 5:1 and the TFR was 6 mL/min. The mixing process was carried out at room temperature. The nanoparticles were

collected at the microfluidic chip's outlet channel. The pH of the resultant nanoparticles was increased to 10 by the addition of NaOH (1 N) to allow the nanoparticles to be resuspended after centrifugation. The nanoparticles were pelleted following one cycle of centrifugation (10,000 g, 1 h, 20ºC) to remove ethanol and free CR6. Pellets were resuspended in 1 mL Milli-Q® water and were left to settle at room temperature for 1 h before analysis.

4.4.2.2 Nanoprecipitation

Zein and CR6 solution were prepared and mixed using the same protocol as described in 4.4.2.1. Nanoparticles were produced by nanoprecipitation method as described in 4.4.1.2. The volume ratio of aqueous to organic phase was 5:1. The resultant nanoparticle suspension was adjusted to pH 10 and purified as described in 4.4.2.1.

4.4.3 Preparation of mPEG-zein nanoparticles entrapping CR6

mPEG-zein nanoparticles were prepared from mPEG-zein conjugates (see detailed in Chapter 2) by nanoprecipitation Method 2, as described above in Section 4.4.2.2.

4.4.4 Nanoparticle characterisation

4.4.4.1 Nanoparticle morphology

The morphology of the prepared nanoparticles was assessed by TEM, using a JEOL JEM-1200EX® transmission electron microscope (Jeol, Tokyo, Japan) operating at an accelerating voltage of 80 kV. Each sample was diluted at 1/5 using distilled water before being drop cast (3 μL) onto a carbon-coated copper grid (400 mesh size) and was air-dried overnight before imaging.

4.4.4.2 Determination of particle diameter, size distribution, and zeta potential

The size, PDI, and zeta potential of zein, mPEG5K-zein (0.5:1), mPEG5K-zein (1:1), and mPEG10K-zein nanoparticles loading CR6 were measured by photon correlation spectroscopy and laser Doppler electrophoresis, using a Malvern Zetasizer Nano-ZS® at 25°C (Malvern Instruments Ltd, Malvern, UK). All samples were diluted with Milli-Q® water to the desired concentration (at 1/5 for samples prepared by microfluidics, 1/10 for samples prepared by nanoprecipitation) up to 1 mL before measurement.

4.4.4.3 CR6 encapsulation efficiency

CR6-loaded zein/mPEG-zein nanoparticles (50 µL) were dissolved in 950 µL methanol and centrifuged at 9300 g for 15 min at room temperature using an IEC Micromax® centrifuge (Thermo Scientific, Loughborough, UK). The amount of CR6 entrapped in the nanoparticles was quantified by spectrofluorometry (λ_{exc}: 456 nm, λ_{em}: 500 nm, slit widths: 5 nm), using a Varian Cary Eclipse® spectrofluorometer (Agilent Technologies, Santa Clara, CA). The encapsulation efficiency (EE) was calculated as follows:

$$\text{EE (\%)} = \frac{\text{Amount of CR6 in the nanoparticles} \times 100}{\text{Amount of CR6 used for the preparation of nanoparticles}}$$

4.4.4.4 Nanoparticle yield

The amount of zein before and after nanoparticle preparation was determined by Lowry assay, as previously reported (Dufès *et al*., 2000). Briefly, 1 mL of potassium sodium tartrate solution (2% w/v in distilled water) and 1 mL of copper sulphate solution (1% w/v in distilled water) were added dropwise into 50 mL of sodium

carbonate solution (2% w/v in 0.1 N NaOH) (under continuous stirring to avoid precipitation) to make up solution A. Bovine serum albumin (BSA) was used as a standard protein solution (concentration ranging from 5 to 500 µg/mL). One hundred microlitres of nanoparticle samples (diluted 1/10 in distilled water) or BSA standard solutions was mixed with 1 mL of solution A and incubated at room temperature for 10 min. Subsequently, 100 µL of 1 N Folin Ciocalteu's reagent was added to these samples (with immediate vortexing), followed by incubation at room temperature for 30 min (protected from light). The absorbance of each sample was measured at 750 nm using an Agilent Varian Cary® 50 UV-Vis spectrophotometer (Agilent Technologies, Santa Clara, CA). BSA (0 µg/mL) was used as the reference cell to set zero. The experiment was done in triplicates. The amount of zein was calculated by correlating the absorbance of each sample with the standard curve of BSA. The particle yield was calculated as follows:

$$\text{Yield (\%)} = \frac{\text{Amount of zein in the nanoparticles} \times 100}{\text{Amount of zein used for the preparation of nanoparticles}}$$

4.4.5 Stability study

The stability of zein and mPEG-zein formulations (prepared in 4.4.2.2 and 4.4.3) was assessed by measuring particle size on a Malvern Zetasizer Nano-ZS® at specific time points (Days 0, 7, 14, 21, and 28). All samples were kept in glass vials under storage condition at 4°C for 4 weeks (protected from light). Each sample (100 µL) was diluted with Milli-Q® water up to 1 mL before size measurement at 25°C.

4.4.6 *In vitro* analysis

4.4.6.1 Cellular uptake

4.4.6.1.1 Qualitative analysis

Imaging of the cellular uptake of CR6 loaded in zein and mPEG-zein nanoparticles was conducted using confocal microscopy. B16-F10-luc-G5 cells were seeded on coverslips in 6-well plates (1 x 10^5 cells/well) and allowed to adhere overnight. They were then treated with CR6 (1 µg per well), either loaded in zein/mPEG-zein nanoparticles or in solution. After 2-h incubation, cells were washed twice with 3 mL PBS before being fixed with 2 mL formaldehyde solution (4%) for 10 min. Cells were permeabilised with 2 mL Triton-X 100 solution (0.1% v/v in PBS) for 10 min, before a further incubation with 3 mL BSA (1% w/v in PBS) for 30 min to reduce non-specific binding. Cells were stained with Alexa Fluor® 647 dye (one unit of dye diluted in 200 µL PBS) for 30 min to visualise cell membranes, before a final wash with 3 mL PBS. After staining, they were mounted in Vectashield® containing DAPI for nuclei staining. The cells were examined using a Leica TCS SP8® confocal microscope (Wetzlar, Germany) at x63 magnification (zoom factor of 1.25). DAPI was excited with the 405 nm laser line (emission bandwidth: 415-491 nm), Alexa Fluor® 647 was excited with the 633 nm laser line (emission bandwidth: 645-710 nm), and CR6 was excited with the 488 nm laser line (emission bandwidth: 515-558 nm).

4.4.6.1.2 Quantitative analysis

The quantification of the cellular uptake of CR6 loaded in zein/mPEG-zein nanoparticles was carried out by flow cytometry. B16-F10-luc-G5 cells were seeded into 6-well plates at a density of 2 x 10^5 cells/well and allowed to grow at 37°C for 24

h, before being treated with CR6 (50 ng per well), either loaded in zein/mPEG-zein nanoparticles or in solution. After 2-h incubation, adherent cells were washed and detached (using 200 µL TrypLE® Express and 400 µL complete medium per well). The mean fluorescence intensity (MFI) of CR6 taken up by the cells was analysed by an Attune NxT® flow cytometer (Thermo Fisher Scientific, Waltham, MA), counting 10,000 cells (gated events) for each sample.

4.4.6.1.3 Mechanisms of cellular uptake

The mechanisms involved in the cellular uptake of CR6 loaded in zein/mPEG-zein nanoparticles were investigated using various uptake inhibitors. B16-F10-luc-G5 cells were seeded as described in 4.4.6.1.2. After removal of the medium, the cells were pre-incubated with endocytosis inhibitors chlorpromazine (10 µg/mL), filipin (4 µg/mL), and colchicine (40 µg/mL) for 30 min. The treatments were then removed and replaced with co-incubation of CR6-loaded zein/mPEG-zein nanoparticles (50 ng CR6 per well) with the same concentration of each inhibitor for another 2 h. The cells were then washed and processed for flow cytometry analysis as previously described.

4.4.7 Statistical analysis

The results were expressed as means ± SEM unless stated otherwise. Statistical analysis was assessed by one-way analysis of variance (ANOVA) followed by Tukey multiple comparison post-test and unpaired *t*-test was performed for paired comparisons (Minitab® software, State College, PE) at a significance level of 0.05.

4.5 Results

4.5.1 Optimisation of production parameters

4.5.1.1 Microfluidic system

In order to determine the critical parameters during microfluidic manufacture, zein nanoparticles encapsulating CR6 were screened for the effect of zein concentration and CR6 loading on particle size, PDI, zeta potential, and EE. In this study, ethanol 80% v/v was used as the organic phase for zein and CR6, as a result of previous work done by van Ballegooie *et al*. (2019). Results in **Table 4-1** show a gradual trend of increasing particle size (140.20 ± 2.51 nm to 171.57 ± 4.02 nm) as the zein concentration increased. All nanoparticles obtained were uniform (PDI < 0.1) and exhibited cationic surface charges. CR6 EE was in the range of 10-15%. The smallest size and highest EE was observed from zein concentration of 0.5% w/v. CR6 loading had a minimal effect on the particle size but does not seem to affect the PDI, surface charge, and EE. All of the nanoparticles produced displayed size between 150 and 160 nm, PDI lower than 0.1, positive zeta potential values, and EE of approximately 10%. Hence, CR6 loading at 0.1% w/w of zein was selected to prepare the nanoparticles as it gave a maximum drug loading without compromising the properties of the resulting nanoparticles.

Table 4-1. Characteristics of zein nanoparticles synthesised in the microfluidic Y-junction and the effect of various experimental parameters used in this work. Results represent mean ± SD of triplicate readings.

Parameters		Size (nm)	PDI	Zeta potential (mV)	EE (%)
Zein (% w/v)	0.5	140.20 ± 2.51	0.07 ± 0.01	25.70 ± 1.61	14.50 ± 0.15
	1	153.07 ± 2.95	0.07 ± 0.01	30.97 ± 0.06	11.19 ± 0.35
	2	158.10 ± 1.57	0.06 ± 0.02	30.70 ± 0.87	12.66 ± 0.62
	3	171.57 ± 4.02	0.04 ± 0.03	34.53 ± 0.95	10.38 ± 0.47
CR6 loading	0.02	157.47 ± 1.20	0.06 ± 0.01	25.70 ± 0.30	10.81 ± 0.16
(% w/w)	0.05	151.17 ± 0.45	0.05 ± 0.02	27.33 ± 0.81	10.06 ± 0.07
	0.1	152.07 ± 0.75	0.08 ± 0.03	25.47 ± 0.87	10.25 ± 0.17
Flow Rate Ratio	1:1	Aggregation			
(FRR)	3:1	151.17 ± 0.45	0.05 ± 0.02	27.33 ± 0.81	10.06 ± 0.07
	5:1	92.57 ± 0.61	0.16 ± 0.01	20.00 ± 1.45	5.50 ± 0.05
Total Flow Rate	0.5	211.57 ± 4.17	0.13 ± 0.04	34.63 ± 0.40	7.80 ± 0.33
(TFR)	2	165.10 ± 5.31	0.09 ± 0.04	32.17 ± 0.47	6.80 ± 0.10
	6	158.10 ± 1.57	0.06 ± 0.02	30.70 ± 0.87	12.66 ± 0.62

The effect of microfluidic operating parameters, including FRR and TFR, was also investigated. The FRR between aqueous and organic phases was found to impact nanoparticle characteristics. While the TFR was fixed at 6 mL/min, nanoparticles were aggregated after centrifugation when a FRR of 1:1 was applied. As the FRR increased from 3:1 to 5:1, there was a significant decrease in particle size (151.17 ± 0.45 nm to 92.57 ± 0.61 nm) and EE (10.06 ± 0.07% to 5.50 ± 0.05%). Thus, a 3:1 FRR provided

the best zein nanoparticles in term of size and EE. Nanoparticles were also assessed for their size and ability to entrap CR6 across manufacturing flow rate speeds between 0.5-6 mL/min. Following manufacture at 3:1 FRR, particle size decreased as the speed increased. The size of the nanoparticles was largest at a TFR of 0.5 mL/min (211.57 ± 4.17 nm) and decreased significantly to 165.10 ± 5.31 nm when the TFR was increased to 2 mL/min. The nanoparticles produced using TFR at 6 mL/min exhibited the smallest size (158.10 ± 1.57 nm) and highest EE (~13%). Zeta potentials were found to be between 30-35 mV across all three TFRs.

Because of their small size and high EE, the most optimal parameters for CR6-loaded zein nanoparticles produced using a Y-junction microfluidic system were therefore a zein concentration of 0.5% w/v, a CR6 loading of 0.1% w/w, a 3:1 FRR, and a TFR of 6 mL/min.

4.5.1.2 Nanoprecipitation method

Before comparing microfluidic and manual approaches for the production of CR6-loaded zein nanoparticles, it is crucial to determine the preparation method and volume ratio of aqueous to organic phase for the nanoprecipitation process, while controlling other formulation parameters, including zein concentration and CR6 loading, that could influence nanoparticle physicochemical attributes. Thus, the effects of mixing process and aqueous to organic phase volume ratio on nanoparticle characteristics were tested under the same conditions (0.5% w/v zein concentration, 0.1% w/w CR6 loading). As shown in **Table 4-2**, the mixing process significantly affected the size and EE of the particles. Method 1, where zein solution was added to water, showed a trend of decreasing particle size (from 675.83 ± 36.32 nm to 60.50 ± 0.68 nm) when

aqueous to organic phase volume ratio increased from 1:1 to 5:1. The EEs were very low across all the volume ratios tested (2-5%). For Method 2, nanoparticles were produced by dropwise addition of water to zein solution. When volume ratios of 1:1 and 2:1 were applied, large levels of aggregation were observed after centrifugation. At the volume ratio above 2:1, Method 2 generated large nanoparticles (340-540 nm) with significantly improved EEs (about 55-65%) when the volume ratios were matched with Method 1. Although increasing aqueous:organic phase volume ratio from 4:1 to 5:1 decreased EE (64.01 ± 1.02% to 55.60 ± 0.39%), it significantly reduced the size of the particles (388.10 ± 4.36 nm to 343.93 ± 13.61 nm). Therefore, nanoprecipitation Method 2 at 5:1 aqueous to organic volume ratio was selected for producing zein nanoparticles.

Table 4-2. Characteristics of zein nanoparticles prepared by nanoprecipitation method optimised by variation of the following parameters: preparation method and volume ratio of aqueous to organic phase. Results represent mean ± SD of triplicate readings.

Method	Aqueous to organic phase volume ratio	Size (nm)	PDI	Zeta potential (mV)	EE (%)
Method 1	1:1	675.83 ± 36.32	0.22 ± 0.08	41.43 ± 0.40	4.94 ± 0.20
	2:1	165.90 ± 1.81	0.07 ± 0.03	34.20 ± 1.37	4.10 ± 0.09
	3:1	104.80 ± 1.73	0.09 ± 0.02	34.03 ± 2.22	3.56 ± 0.12
	4:1	70.20 ± 0.62	0.24 ± 0.02	32.80 ± 2.72	2.17 ± 0.02
	5:1	60.50 ± 0.68	0.25 ± 0.02	35.57 ± 3.12	2.03 ± 0.01
Method 2	1:1	Aggregation			
	2:1	Aggregation			
	3:1	538.73 ± 13.22	0.03 ± 0.03	30.50 ± 0.46	56.09 ± 1.93
	4:1	388.10 ± 4.36	0.24 ± 0.02	31.07 ± 0.76	64.01 ± 1.02
	5:1	343.93 ± 13.61	0.27 ± 0.01	27.80 ± 0.26	55.60 ± 0.39

4.5.2 Impact of manufacturing method on zein nanoparticle characteristics

To compare microfluidic versus manual manufacturing, the volume of water to zein phase at 5:1 was selected as a result of the nanoparticles of acceptable size with high EE obtained from nanoprecipitation Method 2 in 4.5.1.2. Hence, a FRR at 5:1 and a TFR of 6 mL/min were applied for microfluidic production. In addition, the pH of nanoparticle suspension was increased to 10 to stabilise the nanoparticles before high speed centrifugation (10,000 g). As shown in **Figure 4-3,** TEM images revealed the presence of spherical-shaped nanoparticles, demonstrating a successful production of

CR6-loaded zein nanoparticles by both microfluidic and manual methods. The size of the zein nanoparticles was dependent on the manufacturing approaches.

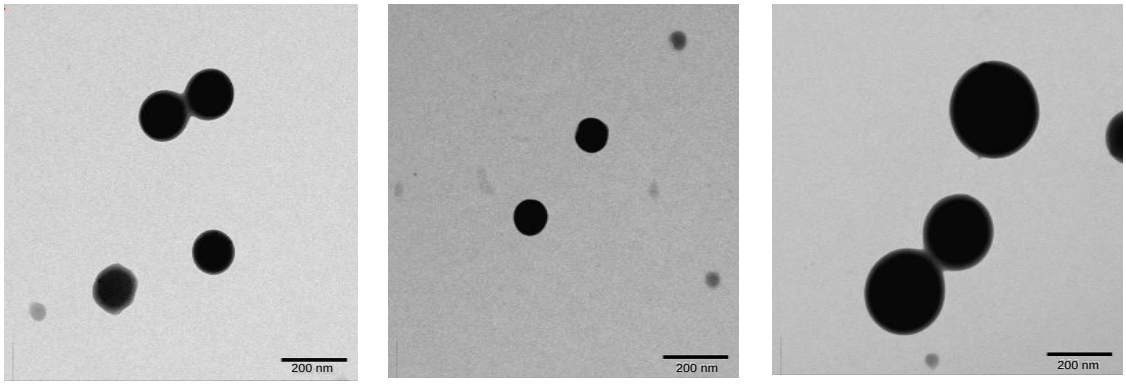

Figure 4-3. Morphology of CR6-loaded zein nanoparticles using TEM (scale bar: 200 nm).

This was further confirmed by DLS measurements. The size of zein nanoparticles ranged from 98 to 243 nm, with narrow size distributions (PDI ~0.1) following preparation with all three manufacturing methods. The nanoparticles displayed a negative surface charge (about -26 mV), independently of the preparation method used (**Figure 4-4**). The CR6 EEs of the nanoparticles prepared by microfluidics, nanoprecipitation Method 1, and nanoprecipitation Method 2 were 29.72 ± 0.61%, 24.67 ± 2.60%, and 68.92 ± 1.91%, respectively.

Nanoparticles produced by microfluidic manufacturing, compared to nanoprecipitation Method 1 (addition of the organic phase to the aqueous phase), displayed no statistical differences in size, PDI, surface charge, or EE. Although the particle size (115.26 ± 6.55 nm for microfluidics and 98.29 ± 1.97 nm for

nanoprecipitation Method 1) was optimal for cancer drug delivery, these 2 methods gave low yields and EEs. Microfluidic manufacturing, however, seem to be superior over the nanoprecipitation Method 1, as the yield increased from 22.80 ± 2.28% when using nanoprecipitation Method 1 to 29.84 ± 1.58% when using microfluidics. Although the nanoprecipitation Method 2 (addition of water to the organic phase) generated the largest particle size (242.77 ± 1.97 nm), it showed a significantly improved EE (68.92 ± 1.91%) and yield (62.21 ± 1.39%) when compared to the other two methods. Among the three manufacturing approaches, nanoprecipitation Method 2 was therefore the best method for the preparation of zein nanoparticles entrapping CR6 for subsequent studies.

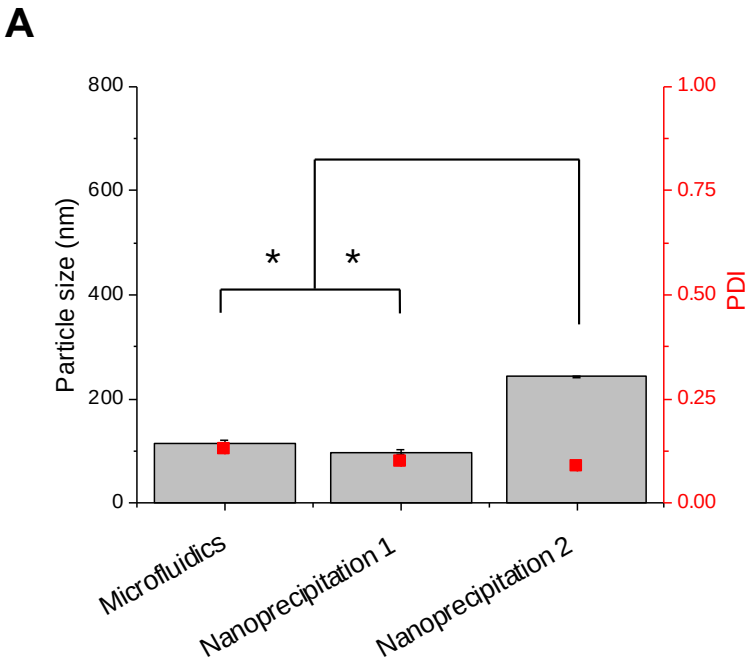

B

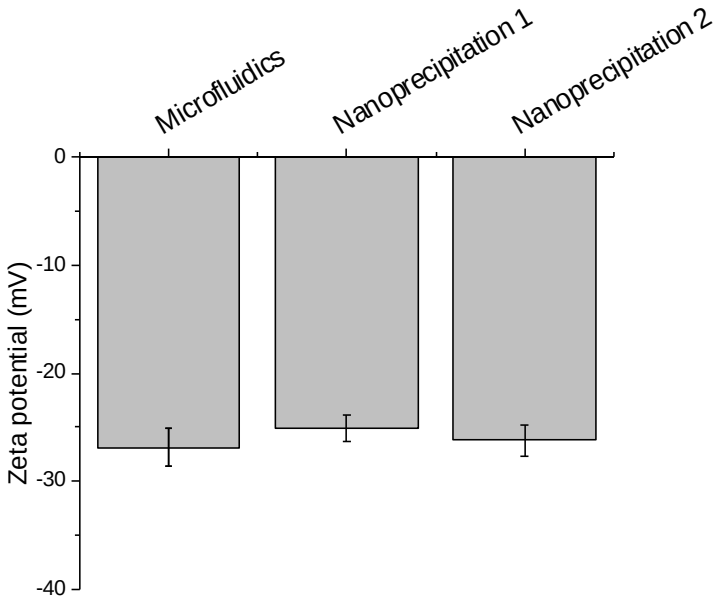
Microfluidics
Nanoprecipitation 1
Nanoprecipitation 2
Zeta potential (mV)
0
-10
-20
-30
-40

C

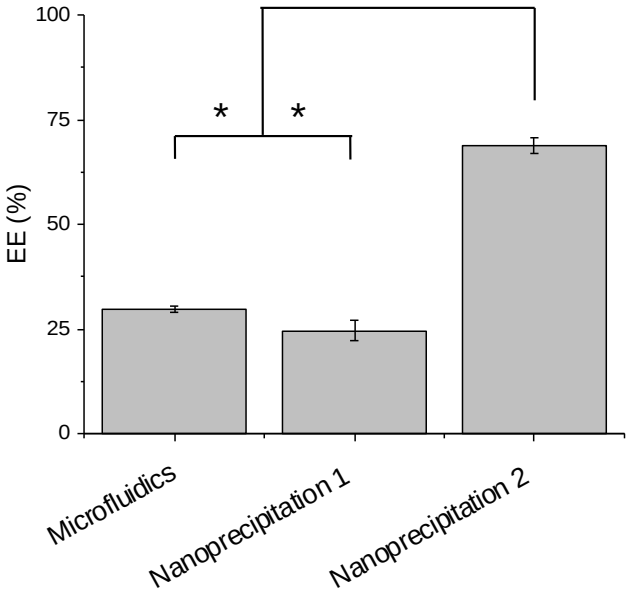
EE (%)
100
75
50
25
0
*
*
Microfluidics
Nanoprecipitation 1
Nanoprecipitation 2

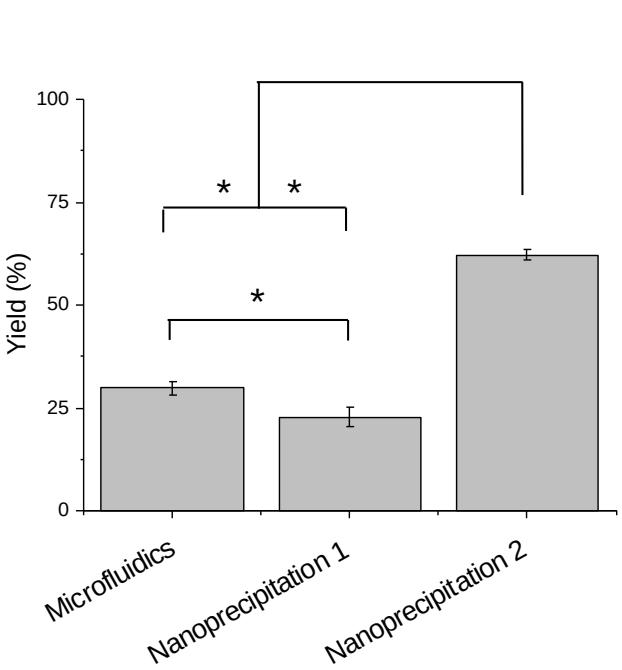

Figure 4-4. Size and polydispersity index (PDI) (A), zeta potential (B), encapsulation efficiency (EE) (C), and yield (D) of CR6-loaded zein nanoparticles (*: $P < 0.05$). Results represent mean ± SEM of 3 samples.

4.5.3 Characterisation of PEGylated zein nanoparticles entrapping CR6

The morphology of PEGylated zein nanoparticles produced by nanoprecipitation Method 2 was visualised using TEM **(Figure 4-5)**. The nanoparticles were spherical in shape. The size of mPEG5K-zein formulations appeared to be much smaller than that of their 10K counterpart and the control zein.

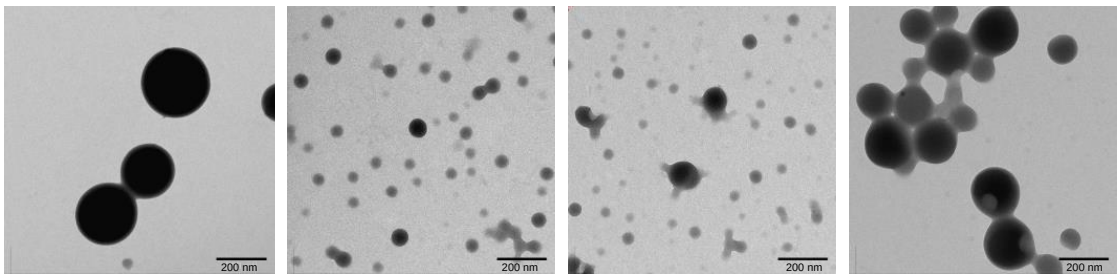

Zein | mPEG5K-zein (0.5:1) | mPEG5K-zein (1:1) | mPEG10K-zein

Figure 4-5. Unstained TEM images of zein, mPEG5K-zein (0.5:1), mPEG5K-zein (1:1), and mPEG10K-zein nanoparticles. All nanoparticles were prepared using nanoprecipitation Method 2 (scale bar: 200 nm).

The hydrodynamic diameter, PDI, zeta potential, and EE of zein and mPEG-zein nanoparticles are summarised in **Table 4-3**. PEGylation significantly decreased the size of zein nanoparticles. At constant PEG chain length (5K), the particle size slightly decreased when PEG concentration was doubled. When nanoparticles were prepared with constant PEG to zein molar ratio (mPEG5K-zein (0.5:1) versus mPEG10K-zein), their size increased with increasing the chain length. All formulations showed a monodisperse size distribution. Both zein and mPEG-zein nanoparticles displayed a negative surface charge: with a zeta potential of -26 mV for zein and less negative zeta potential values (ranging from -17 to -12 mV) for PEGylated systems. The EE of CR6 in zein-based nanoparticles was dependent on parameters including nanoparticle composition and PEG content. PEGylation of the nanoparticles resulted in a lower CR6 entrapment. Among PEGylated systems, mPEG10K-zein displayed the highest EE, followed by mPEG5K-zein (0.5:1) and mPEG5K-zein (1:1), respectively.

Table 4-3. Characteristics of zein and mPEG-zein nanoparticles prepared by nanoprecipitation Method 2. Results represent mean ± SEM of 3 samples.

Formulations	Size (nm)	PDI	Zeta potential (mV)	EE (%)
Zein	242.77 ± 1.97	0.09 ± 0.01	-26.17 ± 1.42	68.92 ± 1.91
mPEG5K-zein (0.5:1)	138.55 ± 1.84	0.12 ± 0.01	-12.38 ± 0.60	50.95 ± 1.46
mPEG5K-zein (1:1)	133.27 ± 1.71	0.11 ± 0.00	-16.55 ± 0.93	35.62 ± 0.88
mPEG10K-zein	197.30 ± 3.19	0.02 ± 0.00	-13.92 ± 0.42	58.35 ± 3.90

4.5.4 Stability of zein and mPEG-zein nanoparticles

The size of the zein nanoparticles (242.77 ± 1.97 nm at Day 0) was stable for 2 weeks, but significantly increased from Day 15 to reach 929.92 ± 277.90 nm at Day 28 **(Figure 4-6**). PEGylation, however, was shown to improve the stability of the zein nanoparticles, as PEGylated formulations were found to be stable for at least 4 weeks when stored at 4°C. Their sizes remained unchanged (from 138.55 ± 1.84 nm at Day 0 to 137.42 ± 2.04 nm at Day 28 for mPEG5K-zein (0.5:1) and from 133.27 ± 1.71 nm at Day 0 to 131.35 ± 1.18 nm at Day 28 for mPEG5K-zein (1:1)). In the case of mPEG10K-zein nanoparticles, their size increased slightly from 197.30 ± 3.19 nm at Day 0 to 207.85 ± 6.82 nm and 222.82 ± 12.83 nm at Days 14 and 21, respectively, before dropping to 197.03 ± 2.92 nm at Day 28. However, there was no statistical difference in the size increases at Days 14 and 21.

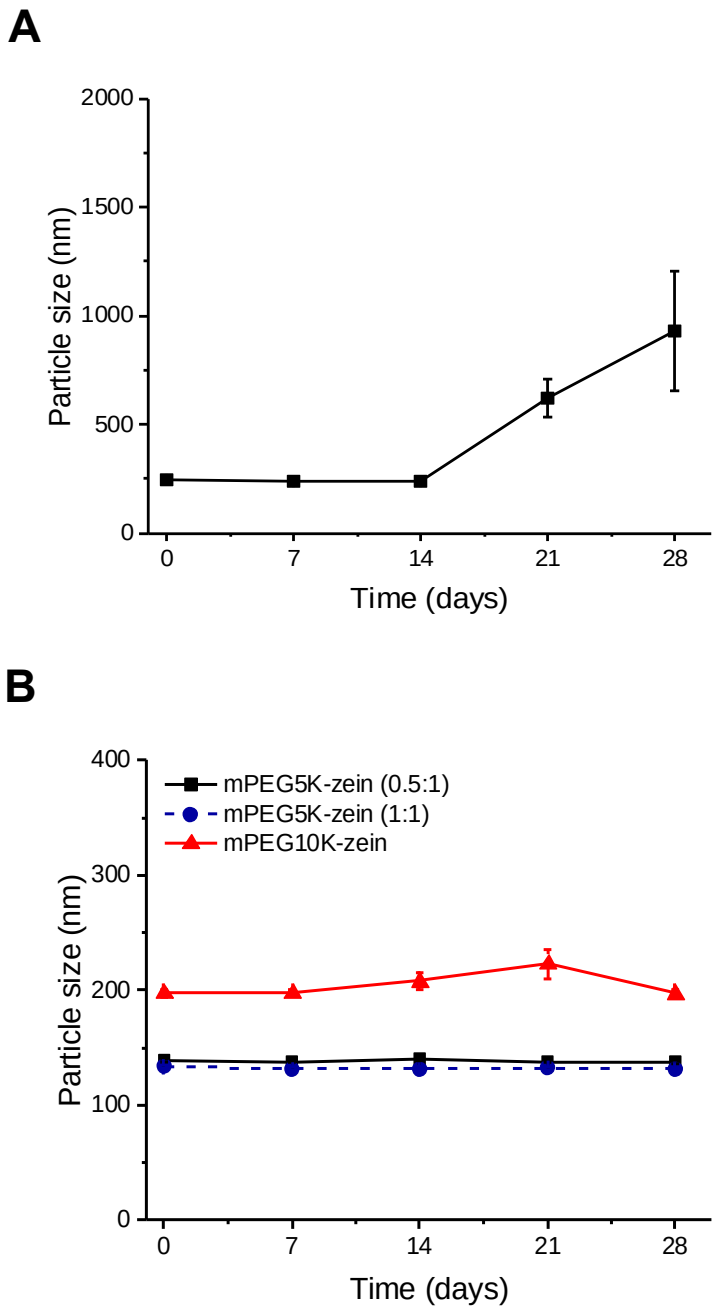

Figure 4-6. Stability of zein (A) and mPEG-zein (B) nanoparticles loading CR6 after storage at 4°C for 4 weeks. Results represent mean ± SEM of 3 samples. Nanoparticles were prepared by nanoprecipitation Method 2. Error bars are smaller than the symbols when not visible.

4.5.5 Cellular uptake

The uptake of zein-based nanoparticles encapsulating CR6 by B16-F10-luc-G5 melanoma cancer cells was qualitatively evaluated using confocal microscopy (**Figure 4-7**). Following 2-h incubation, zein and mPEG-zein nanoparticles were able to deliver CR6 into the cells. PEGylation of the nanoparticles led to a lower cellular uptake than that observed with non-PEGylated formulation. Fluorescent CR6 was predominantly localised in the cytoplasm of the cells after treatment with all nanoparticle formulations. It was also found to be co-localised in the nuclei following treatment with mPEG-zein formulations, unlike zein nanoparticles. CR6 accumulation in the cells was higher after treatment with CR6 solution than the nanoparticles.

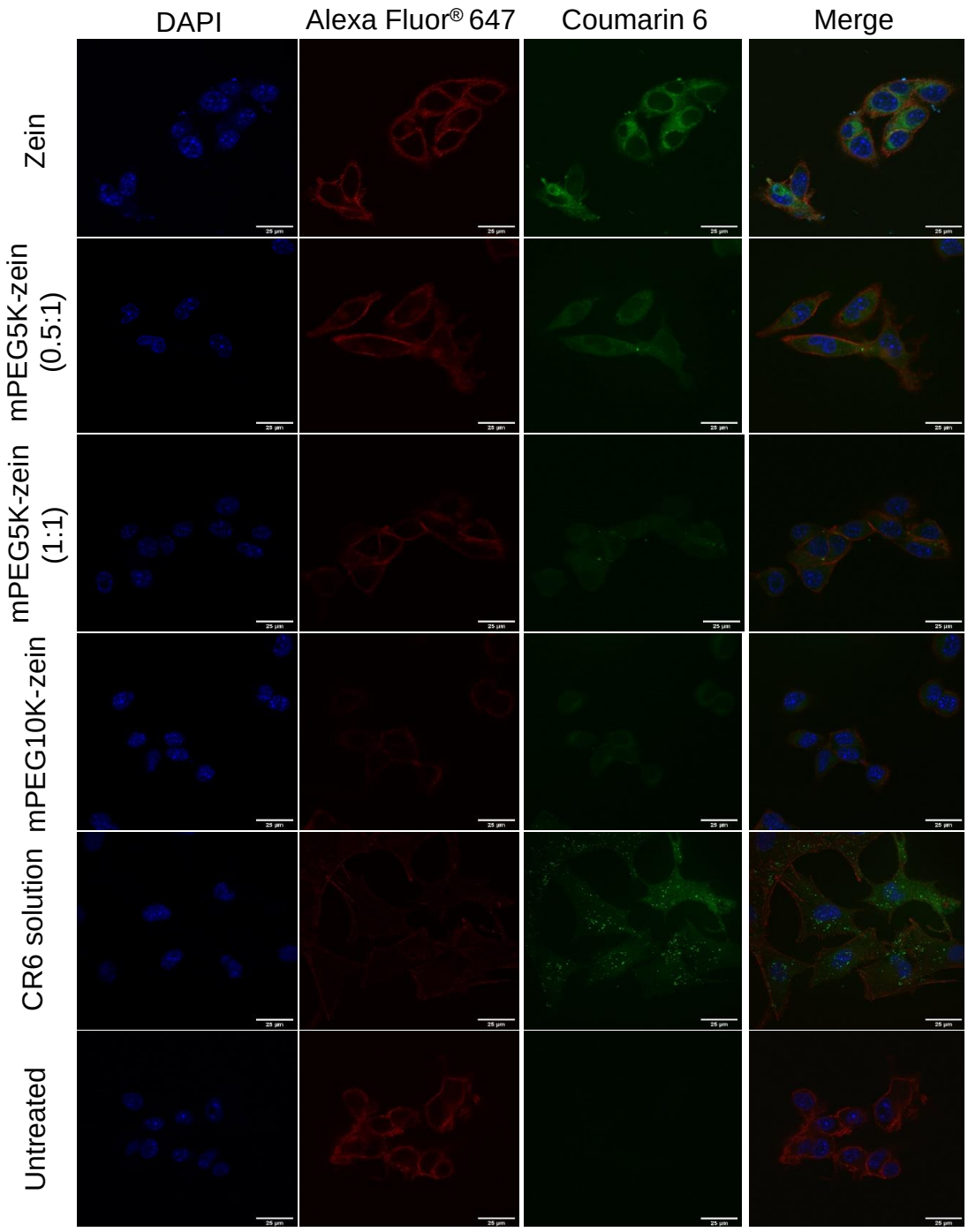

Figure 4-7. Confocal images of the cellular uptake of CR6 loaded in zein and mPEG-zein nanoparticles, or as a solution, in B16-F10-luc-G5 cells (scale bar: 25 µm).

The cellular uptake was also quantitatively confirmed by flow cytometry (**Figure 4-8**). The highest cellular fluorescence of CR6 was observed following treatment with CR6 solution (MFI 6047 ± 187 a.u.), which was 1.3-fold higher than that obtained with zein nanoparticles (MFI 4602 ± 148 a.u.). PEGylation significantly decreased the uptake of the zein nanoparticles. Among PEGylated formulations, mPEG5K-zein (0.5:1) was more efficacious in delivering CR6 into the cells by 1.3-fold and 1.7-fold in comparison with mPEG5K-zein (1:1) and mPEG10K-zein, respectively. These results indicate that PEGylation with a shorter PEG chain length and less PEG density led to higher nanoparticle uptake by the cells.

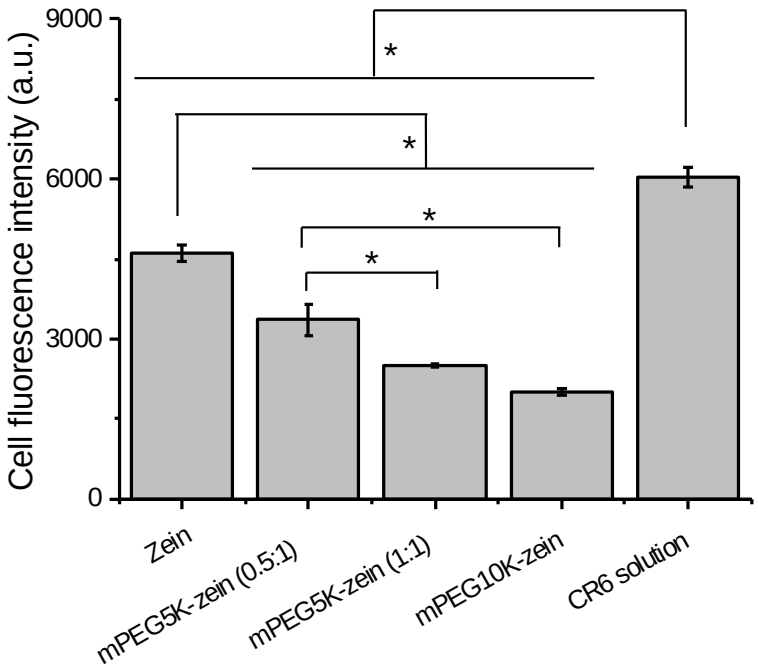

Figure 4-8. Flow cytometry analysis of the cellular uptake of CR6 loaded in zein and mPEG-zein nanoparticles, or as a solution (a.u.: arbitrary units) (*: $P < 0.05$). Results represent mean ± SEM of 3 independent experiments.

4.5.6 Mechanisms of cellular uptake

To investigate the cellular uptake mechanism of zein-based nanoparticles, B16-F10-luc-G5 cells were treated with CR6-loaded zein/mPEG-zein nanoparticles in the presence of various endocytosis inhibitors. The pre-treatment of the cells with chlorpromazine and colchicine significantly decreased the cellular uptake of all nanoparticle formulations (**Figure 4-9**). Chlorpromazine, however, inhibited zein-based nanoparticle uptake more than colchicine (by 10-15% with chlorpromazine versus 6-13% with colchicine), indicating that clathrin-mediated endocytosis was the primary route of internalisation. Macropinocytosis was also involved in the cellular uptake to a lesser extent. Filipin decreased the cellular uptake of the zein nanoparticles by about 4%, but did not affect the uptake of their PEGylated counterparts. This suggested that caveolae-mediated endocytosis was involved in the cellular uptake of zein nanoparticles, but did not participate in the uptake of the mPEG-zein formulations. As a result, the cellular uptake of zein nanoparticles involved all three endocytosis pathways, while the cellular uptake mechanisms of PEGylated zein nanoparticles were clathrin-mediated and macropinocytosis-mediated endocytosis.

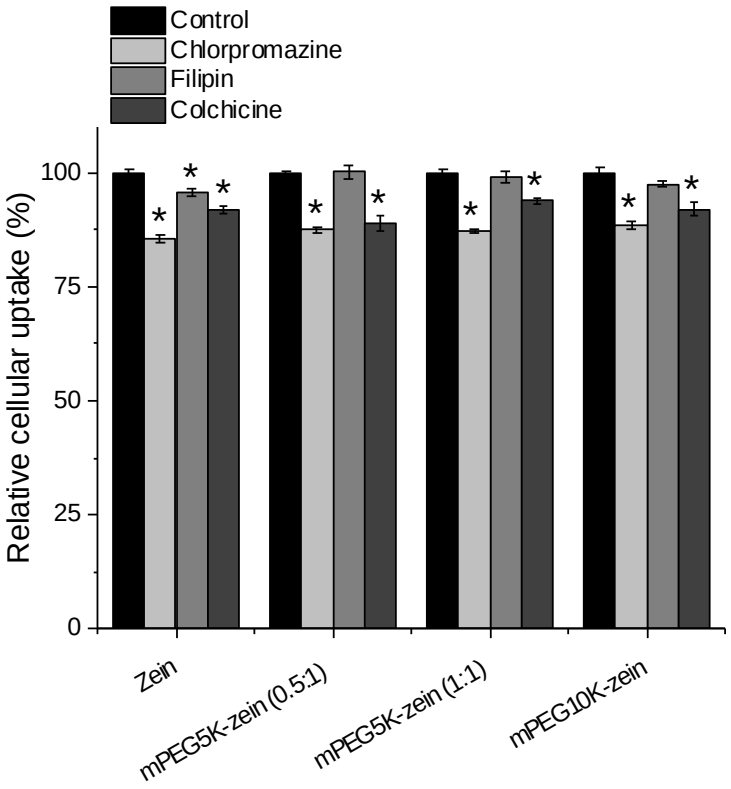

Figure 4-9. Effects of endocytosis inhibitors on the cellular uptake of CR6-loaded zein/mPEG-zein nanoparticles (*: $P < 0.05$, compared with control of each system). Results represent mean ± SEM of 3 independent experiments.

4.6 Discussion

Due to different solubilities of zein in ethanol and water, zein nanoparticles loaded with various active compounds can be produced using nanoprecipitation. The supersaturation of zein occurs when the concentration of the solvent is reduced by shearing a zein ethanolic solution into water, resulting in precipitation and the formation of nanoparticles. The particle size is dependent on parameters such as the preparation method, agitation speed, and volume ratio between the two phases (Pascoli *et al*., 2018). However, the manufacture at larger scales is often inconsistent in replicating particle size because nanoprecipitation is a batch process, which involves the variation of shear forces and spatial shear intensity within the solution between batches. Therefore, improved production techniques are required to limit the effects of these factors. Shifting from batch to continuous manufacturing to fabricate zein nanoparticles has been explored to improve particle homogeneity and minimise batch variations (Olenskyj *et al*., 2017; van Ballegooie *et al*., 2019). Microfluidics is one such tool that is being adopted by the industry to produce nanoparticles in a highly reproducible manner and was hence assessed in the present study.

Zein nanoparticles entrapping CR6 were produced by both microfluidic and manual-based production processes. Using a Y-junction microfluidic system, the modification of zein concentration, total flow rate of the fluidic system, and relative flow rate of the aqueous and organic phases allowed for nanoparticle size and PDI to be controlled. Increasing zein concentration increased nanoparticle size while increasing TFR and FRR (aqueous to organic phase ratio) led to a decrease in size. Our result was in good agreement with that published by van Ballegooie *et al.* (2019). Using microfluidics, the most optimal conditions for achieving the highest CR6 entrapment were found to

be a zein concentration of 0.5% w/v, a CR6 loading of 0.1% w/w, and a TFR of 6 mL/min at a 3:1 FRR.

Zein nanoparticles were also manually prepared using nanoprecipitation process. To investigate the effects of method preparation and aqueous to organic phase volume ratio on nanoparticle characteristics, zein concentration of 0.5% w/v and CR6 loading of 0.1% w/w were fixed. The mixing process has a significant impact on the size and EE of the particles. Method 1, where zein solution was added to water, yielded nanoparticles with very low EE, unlike nanoparticles that formed when adding water to zein solution (Method 2). Although a large particle size was observed, CR6 entrapment was significantly improved. The increase of the volume ratio from 4:1 to 5:1 decreased CR6 entrapment. The lower EE with increasing aqueous to organic phase volume ratio was found to be similar to the results of previous studies (Chorny *et al*., 2002; Song *et al*., 2008). However, it significantly reduced the size of the particles. Our results suggested that nanoprecipitation Method 2 (addition of water to organic phase) at 5:1 volume ratio was suitable for producing zein nanoparticles. According to our results, further formulation optimisation was needed to achieve a smaller particle size combined with high CR6 entrapment.

To compare microfluidic with manual manufacturing, the volume of water to zein phase at 5:1 was applied as a result of previous optimisation studies, meaning that FRR (aqueous to organic phase ratio) of the fluidic system was set at 5:1 and a TFR of 6 mL/min was used. Moreover, the pH of nanoparticle suspension was increased to 10 once the nanoparticles were formed in order to stabilise them before high speed centrifugation, as suggested by Regier *et al*. (2012). Raising the pH of nanoparticle suspension to 10 lowered the surface charge of zein nanoparticles from positive to

negative zeta potential values due to the lower isoelectric point of zein at pH 10. This change in charge could prevent irreversible nanoparticle aggregation during handling, which allowed the pellet to be resuspended after centrifugation. The pH adjustment strategy was successful in improving the EE of zein nanoparticles. It also significantly decreased the size of the nanoparticles prepared by nanoprecipitation Method 2.

Nanoparticles of similar properties were obtained using microfluidics and nanoprecipitation Method 1. These two approaches could produce highly monodisperse zein nanoparticles with the desired size, but yield and EE were comparatively low. EE was found to correlate with nanoparticle yield. Nanoprecipitation Method 2, on the other hand, generated zein nanoparticles with the largest size among the three tested manufacturing processes. However, their size remained below 400 nm, which is the cut-off size for extravasation for most tumours (Yuan *et al*., 1995). Besides, it significantly improved EE and nanoparticle yield. Increased EE allows the same amount of drug to be delivered with fewer nanoparticles. Therefore, we decided not to further explore the preparation of zein-based nanoparticles in the microfluidic setup due to low EE and yield, but instead focused on manual production using nanoprecipitation Method 2 (addition of water to organic phase).

PEGylated zein nanoparticles were prepared from mPEG-zein conjugates (see details in Chapter 2) using nanoprecipitation Method 2, and the effect of the PEG chain length and PEG density on nanoparticle physicochemical properties was investigated. In this Chapter, PEGylated zein nanoparticles were actually PEGylated zein micelles. Because micelles are another type of nanoparticles that are prepared using amphiphilic molecules, we used the common term “nanoparticles” to define the particles produced

from both zein and mPEG-zein. Therefore, two types of nanoformulations were actually compared: zein nanoparticles and PEGylated zein micelles. PEGylation led to a decrease in the size of zein nanoparticles, possibly due to more amphiphilic nature of the mPEG-zein conjugates in comparison with zein, which reduced the interfacial tension between the aqueous and the organic phases (Gref *et al*., 2000). When nanoparticles were prepared using the same PEG MW, their size slightly decreased with increasing PEG content. The smaller size with the higher PEG density was also observed in PEG-PLA and PEG-PLGA nanoparticles (Gref *et al*., 2000; Xu *et al*., 2015). At constant PEG to zein molar ratio, the particle size increased with increasing PEG chain length. This is likely a result of the increase in the viscosity of the organic phase during particle preparation and the increase of the extending PEG chain on the final particles (Gref *et al*., 2000).

PEGylation is known to shield either negative or positive charge on the surface of particles, resulting in less negative or less positive zeta potential. As expected, incorporating PEG in the formulations decreased zeta potential absolute values of zein nanoparticles. Besides, PEGylation had an impact on the entrapment of CR6 in the nanoparticles. CR6 EE appeared to correlate with the particle size, in agreement with a previous study that has shown that smaller size nanoparticles are subject to a more extensive drug loss by diffusion towards the suspending medium due to their larger surface to volume ratio (Chorny *et al*., 2002). Nonetheless, when compared between two mPEG5K-zein formulations, a substantial EE reduction was observed with a small decrease in particle size when using high PEG density. Apart from the size effect, this EE reduction would be due to a smaller space left for hydrophobic interaction between

CR6 and zein compartment as the PEG content over zein increased, resulting in a significantly decreased EE.

The long-term stability of zein-based nanoparticles during storage was also examined. In the absence of PEG, zein nanoparticles appeared to form large aggregates, which was observed by the size change after 2 weeks. PEG coating effectively prevented the aggregation of the nanoparticles, showing better colloidal stability for all three PEGylated formulations. Improved nanocarrier stability as a result of surface modification with PEG is well established (Xu *et al*., 2015; Suk *et al*., 2016; Bachir *et al*., 2018).

In vitro studies demonstrated that PEGylation resulted in a significant reduction in cellular uptake efficiency. This could be explained by the effect of steric shielding of the PEG chains that hinders the interactions between the nanoparticles and the cell surface (Du *et al*., 1997). Among PEGylated formulations, the cellular uptake of CR6 was highest after incubation with mPEG5K-zein (0.5:1), followed by mPEG5K-zein (1:1) and mPEG10K-zein, respectively. Higher uptake with shorter PEG chain length and less PEG density was consistent with other previously reported nanocarriers (Cruje and Chithrani, 2014; Pozzi *et al*., 2014; Bachir *et al*., 2018). PEGylation was shown to strongly reduce protein binding. Cruje and Chithrani reported that non-specific protein adsorption may facilitate cancer cell entry. Hence, the highest uptake observed in non-PEGylated nanoparticles was due to the absence of PEG molecules that repel adsorbed proteins. Non-specific protein adsorption was found to increase with shorter PEG chain lengths and lower grafting densities. This in turn resulted in higher nanoparticle internalisation by cancer cells (Cruje and Chithrani, 2014).

To elucidate which pathways are involved in the endocytosis of zein-based nanoparticles, the inhibitory effect of pathway specific inhibitors on cellular uptake was assessed. The cellular uptake of zein and mPEG-zein nanoparticles was partially inhibited by chlorpromazine and colchicine. The stronger inhibition by chlorpromazine suggested that the nanoparticles were mainly internalised into the cells via clathrin-mediated endocytosis. Macropinocytosis was also involved in the endocytosis. Filipin resulted in a small decrease in the cellular uptake of zein nanoparticles, but did not inhibit the uptake of PEGylated formulations. Our results therefore indicated the involvement of three endocytosis pathways (clathrin-mediated, caveolae-mediated, and macropinocytosis-mediated endocytosis) in the internalisation of zein nanoparticles, while clathrin-mediated and macropinocytosis-mediated endocytosis were involved in the cellular uptake of PEGylated zein formulations. In cellular uptake studies, higher CR6 accumulation in the cells was observed following treatment with CR6 solution over the nanoparticles. The reason for such observation could be explained by the different cellular uptake mechanisms used. Free CR6 entered cells by passive diffusion, while the nanoparticles were taken up by endocytosis, a slower but highly specific process.

CHAPTER 5

Conclusions and future works

5.1 Conclusions

Zein, a hydrophobic protein from corn, presents some unique advantages such as FDA "GRAS" status, low cost, biocompatibility, biodegradability, and ease of modification that make it an attractive material for use as delivery systems (Paliwal and Palakurthi, 2014). However, as a protein nanocarrier, its immunogenicity has raised concerns about their potential use as drug and vaccine delivery vehicles (Hurtado-Lopez and Murdan, 2006). The conjugation of zein with PEG has been proposed as a means to overcome this issue by creating a steric shielding of the delivery system, thus reducing opsonisation and extending circulation half-life.

As PEG density and chain length are crucial determinants of shielding efficacy, the modification of zein with PEG of different lengths and densities requires investigation to determine the optimal combination of these two materials that provides stealth efficacy for the delivery system. **Chapter 2** demonstrated that yellow zein could be successfully conjugated with mPEG-SCM and was able to self-assemble into micelles with hydrophobic zein forming the inner core while the hydrophilic mPEG is in the outer shell. mPEG-zein could entrap a model hydrophobic substance, Nile red, resulting in micelles of size between 100 and 300 nm. The difference in size depended on the MW of PEG and PEG density. The zeta potential of the micelles was positive in all formulations. Loading Nile red did not change the surface charge of the micelles, suggesting that Nile red was entrapped in the hydrophobic inner core of the micelles. *In vitro* studies revealed that mPEG-zein micelles could deliver Nile red into the B16-F10-luc-G5 melanoma cell line mainly via clathrin-mediated endocytosis, with higher cellular uptake observed when using smaller chain length PEG5K and less PEG

density. Cell viability study also indicated that the micelles were relatively safe to B16-F10-luc-G5 and T98G cancer cells.

Nevertheless, it has been established that the properties of nanoparticles can be affected by the adsorption of proteins "corona" on their surface once in contact with biological fluids, giving it a new biological identity which subsequently impacts their cellular responses *in vivo* (Monopoli *et al*., 2012; Nguyen and Lee, 2017). Although PEGylation is often used to reduce corona formation on nanoparticles (Gref *et al*., 2000; Owens and Peppas, 2006), a full understanding of the effect of the protein corona on PEGylated zein micelles and their interactions with cells is needed.

Chapter 3 provided the first investigation of the impact of the protein corona on mPEG-zein micelle uptake by cancer cells and immune cells. Overall, PEGylation of zein could confer stealth effects on the micelle surface, regardless of PEG chain length, as it minimised the adsorption of proteins on the mPEG-zein micelles. The presence of FBS slightly reduced the uptake of mPEG5K-zein (0.5:1) and mPEG10K-zein micelles by cancer cells and immune cells. On the other hand, the presence of HP did not have any impact on the uptake of PEGylated zein micelles by the melanoma cancer cells, independently of the MW PEG used in the formulations. It decreased the uptake of the micelles by macrophages, with a higher decrease observed with mPEG10K-zein micelles, and by dendritic cells for both micelle formulations. However, smaller chain length PEG5K showed an advantage in cellular uptake efficiency over longer chain PEG10K. These results, therefore, make mPEG5K-zein (0.5:1) micelles the best compromise between anti-opsonisation strategy and cancer cell targeting.

The potential of using microfluidic-assisted technologies to manufacture zein nanoparticles was also assessed. **Chapter 4** revealed that zein nanoparticles could be produced by both manual and microfluidic approaches. Parameters such as total flow rate and flow rate ratio of the aqueous and organic phase for microfluidics, as well as method preparation and aqueous to organic phase volume ratio for nanoprecipitation, strongly impacted nanoparticle properties. Continuous microfluidic manufacturing was not the best choice for making zein nanoparticles in this study, because it gave low nanoparticle yield and EE compared with nanoprecipitation Method 2. Hence, to produce zein nanoparticles using microfluidics, further studies will be required to improve yield and achieve high drug entrapment. Furthermore, PEGylation of zein with shorter PEG chain length and lower PEG density made mPEG5K-zein (0.5:1) the most favourable formulation, as it improved nanoparticle stability and provided higher uptake efficiency by melanoma cancer cells.

5.2 Future works

The results obtained from this thesis suggest that PEGylated zein, in particular mPEG5K-zein (0.5:1), is an interesting biopolymer that shows high potential for use in drug delivery applications. However, there are many areas that can be improved and require further investigation.

In Chapter 2, although PEG with various chain lengths and densities was successfully conjugated to zein, as confirmed by ATR-FTIR, more in depth investigation of PEGylation efficiency should be carried out to determine the ratio of PEG that actually attached to zein after PEGylation. The effect of protein corona on two mPEG-zein micelle formulations was evaluated in Chapter 3. However, this investigation should be tested on all three formulations to gain a better understanding of the protein adsorbed on the micelles with low and high PEG densities and their correlation with the interaction with cells. In Chapter 4, microfluidic-assisted manufacture was shown to produce uniform zein nanoparticles in a range of sizes for tumour retention. However, nanoparticle yield and drug EE were found to be low. To improve nanoparticle yield, tangential flow filtration could be used for the purification of the nanoparticles, instead of centrifugation. In addition, to improve drug entrapment, the next step would consider encapsulating the drug via active loading. This technique involves incubating drug solution with pre-formed nanoparticles in a water bath. By this means, parameters that affect the amount of drug encapsulated, including the time and temperature applied during the loading process, will be determined to achieve high drug entrapment.

To assess the feasibility of using PEGylated zein as a carrier for cancer therapy, the next study will focus on encapsulating chemotherapeutic agents such as doxorubicin in the delivery systems in order to examine anticancer activity. Future studies could potentially investigate surface modification of mPEG-zein conjugates to improve tumour specificity. PEG molecules can be functionalised with targeting ligands, i.e. transferrin, to enhance cellular internalisation into target cells via receptor-mediated endocytosis. This would allow payloads to be delivered specifically to cancer cells while minimising secondary effects to healthy tissues. To prove tumour targeting efficiency, for example of transferrin-bearing mPEG-zein nanoparticles, *in vitro* evaluation on cancer cell lines that overexpress transferrin receptors, such as MCF-7 breast cancer cells and PC-3 prostate cancer cells, will be required.

In vitro drug release profile should also be performed using a dialysis technique under three different pHs (5.5, 6.5, and 7.4) to mimic the subcellular endosome, the tumour extracellular environment, and the physiological pH in normal tissues and blood, respectively. Sustained release of the drug is essential to exert its therapeutic effect. Ideally, the drug should be retained within the nanoparticles at the physiological pH (pH 7.4) after intravenous injection to minimise off-site toxicity. Once the nanoparticles reach the tumour sites, the drug is preferentially released due to the acidic tumour microenvironments (pH 5.5-6.5). The results from this study would allow us to further develop pH-responsive PEGylated zein nanoparticles that favour drug release at the target site over surrounding tissues.

Although promising results in using PEGylated zein nanocarriers to deliver lipophilic drug models into cancer cells *in vitro* are demonstrated, *in vitro* studies cannot fully mimic the tumour microenvironment and predict the biological fate of the nanocarriers

after intravenous administration. Therefore, *in vivo* studies will be required to gain a full understanding of the therapeutic efficacy and associated toxicity of systemic administration of PEGylated zein nanocarriers. They would use mice bearing subcutaneous tumours as an animal model and would evaluate tumour volume, mice weight changes, and survival rate. Additionally, the pharmacokinetics and biodistribution of the PEGylated zein nanocarriers following intravenous injection will be examined to confirm that PEGylation could prevent opsonisation and prolong blood circulation, thus allowing sufficient time for our delivery systems to reach tumour areas.

References

ABDELLATIF, A. A. H., EL-TELBANY, D. F. A., ZAYED, G. & AL-SAWAHLI, M. M. 2019. Hydrogel containing PEG-coated fluconazole nanoparticles with enhanced solubility and antifungal activity. *Journal of Pharmaceutical Innov*ation, 14, 112-122.

AGGARWAL, P., HALL, J. B., MCLELAND, C. B., DOBROVOLSKAIA, M. A. & MCNEIL, S. E. 2009. Nanoparticle interaction with plasma proteins as it relates to particle biodistribution, biocompatibility and therapeutic efficacy. *Advanced Drug Delivery Reviews*, 61, 428-437.

AHSAN, S. M., RAO, C. M. & AHMAD, M. F. 2018. Nanoparticle-protein interaction: The significance and role of protein corona. *Advances in Experimental Medicine and Biology*, 1048, 175-198.

ALBANESE, A., TANG, P. S. & CHAN, W. C. W. 2012. The effect of nanoparticle size, shape, and surface chemistry on biological systems. *Annual Review of Biomedical Engineering*, 14, 1-16.

ALEXIS, F., PRIDGEN, E., MOLNAR, L. K. & FOROKHZAD, O. C. 2008. Factor affecting the clearance and biodistribution of polymeric nanoparticles. *Molecular Pharmaceutics*, 5, 505-515.

ANDERSON, T. J. & LAMSAL, B. P. 2011. Zein extraction from corn, corn products, and coproducts and modifications for various applications: a review. *Cereal Chemistry*, 88, 159-173.

BACHIR, Z. A., HUANG, Y., HE, M., HUANG, L., HOU, X., CHEN, R. & GAO, F. 2018. Effect of PEG surface density and chain length on the pharmacokinetics and biodistribution of methotrexate-loaded chitosan nanoparticles. *International Journal of Nanomedicine*, 13, 5657-5671.

BARENHOLZ, Y. C. 2012. Doxil® - the first FDA-approved nano-drug: lessons learned. *Journal of Controlled Release*, 160, 117-134.

BEHZADI, S., SERPOOSHAN, V., TAO, W., HAMALY, M. A., ALKAWAREEK, M. Y., DREADEN, E. C., BROWN, D., ALKILANY, A. M., FAROKHZAD, O. C. & MAHMOUDI, M. 2017. Cellular uptake of nanoparticles: journey inside the cell. *Chemical Society Reviews*, 46, 4218-4244.

BLANCO, E., SHEN, H., & FERRARI, M. 2015. Principles of nanoparticle design for overcoming biological barriers to drug delivery. *Nature Biotechnology*, *33*, 941-951.

CANCER RESEARCH UK. Treatment for cancer. Available at: https://www.cancerresearchuk.org/about-cancer/cancer-in-general/treatment [Accessed 12 June 2021].

CAO, X., GENG, J., SU, S., ZHANG, L., XU, Q., ZHANG, L., XIE, Y., WU, S., SUN, Y. & GAO, Z. 2012. Doxorubicin-loaded zein *in situ* gel for interstitial chemotherapy. *Chemical and Pharmaceutical Bulletin*, 60, 1227-1233.

CHAN, D., YU, A. C. & APPEL, E. A. 2017. Single-chain polymeric nanocarriers: a platform for determining structure-function correlations in the delivery of molecular cargo. *Biomacromolecules*, 18, 1434-1439.

CHEN, H. & ZHONG, Q. 2014. Processes improving the dispersibility of spray-dried zein nanoparticles using sodium caseinate. *Food Hydrocolloids*, 35, 358-366.

CHENG, L., HUANG, F.-Z., CHENG, L.-F., ZHU, Y.-Q., HU, Q., LI, L., WEI, L. & CHEN D.-W. 2014. GE11-modified liposomes for non-small cell lung cancer targeting: preparation, *ex vitro* and *in vivo* evaluation. *International Journal of Nanomedicine*, 9, 921-935.

CHORNY, M., FISHBEIN, I., DANENBERG, H. D. & GOLOMB, G. 2002. Lipophilic drug loaded nanospheres prepared by nanoprecipitation: effect of formulation variables on size, drug recovery and release kinetics. *Journal of Controlled Release*, 83, 389-400.

CHOU, L. Y., MING, K. & CHAN, W. C. 2011. Strategies for the intracellular delivery of nanoparticles. *Chemical Society Reviews*, 40, 233-245.

CORBO, C., MOLINARO, R., PORODI, A., TOLEDANO FURMAN, N. E., SALVATORE, F. & TASCIOTTI, E. 2016. The impact of nanoparticle protein corona on cytotoxicity, immunotoxicity and target drug delivery. *Nanomedicine*, 11, 81-100.

CRUJE, C. & CHITHRANI, D. B. 2014. Polyethylene glycol density and length affects nanoparticle uptake by cancer cells. *Journal of Nanomedicine Research*, 1, 6-11.

CRUZ, L. J., TACKEN, P. J., FOKKINK, R. & FIGDOR, C. G. 2011. The influence of PEG chain length and targeting moiety on antibody-mediated delivery of nanoparticle vaccines to human dendritic cells. *Biomaterial*s, 32, 6791-6803.

DABHOLKAR, R. D., SAWANT, R. M., MONGAYT, D. A., DEVARAJAN, P. V. & TORCHILIN, V. P. 2006. Polyethylene glycol-phosphatidylethanolamine conjugate (PEG-PE)-based mixed micelles: some properties, loading with paclitaxel, and modulation of P-glycoprotein-mediated efflux. *International Journal of Pharmaceutics*, 315, 148-157.

DAI, Q., WALKEY, C. & CHAN, W. C. W. 2014. Polyethylene glycol backfilling mitigates the negative impact of the protein corona on nanoparticle cell targeting. *Angewandte Chemie International Edition*, 53, 5093-5096.

DAVIS, S. S. & ILIUM, L. 1994. Particulate systems for site specific drug delivery. In: Gregoriadis, G., McCormack, B. & Poste, G., eds. *Targeting of Drugs 4*. Boston: Springer, 183-194.

DEL PINO, P., PELAZ, B., ZHANG, Q., MAFFRE, P., NIENHAUS, G. U. & PARAK, W. J. 2014. Protein corona formation around nanoparticles - from the past to the future. *Materials Horizons*, 1, 301-313.

DEMELLO, J. & DEMELLO, A. 2004. Microscale reactors: nanoscale products. *Lab Chip*, 4, 11-15.

DIBIASE, M. D. & MORREL, E. M. 1997. Oral Delivery of microencapsulated proteins. In: Sanders, L. M. & Wayne Hendren, R., eds. *Protein Delivery: Physical Systems*. New York: Plenum Press (10), 255-288.

DICKEN, E. & AHMED, S. 2018. Principles of cancer treatment by chemotherapy. *Surgery (Oxford)*, 36, 134-138.

DONG, F., DONG, X., ZHOU, L., XIAO, H., HO, P. Y., WONG, M. S. & WANG, Y. 2016. Doxorubicin-loaded biodegradable self-assembly zein nanoparticle and its anti-cancer effect: preparation, *in vitro* evaluation, and cellular uptake. *Colloids Surfaces B: Biointerfaces*, 140, 324-331.

DONG, J., SUN, Q. & WANG, J. Y. 2004. Basic study of corn protein, zein, as a biomaterial in tissue engineering, surface morphology and biocompatibility. *Biomaterials*, 25, 4691-4697.

DU, H., CHANDAROY, P. & HUI, S. W. 1997. Grafted poly-(ethylene glycol) on lipid surfaces inhibits protein adsorption and cell adhesion. *Biochimica et Biophysica Acta*, 1326, 236-248.

DUFÈS, C., SCHÄTZLEIN, A. G., TETLEY, L., GRAY, A. I., WATSON, D. G., OVIVER, J. C., COUET, W. & UCHEGBU, I. F. 2000. Niosomes and polymeric chitosan based vesicles bearing transferrin and glucose ligands for drug targeting. *Pharmaceutical Research*, 17, 1250-1258.

ELZOGHBY, A. O., SAMY, W. M. & ELGINDY, N. A. 2012. Protein-based nanocarriers as promising drug and gene delivery systems. *Journal of Controlled Release*, 161, 38-49.

FOROOZANDEH, P. & AZIZ, A. A. 2018. Insight into cellular uptake and intracellular trafficking of nanoparticles. *Nanoscale Research Letters*, 13, 1-12.

FREITAS, S., MERKLE, H. P. & GANDER, B. 2005. Microencapsulation by solvent extraction/evaporation: reviewing the state of the art of microsphere preparation process technology. *Journal of Controlled Release*, 102, 313-332.

FU, J. X., WANG, H. J., ZHOU, Y. Q. & Wang J. Y. 2009. Antibacterial activity of ciprofloxacin-loaded zein microsphere films. *Materials Science and Engineering: C*, 29, 1161-1166.

GABIZON, A. A. 2001. Stealth liposomes and tumor targeting: one step further in the quest for the magic bullet. *Clinical Cancer Research*, 7, 223-225.

GHEZZI, M., PESCINA, S., PADULA, C., SANTI, P., DEL FAVERO, E., CANTÙ, L., & NICOLI, S. 2021. Polymeric micelles in drug delivery: An insight of the techniques for their characterization and assessment in biorelevant conditions. *Journal of Controlled Release*, 332, 312-336.

GIANAZZA, E., VIGLIENGHI, V., RIGHETTI, P. G., SALAMINI, F. & SOAVE, C. 1977. Amino acid composition of zein molecular components. *Phytochemistry*, 16, 315-317.

GONG, S. J., SUN, S. X., SUN, Q. S., WANG, J. Y., LIU, X. M. & LIU, G. Y. 2011. Tablets based on compressed zein microspheres for sustained oral administration: design, pharmacokinetics, and clinical study. *Journal of Biomaterials Applications*, 26, 195-208.

GOSSMANN, R., FAHRLÄNDER, E., HUMMEL, M., MULAC, D., BROCKMEYER, J. & LANGER, K. 2015. Comparative examination of adsorption of serum proteins on HSA- and PLGA-based nanoparticles using SDS-PAGE and LC-MS. *European Journal of Pharmaceutics and Biopharmaceutics*, 93, 80-87.

GRÄFE, C., WEIDNER, A., LÜHE, M. V., BERGEMANN, C., SCHACHER, F. H., CLEMENT, J. H. & SUTZ, S. 2016. Intentional formation of a protein corona on nanoparticles: serum concentration affects protein corona mass, surface charge, and nanoparticle-cell interaction. *The International Journal of Biochemistry & Cell Biology*, 75, 196-202.

GREF, R., LÜCK, M., QUELLEC, P., MARCHAND, M., DELLACHERIE, E., HARNISCH, S., BLUNK, T. & MÜLLER, R. H. 2000. 'Stealth' corona-core nanoparticles surface modified by polyethylene glycol (PEG): influences of the corona (PEG chain length and surface density) and of the core composition on phagocytic uptake and plasma protein adsorption. *Colloids and Surfaces B: Biointerfaces*, 18, 301-313.

HU, K., HUANG, X., GAO, Y., HUANG, X., XIAO, H. & MCCLEMENTS, D. J. 2015. Core–shell biopolymer nanoparticle delivery systems: synthesis and characterization of curcumin fortified zein-pectin nanoparticles. *Food Chemistry*, 182, 275-281.

HURTADO-LÓPEZ, P. & MURDAN, S. 2006. An investigation into the adjuvanticity and immunogenicity of zein microspheres being researched as drug and vaccine carriers. *Journal of Pharmacy and Pharmacology*, 58, 769-774.

ISHIHAMA, Y., ODA, Y., TABATA, T., SATO, T., NAGASU, T., RAPPSILBER, J. & MANN, M. 2005. Exponentially modified protein abundance index (emPAI) for estimation of absolute protein amount in proteomics by the number of sequenced peptides per protein. *Molecular & Cellular Proteomics*, 4, 1265-1272.

JAIN, R. K., & STYLIANOPOULOS, T. 2010. Delivering nanomedicine to solid tumors. *Nature Reviews Clinical Oncology*, *7*, 653-664.

JIANG, Q., REDDY, N. & YANG, Y. 2010. Cytocompatible cross-linking of electrospun zein fibers for the development of water-stable tissue engineering scaffolds. *Acta Biomaterialia*, 6, 4042-4051.

KARNIK, R., GU, F., BASTO, P., CANNIZZARO, C., DEAN, L., KYEI-MANU, W. LANGER, R. & FAROKHZAD, O. C. 2008. Microfluidic platform for controlled synthesis of polymeric nanoparticles. *Nano Letters*, 8, 2906-2912.

KARTHIKEYAN, K., LAKRA, R., RAJARAM, R. & KORRAPATI, P. S. 2012. Development and characterization of zein-based micro carrier system for sustained delivery of aceclofenac sodium. *AAPS PharmSciTech*, 13, 143-149.

KOBAYASHI, H., WATANABE, R. & CHOYKE, P. L. 2014. Improving conventional enhanced permeability and retention (EPR) effects; what is the appropriate target?. *Theranostics*, 4, 81-89.

KONG, B. & XIONG, Y. L. 2006. Antioxidant activity of zein hydrolysates in a liposome system and the possible mode of action. *Journal of Agricultural and Food Chemistry*, 54, 6059-6068.

LAI, L. F. & GUO, H. X. 2011. Preparation of new 5-fluorouracil-loaded zein nanoparticles for liver targeting. *International Journal of Pharmaceutics*, 404, 317-323.

LASKAR, P., SAMANTA, S., GHOSH, S. K. & DEY, J. 2014. In vitro evaluation of pH-sensitive cholesterol-containing stable polymeric micelles for delivery of camptothecin. *Journal of Colloid and Interface Science*, 430, 305-314.

LASKAR, P. SOMANI, S., ALTWAIJRY, N., MULLIN, M., BOWERING, D., WARZECHA, M., KEATING, P., TATE, R. J., LEUNG, H. Y. & DUFÈS, C. 2018. Redox-sensitive, cholesterol-bearing PEGylated poly(propylene imine)-based dendrimersomes for drug and gene delivery to cancer cells. *Nanoscale*, 10, 22830-22847.

LAWTON, J. W. 2002. Zein: a history of processing and use. *Cereal Chemistry*, 79, 1-18.

LEE, S., KIM, Y. C. & PARK, J. H. 2016. Zein-alginate based oral drug delivery systems: protection and release of therapeutic proteins. *International Journal of Pharmaceutics*, 515, 300-306.

LESNIAK, A., FENAROLI, F., MONOPOLI, M. P., ÅBERG, C., DAWSON, K. A. & SALVATI, A. 2012. Effect of the presence or absence of a protein corona on silica nanoparticle uptake and impact on cells. *ACS Nano*, 6, 5845-5857.

LESNIAK, A., SALVATI, A., SANTOS-MARTINEZ, M. J., RADOMSKI, M. W., DAWSON, K. A. & ÅBERG, C. 2013. Nanoparticle adhesion to the cell membrane and its effect on nanoparticle uptake efficiency. *Journal of the American Chemical Society*, 135, 1438-1444.

LETCHFORD, K. & BURT, H. 2007. A review of the formation and classification of amphiphilic block copolymer nanoparticulate structures: micelles, nanospheres, nanocapsules and polymersomes. *European Journal of Pharmaceutics and Biopharmaceutics*, 65, 259-269.

LIN, T., LU, C., ZHU, L. & LU, T. 2011. The biodegradation of zein *in vitro* and *in vivo* and its application in implants. *AAPS PharmSciTech*, 12, 172-176.

LI, M. & YU, M. 2020. Development of a nanoparticle delivery system based on zein/polysaccharide complexes. *Journal of Food Science,* 85, 4108-4117.

LUO, Y., TENG, Z., WANG, T. T. Y. & WANG, Q. 2013. Cellular uptake and transport of zein nanoparticles: effects of sodium caseinate. *Journal of Agricultural and Food Chem*istry, 61, 7621-7629.

LUO, Y. & WANG, Q. 2014. Zein-based micro- and nano-particles for drug and nutrient delivery: a review. *Journal of Applied Polymer Science*, 131, 40696.

LUO, Y., ZHANG, B., WHENT, M., YU, L. L. & WANG, Q. 2011. Preparation and characterization of zein/chitosan complex for encapsulation of α-tocopherol, and its *in vitro* controlled release study. *Colloids and Surfaces B: Biointerfaces*, 85, 145-152.

MAEDA, H. 2015. Toward a full understanding of the EPR effect in primary and metastatic tumors as well as issues related to its heterogeneity. *Advanced Drug Delivery Reviews*, 91, 3-6.

MATSUSHIMA, N., DANNO, G. I., TAKEZAWA, H. & IZUMI, Y. 1997. Three-dimensional structure of maize α-zein proteins studied by small-angle X-ray scattering. *Biochimica et Biophysica Acta*, 1339, 14-22.

MISHRA, P., NAYAK, B. & DEY, R. K. 2016. PEGylation in anti-cancer therapy: An overview. *Asian Journal of Pharmaceutical Sciences,* 11, 337–348.

MIYOSHI, S., ISHIKAWA, H., KANEKO, T., FUKUI, F., TANAKA., H & MARUYAMA, S. 1991. Structures and activity of angiotensin-converting enzyme inhibitors in an α-zein hydroxylate. *Agricultural and Biological Chemistry*, 55, 1313-1318.

MO, J., XIE, Q., WEI, W. & ZHAO, J. 2018. Revealing the immune perturbation of black phosphorus nanomaterials to macrophages by understanding the protein corona. *Nature Communications*, 9, 2480.

MOMANY, F. A., SESSA, D. J., LAWTON, J. W., SELLING, G. W., HAMAKER, S. A. H. & WILLETT, J. L. 2006. Structural characterization of α-zein. *Journal of Agricultural and Food Chemistry,* 54, 543-547.

MONOPOLI, M. P., WALCZYK, D., CAMPBELL, A., ELIA, G., LYNCH, I., BALDELLI, B. F. & DAWSON, K. A. 2011. Physical-chemical aspects of protein corona: relevance to *in vitro* and *in vivo* biological impacts of nanoparticles. *Journal of the American Chemical Society*, 133, 2525-2534.

MONOPOLI, M. P., ÅBERG, C., SALVATI, A. & DAWSON, K. A. 2012. Biomolecular coronas provide the biological identity of nanosized materials. *Nature Nanotechnology*, 7, 779-786.

NAKAMURA, Y., MOCHIDA, A., CHOYKE, P. L. & KOBAYASHI, H. 2016. Nanodrug delivery: is the enhanced permeability and retention effect sufficient for curing cancer?. *Bioconjugate Chemistry*, 27, 2225-2238.

NAM, H. Y., KWON, S. M., CHUNG, H., LEE, S.-Y., KWON, S.-H., JEON, H., KIM, Y., PARK, J. H., KIM, J., HER, S., OH, Y. K., KWON, I. C., KIM, K. & JEONG, S. Y. 2009. Cellular uptake mechanism and intracellular fate of hydrophobically modified glycol chitosan nanoparticles. *Journal of Controlled Release*, 135, 259-267.

NELEMANS, L. C., & GUREVICH, L. 2020. Drug delivery with polymeric nanocarriers-cellular uptake mechanisms. *Materials*, 13, 366.

NGUYEN, V. H. & LEE, B. J. 2017. Protein corona: a new approach for nanomedicine design. *International Journal of Nanomedicine*,12, 3137-3151.

NITTA, S. K., & NUMATA, K. 2013. Biopolymer-based nanoparticles for drug/gene delivery and tissue engineering. *International Journal of Molecular Sciences*, *14*, 1629-1654.

O'BRIEN, M. E. R., WIGLER, N., INBAR, M., ROSSO, R., GRISCHKE, E., SANTORO, A., CATANE, R., KIEBACK, D. G., TOMCZAK, P., ACKLAND, S. P., ORLANDI, F., MELLARS, L., ALLAND, L. & TENDLER, C. 2004. Reduced cardiotoxicity and comparable efficacy in a phase III trial of pegylated liposomal doxorubicin HCl (CAELYX™/Doxil®) versus conventional doxorubicin for first-line treatment of metastatic breast cancer. *Annals of Oncology*, 15, 440-449.

OGAWARA, K., FURUMOTO, K., NAGAYAMA, S., MINATO, K., HIGAKI, K., KAI, T. & KIMURA, T. 2004. Pre-coating with serum albumin reduces receptor-mediated hepatic disposition of polystyrene nanosphere: implications for rational design of nanoparticles. *Journal of Controlled Release*, 100, 451-455.

OLENSKYJ, A. G., FENG, Y. & LEE, Y. 2017. Continuous microfluidic production of zein nanoparticles and correlation of particle size with physical parameters determined using CFD simulation. *Journal of Food Engineering*, 211, 50-59.

OPRITA, A. & SEVASTRE, A. S. 2020. New pharmaceutical dosage forms used in the treatment of breast cancer. Polymeric micelles. *Medico Oncology*, 1, 38-52.

OTSUKA, H., NAGASAKI, Y. & KATAOKA, K. 2012. PEGylated nanoparticles for biological and pharmaceutical applications. *Advanced Drug Delivery Reviews*, 64, 246–255.

OWENS III, D. E. & PEPPAS, N. A. 2006. Opsonization, biodistribution, and pharmacokinetics of polymeric nanoparticles. *International Journal of Pharmaceutics*, 307, 93-102.

PALIWAL, R. & PALAKURTHI, S. 2014. Zein in controlled drug delivery and tissue engineering. *Journal of Controlled Release*, 189, 108-122.

PANARITI, A., MISEROCCHI, G., & RIVOLTA, I. 2012. The effect of nanoparticle uptake on cellular behavior: disrupting or enabling functions?. *Nanotechnology, Science and Applications*, 5, 87-100.

PARRIS, N., COOKE, P. H. & HICKS, K. B. 2005. Encapsulation of essential oils in zein nanospherical particles. *Journal of Agricultural and Food Chemistry*, 53, 4788-4792.

PARRIS, N. & DICKEY, L. C. 2001. Extraction and solubility characteristics of zein proteins from dry-milled corn. *Journal of Agricultural and Food Chemistry*, 49, 3757-3760.

PARTIKEL, K., KORTE, R., STEIN, N. C., MULAC, D., HERRMANN, F. C., HUMPF, H.-U. & LANGER, K. 2019. Effect of nanoparticle size and PEGylation on the protein corona of PLGA nanoparticles. *European Journal of Pharmaceutics and Biopharmaceutics*, 141, 70-80.

PASCOLI, M., DE LIMA, R. & FRACETO, L. F. 2018. Zein nanoparticles and strategies to improve colloidal stability: a mini-review. *Frontiers in Chemistry*, 6, 1-5.

PAULIS, J. W. & WALL, J. S. 1977. Fractionation and characterization of alcohol-soluble reduced corn endosperm glutelin proteins. *Cereal Chemistry*, 54, 1223-1228.

PHILLIPS, R. L. & MCCLURE, B. A. 1985. Elevated protein-bound methionine in seeds of maize line resistant to lysine plus threonine. *Cereal Chemistry*, 62, 213-218.

PODARALLA, S., AVERINENI, R. ALQAHTANI, M & PERUMAL, O. 2012. Synthesis of novel biodegradable methoxy poly(ethylene glycol)–zein micelles for effective delivery of curcumin. *Molecular Pharmaceutics*, 9, 2778-2786.

PODARALLA, S. & PERUMAL, O. 2012. Influence of formulation factors on the preparation of zein nanoparticles. *AAPS PharmSciTech*, 13, 919-927.

POZZI, D., COLAPICCHIONI, V., CARACCIOLO, G., PIOVESANA, S., CAPRIOTTI, A. L., PALCHETTI, S., GROSSI, S. D., RICCIOLI, A., AMENITSCH, H. & LAGANÀ, A. 2014. Effect of polyethyleneglycol (PEG) chain length on the bio-nano-interactions between PEGylated lipid nanoparticles and biological fluids: from nanostructure to uptake in cancer cells. *Nanoscale*, 6, 2782-2792.

QU, Z. H., WANG, H. J., TANG, T. T., ZHANG, X. L., WANG, J. Y. & DAI, K. R. 2008. Evaluation of the zein/inorganics composite on biocompatibility and osteoblastic differentiation. *Acta Biomaterialia*, 4, 1360-1368.

RAHMAN, M., LAURENT, S., TAWIL, N., YAHIA, L. & MAHMOUDI, M. 2013. Protein-nanoparticle interactions (Vol. 15). Berlin, Germany: Springer.

RANGANATHAN, R., MADANMOHAN, S., KESAVAN, A., BASKAR, G., KRISHNAMOORTHY, Y. R., SANTOSHAM, R., PONRAJU, D., RAYALA, S. K. & VENKATRAMAN, G. 2012. Nanomedicine: towards development of patient-friendly drug-delivery systems for oncological applications. *International Journal of Nanomedicine, 7*, 1043-1060.

RAO, J. P. & GECKELER, K. E. 2011. Polymer nanoparticles: preparation techniques and size-control parameters. *Progress in Polymer Science*, 36, 887-913.

REDDY, N. & YANG, Y. 2011. Potential of plant proteins for medical applications. *Trends in Biotechnology*, 29, 490-498.

REGIER, M. C., TAYLOR, J. D., BORCYK, T., YANG, Y. & PANNIER, A. K. 2012. Fabrication and characterization of DNA-loaded zein nanospheres. *Journal of Nanobiotechnology*, 10, 44.

RIGANTI, C., VOENA, C., KOPECKA, J., CORSETTO, P. A., MONTORFANO, G., ENRICO, E., COSTAMAGNA, C., RIZZO, A. M., GHIGO, D. & BOSIA, A. 2011. Liposome-encapsulated doxorubicin reverses drug resistance by inhibiting P-glycoprotein in human cancer cells. *Molecular Pharmaceutics*, 8, 683-700.

RIGHETTI, P. G., CASTAGNAA, A., ANTONUCCIA, F., PIUBELLIB, C., CECCONIA, D., CAMPOSTRINIA, N., RUSTICHELLIA, C., ANTONIOLIA, P., ZANUSSOB, G., MONACOB, S., LOMASC, L. & BOSCHETTIC, E. 2005. Proteome analysis in the clinical chemistry laboratory: myth or reality?. *Clinica Chimica Acta*, 357, 123-139.

ROMBERG, B., HENNINK, W. E. & STORM, G. 2008. Sheddable coatings for long-circulating nanoparticles. *Pharmaceutical Research*, 25, 55-71.

SAHAY, G., ALAKHOVA, D. Y. & KABANOV, A. V. 2010. Endocytosis of nanomedicines. *Journal of Controlled Release*, 145, 182-195.

SAGNELLA, S. M., MCCARROLL, J. A. & KAVALLARIS, M. 2014. Drug delivery: Beyond active tumour targeting. *Nanomedicine: Nanotechnology, Biology and Medicine*, 10, 1131-1137.

SAWANT, R. R. & TORCHILIN, V. P. 2010. Polymeric micelles: polyethylene glycol-phosphatidylethanolamine (PEG-PE)-based micelles as an example. In *Cancer Nanotechnology* (pp. 131-149). Humana Press.

SCHÖTTLER, S., BECKER, G., WINZEN, S., STEINBACH, T., MOHR, K., LANDFESTER, K., MAILÄADER, V. & WURM, F. R. 2016. Protein adsorption is required for stealth effect of poly(ethylene glycol)- and poly(phosphoester)-coated nanocarriers. *Nature Nanotechnology*, 11, 372-377.

SHI, Y., VAN DER MEEL, R., CHEN, X. & LAMMERS, T. 2020. The EPR effect and beyond: Strategies to improve tumor targeting and cancer nanomedicine treatment efficacy. *Theranostics*, 10, 7921-7924.

SHUKLA, R. & CHERYAN, M. 2001. Zein: the industrial protein from corn. *Industrial Crops and Products*, 13, 171-192.

SOE, Z. C., OU, W., GAUTAM, M., POUDEL, K., KIM, B. K., PHAM, L. M., PHUNG, C. D., JEONG, J. H., JIN, S. G., CHOI, H. G., KU, S. K., YONG, C. S. & KIM, J. O. 2019. Development of folate-functionalized PEGylated zein nanoparticles for ligand-directed delivery of paclitaxel. *Pharmaceutics*, 11, 562.

SONG, R., ZHOU, Y., LI, Y., YANG, Z., LI, F., HUANG, Q., SHI, T. & ZHANG, G. 2015. Preparation and characterization of mPEG-g-α-zein biohybrid micelles as a nano-carrier. *Journal of Applied Polymer Science*, 132, 1-6.

SONG, X., ZHAO, Y., HOU, S., XU, F., ZHAO, R., HE, J., CAI, Z., LI, Y. & CHEN, Q. 2008. Dual agents loaded PLGA nanoparticles: systematic study of particle size and drug entrapment efficiency. *European Journal of Pharmaceutics and Biopharmaceutics*, 69, 445-453.

SOUSA, F. F. O., LUZARDO-ÁLVAREZ, A., BLANCO-MÉNDEZ, J., OTERO-ESPINAR, F. J., MARTÍN-PASTOR, M. & MACHO, I. S. 2013. Use of ^{1}H NMR STD, WaterLOGSY, and Langmuir monolayer techniques for characterization of drug-zein protein complexes. *European Journal of Pharmaceutics and Biopharmaceutics*, 85, 790-798.

SOUSA, F. F. O., LUZARDO-ÁLVAREZ, A., PÉREZ-ESTÉVÉZ, A. SEOANE-PRADO, R. & BLANCO-MÉNDEZ, J. 2010. Development of a novel AMX-loaded PLGA/zein microsphere for root canal disinfection. *Biomedical Materials*, 5, 055008.

STOCKHOFE, K., POSTEMA, J. M., SCHIEFERSTEIN, H. & ROSS, T. L. 2014. Radiolabeling of nanoparticles and polymers for PET imaging. *Pharmaceuticals*, 7, 392-418.

SUK, J. S., XU, Q., KIM, N., HANES, J. & ENSIGN, L. M. 2016. PEGylation as a strategy for improving nanoparticle-based drug and gene delivery. *Advanced Drug Delivery Reviews*, *99*, 28-51.

SUN, Q. S., DONG, J., LIN, Z. X., YANG, B. & WANG, J. Y. 2005. Comparison of cytocompatibility of zein film with other biomaterials and its degradability *in vitro*. *Biopolymers*, 78, 268-274.

SUN, T., ZHANG, Y. S., PANG, B., HYUN, D. C., YANG, M. & XIA, Y. 2014. Engineered nanoparticles for drug delivery in cancer therapy. *Angewandte Chemie International Edition*, 53, 12320-12364.

SUNG, H., FERLAY, J., SIEGEL, R. L., LAVERSANNE, M., SOERJOMATARAM, I., JEMAL, A. & BRAY, F. 2021. Global cancer statistics 2020: GLOBOCAN estimates of incidence and mortality worldwide for 36 cancers in 185 countries. *CA: A Cancer Journal for Clinicians*, 71, 209-249.

SUK, J. S., XU, Q., KIM, N., HANES, J. & ENSIGN, L. M. 2016. PEGylation as a strategy for improving nanoparticle-based drug and gene delivery. *Advanced Drug Delivery Reviews*, 99, 28-51.

TARHINI, M., BENLYAMANI, I., HAMDANI, S., AGUSTI, G., FESSI, H., GREIGE-GERGES, H., BENTAHER, A. & ELAISSARI, A. 2018. Protein-based nanoparticle preparation via nanoprecipitation method. *Materials*, 11, 394.

TENZER, S., DOCTER, D., ROSFA, S., WLODARSKI, A., KUHAREV, J., REKIK, A., KNAUER, S. K., BANTZ, C., NAWROTH, T., BIER, C., SIRIRATTANAPAN, J., MANN, W., TREUEL, L., ZELLNER, R., MASKOS, M., SCHILD, H. & STAUBER, R. H. 2011. Nanoparticle size is a critical physicochemical determinant of the human blood plasma corona: a comprehensive quantitative proteomic analysis. *ACS Nano,* 5, 7155-7167.

THAPA, R. K., NGUYEN, H. T., JEONG, J.-H., SHIN, B. S., KU, S. K., CHOI, H.-G., YONG, C. S. & KIM, J. O. 2017. Synergistic anticancer activity of combined histone deacetylase and proteasomal inhibitor-loaded zein nanoparticles in metastatic prostate cancers. *Nanomedicine: Nanotechnology, Biology, and Medicine,* 13, 885-896.

TORCHILIN, V. 2011. Tumor delivery of macromolecular drugs based on the EPR effect. *Advanced Drug Delivery Reviews*, 63, 131-135.

TORCHILIN, V. P. 2007. Micellar nanocarriers: pharmaceutical perspectives. *Pharmaceutical Research,* 24, 1-16.

TORCHILIN, V. P. & TRUBETSKOY, V. S. 1995. Which polymers can make nanoparticulate drug carriers long-circulating?. *Advanced Drug Delivery Reviews,* 16, 141-155.

VAN BALLEGOOIE, C., MAN, A., ANDREU, I., GATES, B. D. & YAPP, D. 2019. Using a microfluidics system to reproducibly synthesize protein nanoparticles: factors contributing to size, homogeneity, and stability. *Processes,* 7, 290.

VAZE, O. S. 2016. Pharmaceutical nanocarriers (liposomes and micelles) in cancer therapy. *Journal of Nanomedicine and Nanotechnology, 7,* 1-2.

VROMAN, L. 1962. Effect of adsorbed proteins on the wettability of hydrophilic and hydrophobic solids. *Nature,* 196, 476–477.

WALKEY, C. D. & CHAN, W. C. 2012. Understanding and controlling the interaction of nanomaterials with proteins in a physiological environment. *Chemical Society Reviews*, 41, 2780-2799.

WALKEY, C. D., OLSEN, J. B., GUO, H., EMILI, A. & CHAN W. C. W. 2012. Nanoparticle size and surface chemistry determine serum protein adsorption and macrophage uptake. *Journal of the American Chemical Society*, 134, 2139-2147.

WANG, H. J., GONG, S. J., LIN, Z. X., FU, J. X., XUE, S. T., HUANG, J. C. & WANG, J. Y. 2007. *In vivo* biocompatibility and mechanical properties of porous zein scaffolds. *Biomaterials*, 28, 3952-3964.

WANG, Q., XIAN, W., LI, S., LIU, C. & PADUA, G. W. 2008. Topography and biocompatibility of patterned hydrophobic/hydrophilic zein layers. *Acta Biomaterialia*, 4, 844-851.

WICKI, A., WITZIGMANN, D., BALASUBRAMANIAN, V. & HUWYLER, J. 2015. Nanomedicine in cancer therapy: challenges, opportunities, and clinical applications. *Journal of Controlled Release, 200*, 138-157.

WILHELM, C., GAZEAU, F., ROGER, J., PONS, J. N. & BACRI, J.-C. 2002. Interaction of anionic superparamagnetic nanoparticles with cells: kinetic analyses of membrane adsorption and subsequent internalization. *Langmuir*, 18, 8148-8155.

WILLIAMS, H. D., TREVASKIS, N. L., CHARMAN, S. A., SHANKER, R. M., CHARMAN, W. N., POUTON, C. W. & PORTER, C. J. H. 2013. Strategies to address low drug solubility in discovery and development. *Pharmacological Reviews*, 65, 315-499.

WONG, H. L., BENDAYAN, R., RAUTH, A. M., XUE, H. Y., BABAKHANIAN, K. & WU, X. Y. 2006. A mechanistic study of enhanced doxorubicin uptake and retention in multidrug resistant breast cancer cells using a polymer-lipid hybrid nanoparticle system. *Journal of Pharmacology and Experimental Therapeutics*, 317, 1372-1381.

XIONG, X. Y., TAM, K. C. & GAN, L. H. 2005. Synthesis and thermal responsive properties of P(LA-*b*-EO-*b*-PO-*b*-EO-*b*-LA) block copolymers with short hydrophobic poly(lactic acid) (PLA) segments. *Polymer*, 46, 1841-1850.

XU, Q., ENSIGN, L. M., BOYLAN, N. J., SCHÖN, A., GONG, X., YANG, J.-C., LAMB, N. W., CAI, S., YU, T., FREIRE, E. & HANES, J. 2015. Impact of surface polyethylene glycol (PEG) density on biodegradable nanoparticle transport in mucus *ex vivo* and distribution *in vivo*. *ACS Nano*, 9, 9217-9227.

YAN, Y., GAUSE, K. T., KAMPHUIS, M. M. J., ANG, C. S., O'BRIEN-SIMPSON, N. M., LENZO, J. C., REYNOLDS, E. C., NICE, E. C. & CARUSO, F. 2013. Differential roles of the protein corona in the cellular uptake of nanoporous polymer particles by monocyte and macrophage cell lines. *ACS Nano*, 7, 10960-10970.

YUAN, F., DELLIAN, M., FUKUMURA, D., LEUNIG, M., BERK, D. A., TORCHILIN, V. P. & JAIN, R. K. 1995. Vascular permeability in a human tumor xenograft: molecular size dependence and cutoff size. *Cancer Research*, 55, 3752-3756.

ZAMAN, M., AHMAD, E., QADEER, A., RABBANI, G. & KHAN, R. H. 2014. Nanoparticles in relation to peptide and protein aggregation. *International Journal of Nanomedicine*, 9, 899-912.

ZHANG, Y., CUI, L., LI, F., SHI, N., LI, C., YU, X., CHEN, Y. & KONG, W. 2016. Design, fabrication and biomedical applications of zein-based nano/micro-carrier systems. *International Journal of Pharmaceutics*, 513, 191-210.

ZHONG, Q., JIN, M., DAVIDSON, P. M. & ZIVANOVIC, S. 2009. Sustained release of lysozyme from zein microcapsules produced by a supercritical anti-solvent process. *Food Chemistry*, 115, 697-700.

ZHONG, Q., JIN, M., XIAO, D., TIAN, H. & ZHANG, W. 2008. Application of supercritical anti-solvent technologies for the synthesis of delivery systems of bioactive food components. *Food Biophysics*, 3, 186-190.

ZOU, T. & GU, L. 2013. TPGS emulsified zein nanoparticles enhanced oral bioavailability of Daidzin: *in vitro* characteristics and *in vivo* performance. *Molecular Pharmaceutics*, 10, 2062-2070.

Appendices

Appendix I

Table A-1. List of hard corona proteins on mPEG5K-zein (0.5:1) and mPEG10K-zein micelles after exposure to human plasma at 37°C for 1 h (n.d.: not detected).

Accession	Description	Mass	mPEG5K-zein (0.5:1)		mPEG10K-zein	
			Score	emPAI	Score	emPAI
NP_000468.1	serum albumin preproprotein	71317	2765	5.74	2552	7.32
CAH18185.1	hypothetical protein (albumin)	71353	2465	4.73	2204	6.46
AAF69644.1	PRO2675 (albumin)	33466	n.d.	n.d.	2093	13.73
AFA52006.1	keratin 1	66197	2910	3.67	1097	2.93
AAG41947.1	keratin 1	66198	n.d.	n.d.	1075	2.93
NP_000414.2	keratin, type II cytoskeletal 2 epidermal	65678	1556	2.15	n.d.	n.d.
AAC83410.1	epidermal cytokeratin 2	66110	n.d.	n.d.	840	2.31
AAC41769.1	keratin type II	60448	549	0.87	n.d.	n.d.
AAA59466.1	keratin type II, partial	60258	538	0.76	n.d.	n.d.
AAH69269.1	Keratin 6A	60323	497	0.87	n.d.	n.d.
AAH24292.1	Keratin 5	62568	358	0.52	207	0.27
NP_000217.2	keratin, type I cytoskeletal 9	62255	2741	1.8	158	0.35
NP_000055.2	complement C3 preproprotein	188569	2720	0.76	1405	0.94
NP_000375.2	apolipoprotein B-100 precursor	516634	1721	0.22	812	0.27
NP_000412.3	keratin, type I cytoskeletal 10	58994	1668	1.97	1173	3.64
AAB35421.1	type I keratin 16	51548	1094	1.59	n.d.	n.d.
AAA59460.1	keratin type 16	51010	n.d.	n.d.	97	0.25
AAH02690.1	Keratin 14	51905	1009	0.92	n.d.	n.d.
NP_705694.3	keratin, type I cytoskeletal 13 isoform a	49900	300	0.35	n.d.	n.d.
BAG56970.1	unnamed protein product	62862	53	0.13	n.d.	n.d.
AMT74554.1	immunoglobulin light chain VRC01c-HuGL, partial	18550	1494	5.03	n.d.	n.d.
AMT74549.1	immunoglobulin light chain VRC01c-HuGL, partial	18437	1282	5.1	n.d.	n.d.
AMT74548.1	immunoglobulin light chain VRC01c-HuGL, partial	18337	1232	4.03	n.d.	n.d.
AAH73794.1	Unknown (protein for MGC:88814)	25236	1108	1.82	245	1.82
1RZ7_L	Chain L, Crystal Structure Of Human Anti-Hiv-1 Gp120-Reactive Antibody 48d	23285	1017	1.61	n.d.	n.d.
AAB50880.1	anitubulin IgG1 kappa VL chain {N-terminal} [human, serum, immunocytic sarcom patient PER isolate, Peptide Partial, 219 aa]	24028	1001	1.54	n.d.	n.d.
5M6A_A	Chain A, Crystal structure of cardiotoxic Bence-Jones light chain dimer H9	22803	967	1.67	n.d.	n.d.
AAF13225.1	immunoglobulin lambda light chain, partial	23197	962	2.07	n.d.	n.d.
ABU90575.2	immunoglobulin lambda 2 light chain, partial	23205	949	1.62	n.d.	n.d.
ABU90604.1	immunoglobulin kappa 1 light chain, partial	23832	944	1.55	n.d.	n.d.
AWH66747.1	immunoglobulin light chain variable region, partial	11751	758	3.71	n.d.	n.d.
BAC85363.1	unnamed protein product	54372	659	0.52	521	0.41
BAC85190.1	unnamed protein product	56528	627	0.49	n.d.	n.d.
BAC85349.1	unnamed protein product	54127	598	0.52	n.d.	n.d.
BAC85432.1	unnamed protein product	54647	n.d.	n.d.	516	0.51
ARA90391.1	immunoglobulin heavy chain, partial	50906	524	0.81	337	0.94
BAC85202.1	unnamed protein product	53997	n.d.	n.d.	260	1.01
AAH28090.1	IGL@ protein	25119	n.d.	n.d.	248	1.83
AXN93649.1	immunoglobulin gamma 1 constant region, partial	36582	n.d.	n.d.	198	1.27
AAH70353.1	IGL@ protein	25475	n.d.	n.d.	189	1.4

Accession	Description	Mass	mPEG5K-zein (0.5:1)		mPEG10K-zein	
			Score	emPAI	Score	emPAI
AAT86037.2	immunoglobulin mu light chain variable region, partial	15959	n.d.	n.d.	168	1
ANH09850.1	immunoglobulin light chain variable region, partial	11778	n.d.	n.d.	122	0.36
P0DOX2.2	Immunoglobulin alpha-2 heavy chain BUT	49816	n.d.	n.d.	113	0.25
AAG00912.1	recombinant IgG4 heavy chain, partial	43465	n.d.	n.d.	92	0.3
AMB38464.1	immunoglobulin heavy chain variable region, partial	15667	502	1.56	n.d.	n.d.
AAD30738.1	immunoglobulin heavy chain variable region, partial	13400	n.d.	n.d.	88	1.27
AAS85877.1	immunoglobulin heavy chain, partial	16502	n.d.	n.d.	88	0.95
AIE56783.1	immunoglobulin heavy chain variable region, partial	10722	n.d.	n.d.	73	0.4
CEF92697.1	immunoglobulin heavy chain variable region, partial	11472	n.d.	n.d.	62	1.6
AAW69278.1	anti-tetanus toxoid immunoglobulin light chain variable region, partial	11764	448	1.53	n.d.	n.d.
AAF79136.1	immunoglobulin light chain variable region, partial	11739	418	0.86	n.d.	n.d.
AAB59396.1	immunoglobulin alpha-2 heavy chain, partial	37212	397	0.5	n.d.	n.d.
CAA06862.1	anti-(ED-B) scFV, partial	25357	384	0.34	n.d.	n.d.
ARA90390.1	immunoglobulin heavy chain, partial	49976	355	0.97	n.d.	n.d.
AAA19493.1	immunoglobulin kappa light chain V-Jk4, partial	12914	324	1.35	n.d.	n.d.
CAE45775.1	hypothetical protein	53011	312	0.89	n.d.	n.d.
CAC43966.1	immunoglobulin kappa light chain variable region, partial	10855	303	0.95	n.d.	n.d.
AAF79134.1	immunoglobulin light chain variable region, partial	12085	286	0.83	n.d.	n.d.
AAA69737.1	immunoglobulin light chain MRNA V-region, partial	13916	223	1.21	38	0.3
CAC85284.1	anti-peptide/MHC complex HLA-A1/MAGE-A1 monoclonal antibody heavy chain, partial	26902	221	0.74	n.d.	n.d.
AAB59394.1	immunoglobulin gamma-4 heavy chain, partial	36360	217	0.51	n.d.	n.d.
BAJ52218.1	immunoglobulin gamma heavy chain, partial	23913	213	0.87	n.d.	n.d.
CAJ75491.1	immunoglobulin lambda light chain, partial	11570	194	0.88	n.d.	n.d.
ABA00093.1	immunoglobulin epsilon heavy chain variable region, partial	13187	173	0.74	n.d.	n.d.
ABU90692.2	immunoglobulin lambda 1 light chain, partial	23106	158	0.62	n.d.	n.d.
AAY33400.1	anti-rabies virus immunoglobulin light chain variable region, partial	11887	85	0.85	n.d.	n.d.
AAD16751.1	immunoglobulin lambda light chain variable region, partial	11759	55	0.86	n.d.	n.d.
NP_000499.1	fibrinogen alpha chain isoform alpha-E preproprotein	95656	1193	0.54	444	0.61
NP_000005.2	alpha-2-macroglobulin isoform a precursor	164614	990	0.32	763	0.38
AAA87674.1	immunoglobulin kappa light chain, partial	23727	n.d.	n.d.	683	2.5
ADX66015.1	immunoglobulin variable region, partial	15515	n.d.	n.d.	321	1.04
NP_000286.3	alpha-1-antitrypsin precursor	46878	921	0.9	926	2.33
AAA51546.1	alpha-1-antitrypsin	46787	n.d.	n.d.	925	2.33
AAH15642.1	Serpin peptidase inhibitor, clade A (alpha-1 antiproteinase, antitrypsin), member 1	46850	n.d.	n.d.	923	2.33
3V83_A	Chain A, The 2.1 Angstrom Crystal Structure Of Diferric Human Transferrin	79280	846	0.69	721	0.95
NP_000032.1	apolipoprotein E isoform b precursor	36246	n.d.	n.d.	686	1.81
EAX03569.1	hCG2001591	194140	802	0.29	1236	0.42
AAB59397.1	apolipoprotein E	36242	768	4.22	n.d.	n.d.
NP_002209.2	inter-alpha-trypsin inhibitor heavy chain H4 isoform 1 precursor	103521	527	0.29	181	0.29
NP_002017.1	fibronectin isoform 3 preproprotein	262656	501	0.06	303	0.07

Accession	Description	Mass	mPEG5K-zein (0.5:1)		mPEG10K-zein	
			Score	emPAI	Score	emPAI
NP_000574.2	vitamin D-binding protein isoform 1 precursor	54480	n.d.	n.d.	279	0.32
NP_000030.1	apolipoprotein A-I isoform 1 preproprotein	30759	480	2.81	779	4.49
AAB22835.1	apolipoprotein AI, apo AI [human, spleen, Peptide Mutant, 88 aa]	10155	199	1.93	302	5
AAA35545.1	proapo-A-I protein	30745	n.d.	n.d.	740	4.49
NP_001636.1	apolipoprotein C-I precursor	9326	n.d.	n.d.	53	0.47
P0DOX6.2	Immunoglobulin mu heavy chain OU	64244	475	0.19	n.d.	n.d.
NP_001076.2	alpha-1-antichymotrypsin precursor	47792	452	0.37	211	0.48
NP_002207.2	inter-alpha-trypsin inhibitor heavy chain H2 precursor	106853	452	0.24	139	0.15
NP_000482.3	complement C1q subcomponent subunit B precursor	26933	443	0.51	180	0.15
NP_001728.1	complement component C9 preproprotein	64615	n.d.	n.d.	63	0.06
NP_002206.2	inter-alpha-trypsin inhibitor heavy chain H1 isoform a preproprotein	101782	355	0.16	321	0.2
NP_000031.1	apolipoprotein C-III precursor	10846	330	0.4	201	1.72
AAB32200.1	apolipoprotein D, apoD	28317	314	0.93	53	0.3
NP_000168.1	gelsolin isoform a precursor	86043	259	0.14	34	0.04
AGP00859.1	immunoglobulin A heavy chain variable region, partial	14039	226	0.3	n.d.	n.d.
NP_005134.1	haptoglobin isoform 1 preproprotein	45861	215	0.64	126	0.28
AAA58902.1	Ig J-chain, partial	16041	214	0.26	75	0.26
NP_001701.2	complement factor B preproprotein	86847	209	0.09	146	0.14
EAW72575.1	alpha-1-B glycoprotein	54809	195	0.07	n.d.	n.d.
NP_000020.1	angiotensinogen preproprotein	53406	194	0.15	111	0.15
NP_000053.2	plasma protease C1 inhibitor precursor	55347	181	0.15	48	0.07
NP_000884.1	kininogen-1 isoform 2 precursor	48936	172	0.17	55	0.17
NP_000473.2	apolipoprotein A-IV precursor	45344	172	0.39	192	0.94
AAF00489.1	hemoglobin beta subunit variant	16086	163	0.58	n.d.	n.d.
BAA00124.1	alpha-2-plasmin inhibitor precursor	54903	158	0.23	n.d.	n.d.
BAB71575.1	unnamed protein product	25941	156	0.33	172	0.54
NP_001725.1	complement C1s subcomponent isoform 1 preproprotein	78174	146	0.05	76	0.05
EAX04934.1	fibrinogen beta chain, isoform CRA_e	40167	124	0.21	n.d.	n.d.
EAX04933.1	fibrinogen beta chain, isoform CRA_d	52759	n.d.	n.d.	108	0.15
1TTC_A	Chain A, Transthyretin	13842	123	0.7	n.d.	n.d.
NP_003652.2	apolipoprotein L1 isoform a precursor	44004	111	0.09	94	0.09
NP_000479.1	antithrombin-III isoform 1 precursor	53025	110	0.15	201	0.53
CAJ75478.1	immunoglobulin heavy chain, partial	23826	105	0.17	60	0.17
NP_001822.3	clusterin preproprotein	53031	104	0.24	179	0.33
AAH34389.1	Leucine-rich alpha-2-glycoprotein 1	38372	103	0.1	65	0.22
AAI44239.1	Peptidoglycan recognition protein 2	68683	97	0.06	n.d.	n.d.
NP_000177.2	complement factor H isoform a precursor	143654	95	0.05	n.d.	n.d.
NP_006735.2	retinol-binding protein 4 isoform a precursor	23337	92	0.38	n.d.	n.d.
NP_001176.1	zinc-alpha-2-glycoprotein precursor	34465	90	0.12	63	0.12
AME15468.1	anti-HIV immunoglobulin heavy chain variable region, partial	13165	89	0.32	n.d.	n.d.
AGR34115.1	anti-HIV-1 immunoglobulin light chain variable region, partial	11208	n.d.	n.d.	44	0.38
3CU7_A	Chain A, Human Complement Component 5	189911	88	0.04	39	0.02
1I5J_A	Chain A, Nmr Structure Of Human Apolipoprotein C-Ii In The Presence Of Sds	8909	83	0.5	n.d.	n.d.
AHZ09405.1	immunoglobulin light chain variable region, partial	11334	83	0.9	n.d.	n.d.
AFQ00545.1	vitronectin, partial	25596	82	0.16	n.d.	n.d.
1JMJ_A	Chain A, Crystal Structure Of Native Heparin Cofactor Ii	55096	77	0.07	62	0.15
ANP95466.1	vitamin D binding protein, partial	3612	71	5.19	n.d.	n.d.

Accession	Description	Mass	mPEG5K-zein (0.5:1)		mPEG10K-zein	
			Score	emPAI	Score	emPAI
NP_000087.2	ceruloplasmin precursor	122997	68	0.03	28	0.03
AGP00850.1	immunoglobulin A heavy chain variable region, partial	13407	67	0.31	n.d.	n.d.
AIU95717.1	immunoglobulin kappa light chain variable region, partial	10697	66	0.41	n.d.	n.d.
AAF03677.1	apolipoprotein(a), partial	12216	66	0.35	n.d.	n.d.
AAA52173.1	serum vitamin D-binding protein precursor	54612	65	0.15	n.d.	n.d.
NP_006503.2	serum amyloid A-4 protein precursor	14851	62	0.28	n.d.	n.d.
NP_000437.3	serum paraoxonase/arylesterase 1 precursor	39877	59	0.1	93	0.1
NP_000706.1	C4b-binding protein alpha chain precursor	69042	56	0.12	n.d.	n.d.
NP_000500.2	fibrinogen gamma chain isoform gamma-A precursor	50092	47	0.08	73	0.35
EAX01790.1	solute carrier family 9 (sodium/hydrogen exchanger), member 4	82210	44	0.05	n.d.	n.d.
NP_001637.1	apolipoprotein C-IV precursor	14886	44	0.28	n.d.	n.d.
AAS19424.1	anti-SARS S protein immunoglobulin heavy chain variable region, partial	12738	44	0.33	n.d.	n.d.
NP_000303.1	vitamin K-dependent protein C preproprotein	53406	42	0.07	n.d.	n.d.
AIZ06499.1	immunoglobulin kappa chain variable region, partial	10228	40	0.43	n.d.	n.d.
BAS02858.1	T cell receptor alpha chain V-J-region, partial	7205	37	0.64	40	0.64
NP_002640.2	phosphatidylinositol 4,5-bisphosphate 3-kinase catalytic subunit gamma isoform	127571	34	0.03	n.d.	n.d.
EAW50979.1	hCG1742973, partial	17765	31	0.23	n.d.	n.d.
EAW55766.1	hCG1984886, isoform CRA_b, partial	24205	30	0.17	n.d.	n.d.
EAX04766.1	hCG2025928	18290	29	0.22	n.d.	n.d.
AAH00539.2	JMJD1B protein, partial	173630	29	0.02	n.d.	n.d.
EAW82627.1	iduronidase, alpha-L-, isoform CRA_j	41521	27	0.09	n.d.	n.d.
CAD39181.1	hypothetical protein, partial	52942	27	0.07	n.d.	n.d.
ABO30676.1	alpha-helix coiled-coil rod homologue, partial	13127	25	0.32	n.d.	n.d.
AAB71646.1	MHC class I chain-related protein, partial	36491	23	0.11	n.d.	n.d.
NP_001013649.2	NHS-like protein 2	133831	23	0.03	n.d.	n.d.
NP_004987.2	multidrug resistance-associated protein 1	172907	22	0.02	n.d.	n.d.
AAL08624.1	NDR1-related protein NDR2	41113	21	0.1	n.d.	n.d.
CAC12843.1	lipoxygenase-3	81856	20	0.05	n.d.	n.d.
ABE97359.1	anti-Rh(D) antibody immunoglobulin heavy chain variable region, partial	14624	20	0.29	n.d.	n.d.
BAB14324.1	unnamed protein product, partial	83252	19	0.05	n.d.	n.d.
NP_001327.2	cathepsin Z preproprotein	34530	19	0.11	n.d.	n.d.
EAW64299.1	EF-hand domain family, member B, isoform CRA_a	130113	16	0.03	n.d.	n.d.
CAB44857.1	immunoglobulin mu heavy chain variable region, partial	13201	16	0.32	n.d.	n.d.
AAS01769.1	monoclonal IgM antibody heavy chain	65126	n.d.	n.d.	244	0.42
1QWH_A	Chain A, A Covalent Dimer Of Transthyretin That Affects The Amyloid Pathway	12836	n.d.	n.d.	217	2.11
NP_001677.2	ATP synthase subunit beta, mitochondrial precursor	56525	n.d.	n.d.	105	0.14
NP_000604.1	hemopexin precursor	52385	n.d.	n.d.	102	0.15
NP_001624.1	protein AMBP preproprotein	39886	n.d.	n.d.	97	0.1
NP_000629.3	vitronectin precursor	55069	n.d.	n.d.	94	0.15
AAL07469.1	alpha-1-B glycoprotein precursor	54746	n.d.	n.d.	72	0.07
AAA35952.1	beta-globin	19204	n.d.	n.d.	63	0.47
NP_001077007.1	POTE ankyrin domain family member E	122882	n.d.	n.d.	58	0.06
NP_001630.1	serum amyloid P-component precursor	25485	n.d.	n.d.	50	0.16
NP_001613.2	alpha-2-HS-glycoprotein isoform 2 preproprotein	40114	n.d.	n.d.	50	0.1

Accession	Description	Mass	mPEG5K-zein (0.5:1)		mPEG10K-zein	
			Score	emPAI	Score	emPAI
1COH_A	Chain A, Structure Of Haemoglobin In The Deoxy Quaternary State With Ligand Bound At The Alpha Haems	15174	n.d.	n.d.	49	0.27
EAX01470.1	hCG23783, isoform CRA_a	23402	n.d.	n.d.	45	0.17
BAG06714.1	MYO5B variant protein	215218	n.d.	n.d.	45	0.02
BAG58506.1	unnamed protein product	113194	n.d.	n.d.	43	0.03
NP_689497.1	charged multivesicular body protein 4c	26394	n.d.	n.d.	38	0.15
AAG44663.1	DC33	30040	n.d.	n.d.	38	0.28
NP_003433.3	zinc finger protein 143 isoform 1 [Homo sapiens]	69709	n.d.	n.d.	36	0.06
NP_001124.1	afamin precursor	70963	n.d.	n.d.	34	0.05
SCW25082.1	Activated tyrosine kinase PDGFRB	92437	n.d.	n.d.	34	0.04
EAX06838.1	Fas (TNFRSF6) associated factor 1, isoform CRA_b	57089	n.d.	n.d.	33	0.07
XP_011524065.1	lethal(3)malignant brain tumor-like protein 4 isoform X6	60648	n.d.	n.d.	28	0.06
BAG60995.1	unnamed protein product	40215	n.d.	n.d.	27	0.1
AAM15772.1	interleukin-1 receptor associated kinase 4	51925	n.d.	n.d.	26	0.08
NP_005989.3	T-complex protein 1 subunit gamma isoform a	61066	n.d.	n.d.	22	0.06
AAG44697.1	DC37	32471	n.d.	n.d.	22	0.12
CAD38880.1	hypothetical protein	58694	n.d.	n.d.	22	0.07
EAW65837.1	tetratricopeptide repeat domain 6, isoform CRA_a	185766	n.d.	n.d.	22	0.02
XP_011536666.1	RNA-binding protein Musashi homolog 1 isoform X5	28085	n.d.	n.d.	21	0.14
AAI13880.1	SH3 domain and tetratricopeptide repeats 2	146697	n.d.	n.d.	19	0.03
BAH11896.1	unnamed protein product	17420	n.d.	n.d.	16	0.24
AAT74746.1	proteoglycan 4, partial	28812	n.d.	n.d.	15	0.14

Appendix II

Conference proceedings

1. Meewan, J., Somani, S. & Dufès, C. Preparation and characterization of mPEG-zein micelles as a delivery vehicle for hydrophobic drugs. The 11th European and Global Summit for Clinical Nanomedicine, Targeted Delivery and Precision Medicine - The Building Blocks to Personalized Medicine 2018, Basel, Switzerland (September 2-5, 2018), Poster presentation.

2. Meewan, J., Somani, S., Laskar, P., Woods, S. & Dufès, C. Effects of protein corona on the cellular uptake of PEGylated zein micelles. British Society of Nanomedicine: Early Career Researchers Meeting 2019. Glasgow, UK (July 25-26, 2019), Poster presentation.

Publications

1. Meewan, J., Somani, S., Laskar, P., Irving, C., Mullin, M., Woods, S., Roberts, C., Alzahrani, A. R., Ferro, V. A., McGill, S., Weidt, S., Burchmore, R. & Dufès, C. 2022. Limited impact of the protein corona on the cellular uptake of PEGylated zein micelles by melanoma cancer cells. *Pharmaceutics*, 14, 439.

2. Almowalad, J., Laskar, P., Somani, S., Meewan, J. & Dufès, C. 2022. Lactoferirin- and dendrimer-bearing gold nanocages for stimulus-free DNA delivery to prostate cancer cells. *International Journal of Nanomedicine*, 17, 1409-1421.

3. Almowalad, J., Somani, S., Laskar, P., Meewan, J., Tate, R. J., Mullin, M. & Dufès, C. 2021. Lactoferrin-bearing gold nanocages for gene delivery in prostate cancer cells in vitro. *International Journal of Nanomedicine*, 16, 4391-4407.

4. Meewan, J., Somani, S., Almowalad, J., Laskar, P., Mullin, M., MacKenzie, G., Khadke, S., Perrie, Y. & Dufès, C. Preparation of zein-based nanoparticles: nanoprecipitation versus microfluidic-assisted manufacture, effects of PEGylation on nanoparticle characteristics and cellular uptake by melanoma cells (Submitted).